HIERARCHICAL STRUCTURE IN ADVANCED POLYMERS: PHASE BEHAVIOR, ORIENTATION PROPERTIES

[illegible] Keller and [illegible]

[illegible] Department of the U.S. Army ERO [illegible]

[illegible] DAJA45 [illegible]

FINAL REPORT

(1)

HIERARCHICAL STRUCTURE IN ADVANCED POLYMERS; PHASE BEHAVIOUR, ORIENTATION,PROPERTIES

Investigators: A. Keller and J.A. Odell

Contractor:Department of the U.S. Army,ERO
Contract Number: DAJA45-89-C-0021

FINAL REPORT

R&D 6011 MS-01

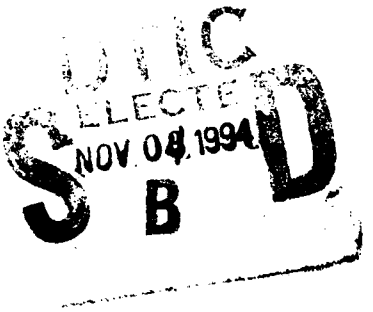

SCOPE & SUMMARY

Relation to Original Proposal

The original proposal was a broad front investigation of the structure hierarchy in advanced materials embracing phase behaviour, orientation and properties. We can state that all these objectives have been pursued in the course of the project leading to substantial amount of new knowledge in the respective fields, as testified also by the publication list appended.

Inevitably there have been some departures in both direction and emphasis since the writing of the original proposal while still in keeping within its broader framework. Some of these changes were in response to the new results arising in the course of the work, as to be expected in an ongoing enquiry, while some were in response to changes in external circumstances. Amongst the latter was the USAF input and interest, subsequent to the preparation of the initial proposal. This created an additional focus on the rigid rod systems PBZT/PBO. Section 4 is our response to their directive, which, as will be seen, has led to a new departure in the study of this kind of system. However, the promised supply of these polymers by the Dow Company, at least in a form suitable for handling in our proposed experiments, has not materialised which, after a while induced us to resort to an alternative model system for the continuation of that part of the program. Another external factor was the inevitable changes in staff with associated changes in research interest and expertise. Thus, while on the one hand a premature departure has left our efforts in the morphological research confined to the large scale end of the structure hierarchy (Section 2), the arrival of new staff with new interests and expertise introduced a new subject area not originally envisaged (Section 5).

In conclusion, when allowing for the changes brought about by circumstances beyond our control, and for the fact that the initial proposal had been knowingly more ambitious than could practically be accomplished in full, we can state that the main objectives have been achieved.

Materials

Most of the materials used were liquid crystal forming polymers (LCP). This choice was dictated by the fact that LCP-s are amongst the most advanced polymeric materials with technological potential both in structural (load bearing) and in device

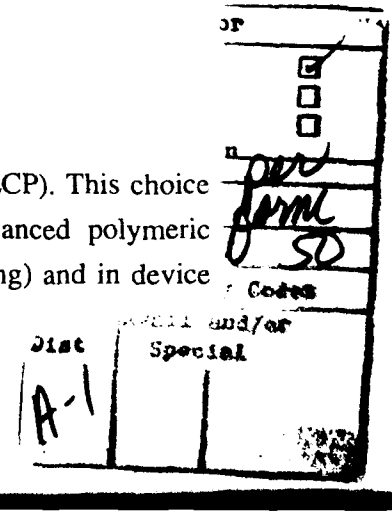

application. Further, from the point of view of fundamental knowledge they add a new dimension to phase behaviour, orientational properties and aspects of structure hierarchy onto what is already known in the more conventional thermoplastic polymers. Thanks to our association with sources of synthesis (Professor Percec, Case Western Reserve University, Cleveland, USA) and at a later stage also with the University Halle, Germany, through our last staff appointment (Dr. H. Fischer) we were in a favourable position to acquire materials best suited for our purposes.

SUBJECT AREAS

1. Banding in liquid crystal polymers

This subject is at the confluence of two important aspects of LCP-s, namely orientation and structure. Broadly, it is a structure feature which arises as an intermediate stage of orientation-relaxation often unintentionally, sometimes unavoidably in processed articles. Here we made three new classes of addition to the knowledge on this effect.

The first is the appearance of banding in multiaxial flow fields, such as could be significant in their own right, but (as in our case) can also appear unintentionally on sample handling. The multiaxial flow fields can give rise to large scale birefringent textures in the isotropic state of the highly orientable LCP-s which mimic genuine LCP texture effects. When passing through the LCP state on cooling, unique combinations of these large scale textures and genuine LCP textures (on the correspondingly smaller scale of the texture hierarchy) can arise which we were now able to analyse. The significance of this attainment is two-fold: Firstly, that we are now in the position to interpret complex birefringence effects that must be widespread amongst LCP-s but could not have been previously interpreted or could have given rise to misinterpretations. Secondly, and more forward looking, through our newly gained insight we can now use such effects to reconstruct complex flow histories and map out associated orientation patterns with consequences for control of processing and properties of LCP products.

The second salient result in the area of banded structure is the recognition that the banding can be self-generated without any external orientation. It can arise on crystallization, in our view, due to the associated anisotropic volume changes. This may provide a major pointer towards fundamental understanding of the banding effect (buckling on resistance to "self extension") and also should have influence on quality control of processed products.

The third advantage is the first ever use of Atomic Force Microscopy in the study of the fine structure of the bands with notably new information gained.

Above, references have been made to the implications of banding for the properties of the corresponding materials. This could be of two kinds. First, the structure underlying the bands may detract from the ultimate properties of a fully oriented product (e.g. in Kevlar) or, alternatively, it could have the positive effect of imparting toughness to such materials (collagen as a biological example). Our advances made through the present work should be in aid of either, namely how to avoid or how to promote the effect, according to intended utilisation.

2. Rheology and flow induced liquid crystal phase transitions

It is well known that thermotropic LCP-s lend themselves particularly well to melt processing due to low flow resistance and absence of flow irregularities and instabilities in the LCP state as compared to the isotropic melt state of conventional thermoplastic polymers. Nevertheless, surprising as this may appear, to our knowledge, there existed no direct comparison between the LCP state and the isotropic state of the same material regards flow behaviour, viscosity in particular: specifically that the viscosity ought to increase on raising the temperature when passing from the LCP into the isotropic state. As soon as we realised this conspicuous gap in existing experience we set out to test for it. Thanks to the acquisition of suitable material from Professor Percec we could probe for the above stated expectation. Not only could the principal effect laid above be verified but its shear rate dependence could also be followed including the effect of molecular weight. These studies then have led to a further new recognition, namely that the flow itself affects the isotropisation temperature, with all its consequences for melt processing. In particular a melt, initially in the high viscosity isotropic state, can convert into a low viscosity LC state in the course of the processing operation itself.

3. Morphology

Here our main concern was the long standing problem of crystallization from the liquid crystal state. Even if we did not get as far down as the molecular and fine structural level within the present program, we succeeded in creating a situation where liquid crystal formation and crystallization could be compared in one and the same

material as regards the optically registerably large scale structure hierarchy and crystallization rate. It was found that in a suitably chosen so called monotropic systems the two types of phase transition can compete, where they can give rise to both structures characteristic of each state and to a combination of both, displaying also some novel features creating as yet a further stratification in the polymeric structure hierarchy. In addition, some important observations were made regards the rate of the final crystallization. Accordingly, the crystalline state was achieved faster when proceeding through the liquid crystal state compared to reaching it directly from the isotropic melt at identical supercoolings.

The work, as it evolved, has raised wider issues ranging beyond the particular system investigated. These issues all relate to non-equilibrium states. Specifically, incomplete liquid crystallinity in addition to and in combination with the more familiar conception of incomplete crystallinity creating, amongst others, a multi-tier hierarchical frame work of structure and/or phase deficiencies. Beyond this, the metastable nature of the liquid crystal phase, in our particular system, raises issues involving metastability in wider generality with consequences for phase transformations in polymers and elsewhere.

In summary, even at this stage of the investigation of crystallization from the liquid crystal state we succeeded in laying down a frame work relating to the thermodynamics, kinetics and polarizing optical structure which we judge as indispensable for continuing work in this area. In addition, the work has highlighted principles of wider generality for phase transitions in polymers and beyond.

4. Phase Behaviour-Crystal Solvates and Solvate Structure

This topic is part of our ongoing involvement in rigid rod systems but was given special topicality by USAF interest and part support. It has arisen from our attempts to study the behaviour of such molecules in solution, the only system in which they are processable, the solvent being polyphosphoric acid. Unfortunately the only sample of PBO we had, supplied by Dow Co. was too concentrated to be useful to us and we could not obtain any recipe of how to dilute it, not to speak of other samples. Under these conditions we were restricted to PBZT of which we had samples from earlier works.

In the course of work on PBZT it became obvious that the system polyphosphoric acid-PBZT was much more involved than implicitly assumed, and there could be no

further progress before the phase diagram was established. In view of the multicomponent nature of polyphosphoric acid itself, and the decisive influence of water this was no simple task. In the course of the investigation the role and importance of crystal solvates has emerged. Crystal solvates in such a system were known to exist before, but in the course of the present study their existence, together with precise composition, could be incorporated within the solvent-solid phase diagram. We consider this result as very significant both practically and fundamentally. In practice, the phase diagram should provide a map for intended processing operations. For fundamental knowledge the principal gain is the recognition of the importance of polymer-solvent associations.

In an attempt to pursue the polymer-solvent association issue we turned to the more tractable LCP, hydroxypropyl cellulose (HPC), where similar investigations could be pursued in aqueous systems. The resemblance of HPC to PBZT regards two component phase behaviour proved to be striking, revealing similar class of crystal solvates calling for further investigations on this related system.

The significance of this work promises to extend beyond it immediate objectives; to the understanding of bicomponent LCP systems and beyond. Within the LCP field it provides a bridge between lyotropic and thermotropic systems as it suggests that the lyotropic phase with heavily solvated chains and no free solvent may be better described as thermotropic. Beyond LCP-s the strong and not uniquely specific association between polymers and solvent, as found even in the isotropic phase of LCP-s, contains pointers to the behaviour of polymers in good solvents in general with potentially far reaching implications.

5. Structure formation in Block Copolymers with one liquid crystalline Block

This line of work, while within the broader framework of the proposal, has not been specifically contemplated initially. It was brought in thanks to our association with the University of Halle, Germany through the appointment of Dr H. Fischer. It involves block copolymers where as familiar, the incompatible blocks segregate forming a micro-phase morphology. This subject one is of course widely familiar and represent an important, typically polymeric facet of phase behaviour creating its own level of phase structure within the overall structure hierarchy of a polymer. The totally new aspect in the present work, (the reason why we took it up when the opportunity arose) is the situation where one of the blocks can also form liquid crystals. This creates yet a

new level of structure hierarchy in a variety of phase combinations. It leads not only to new structure possibilities but is actually probing the limits of our conceptional picture of what represents a phase.

The work that has emerged is truly extensive. It was not all done in Bristol, yet without Dr Fischer masterminding it all from his position in Bristol it would not have materialised: in that sense it was made possible through the present ERO grant and is being reported at this place accordingly. Most of it has become finalised since the last Periodic Report, hence its first inclusion at this point of our reporting on the Grant. In view of the excessive space the full reporting would require we only reproduce here the Abstract of works that are presently in the press with the exception of Abstract 3 (carried out fully in Bristol) where the underlying work is being presented here in full. The texts of the rest are available on request.

LIST OF PUBLICATIONS:

- Hoff M., Keller A., Odell J.A., Percec V., "Large scale textures in nematic polyethers: 1. New aspects of formation", *Mol.Cryst.Liq.Cryst.*, **241**, 221 (1994)
- Hoff M., Keller A., Odell J.A., Percec V., ""Large scale textures in nematic polyethers: 1. New aspects of orientational order and structure hierarchy", *Mol.Cryst.Liq.Cryst.*, **241**, 231 (1994)
- M. Hoff, A. Keller, J. A. Odell, V. Percec, "Crystallisation-induced band formation in nematic polyethers", *Polymer*, **34**, 1800 (1993)
- H. Fischer, M. J. Miles, and J. A. Odell, "Atomic force microscopy of the banded structure of lyotropic polymers", *Macromol.Rapid Commun.*, accepted for publication
- D.P. Heberer, J.A. Odell, and V. Percec"Rheology and Flow-induced Liquid Crystal Phase Transitions in Thermotropic Polyethers", *J. Mater. Sci.*, accepted for publication
- D. Heberer, A. Keller" Interrelation between crystallization and liquid crystal formation; a calorimetric and polarizing microscopical study on a monotropic system" to be published
- H. Fischer, M. Murray, J. A. Odell and A. Keller, "On the phase diagram of the system PBZT/P_2O_5/H_2O", *J. Mater. Sci.*, **29**, 1025 (1994)
- H. Fischer, M. Murray, J. A. Odell and A. Keller, "On the phase diagram of the system Hydroxypropylcellulose/water", *J. Mater. Sci.*, submitted for publication
- H. Fischer, J. A. Odell and A. Keller, "A quick way to prepare concentrated solutions of Hydroxypropylcellulose in water", *J. Adv. Polym. Sci.*, submitted for publication

Arnold, M, Poser, S.; Fischer, H.; Frank, W.; and Utschick, H., "LC side group block copolymers -synthesis, morphology and phase behaviour", *Macromol.Rapid Commun.*, **1994**, *15*, 487

- Fischer, H., Poser, S., Frank, W. and Arnold, M., "On the influence of the morphology on the LC behaviour of LC side chain block copolymers ", *Macromoleclues*, submitted for publication

- Fischer, H., "The Existence of a tetragonal structure in block Copolymers", *Polymer Commun.*, in press

- Fischer, H., *Polymer Commun.*, "Selective staining of the interfacial region in block copolymers ", submitted for publication

- Fischer, H., Poser, S. and Arnold, M., " On the interaction of the morphological structure and the LC behaviour of LC side chain block copolymers", submitted to *Liq.Cryst*

OTHER PAPERS

- H. Fischer, U. Jeschke, C. Vogel and V. Vill, "Discotic hexagonal columnar structures in ACYCLIC carbohydrate S.S.-Diacetals", *Liq. Crystals* **15**, 733 (1993)

- S. Bauer, H. Fischer and H. Ringsdorf, "Highly branched liquid crystalline polymers with chiral end groups", *Angew. Chemie*, **105**, 1658 (1993)

SECTION 1: BANDING IN LIQUID CRYSTALLINE POLYMERS

Recently much attention has focused upon the banded textures formed in liquid crystalline nematic polymers during relaxation of chains previously oriented by external flow. Although the precise mechanism of band formation has not yet been explained satisfactorily, it is generally believed that the bands, a periodical arrangement of the molecular director, form to minimise excess elastic energy of the system. The effect is commonly thought to be driven by distortion of molecules from their equilibrium arrangement and the elasticity of the texture (particularly splay).The Frank elasticity constant for splay is thought to be particularly high (compared to bend and twist), so that any elastic recovery would try to minimise the degree of splay. This might be possible through the co-operative disorientation that we see as banding.

This is clearly of great significance in processing liquid crystalline polymers and has been a major strand of our work under the ERO project. Here we present four representative reports on various aspects of this part of our program.

The first report examines remarkable large-scale textures that nematic polyethers can form, similar to low molecular weight nematic *schlieren* textures, but on a scale of *hundreds of microns*. We demonstrate that they arise from sporadic flow-induced orientation due to external strain fields. Such circumstances may arise during sample handling, yielding effects which are apparently similar to those arising from nematic orientation textures but on a larger scale, overlaying the effects intrinsic to the liquid crystal nature. We thus have a two-tier structure hierarchy, a large-scale structure due to external orientation and a fine scale structure due to the intrinsic nematicity where the latter conforms geometrically to the former. images in samples which display these features.
We believe that the results are of general interest for liquid crystalline polymers, particularly in revealing textures which may arise as a result of melt processing.

In the second report we pursue the structural analysis of the compounded large and fine-scale textures. Characterisation of the two-level hierarchy is an instructive exercise in analysing polarising optical effects, particularly as it is applicable to other situations and systems where similar effects may arise. The fine substructure arises due to nematic self-ordering within the large-scale texture to which it conforms geometrically. The precise nature of this two-tier texture is determined by the interplay between the relaxation of the long-range orientation and the formation of the fine nematic texture.

The flow-induced large-scale textures are investigated by optical and scanning electron microscopy and light diffraction. We found that on a large-scale, molecular arrangement similar to vector fields around disclinations in ordinary nematics, is created due to superposition of radial flow fields. On a fine scale, there are several stages of relaxation of the internal nematic substructure from the highly oriented state; first, a banding appears due to periodic variations of the local director along the long-range orientation, subsequently relaxing gradually to a polydomain texture. We show how the interaction of these two processes on the long and fine scales is responsible for the range of complex textures.

In the third report we show how banding can arise in nematic polymers (specifically thermotropic co-polyethers) spontaneously ***without*** previous orientational treatment, when passing through the nematic-crystal transition, and suggest another possible mechanism leading to its formation. This arises on crystallisation of sufficiently enlarged domains. We propose that the effect is connected with non-uniform volume changes within the crystallising material which may cause buckling of the directionally constrained polymer. In general, this draws attention to the role of volume changes and to that of excess free volume in particular as a source or contributing factor to band formation in the nematic polymers. We also utilise transmission electron microscopy (TEM) to reveal the morphology of the bands after crystallisation of the material and investigate the relationship between crystal morphology and pre-existing band structure.

The last report highlights the nature of the banding texture itself. We use optical, electron and atomic force microscopy (AFM) to try to resolve the long standing question of the morphology of the bands. For this work we have again investigated thermotropic co-polyethers, hydroxypropylcellulose (HPC) and poly(p-phenylene-benz-bis-thiozole) (PBZT). In particular the use of AFM for the first time to investigate banded textures reveals much new information, and provides strong evidence that in at least the latter two systems the director varies sinusoidally with an out of plane component, possibly a helical arrangement. This raises many issues as to the origin of the underlying mechanism, since it is not clear that such an arrangement would minimise splay, thought to be the main criterion driving the banding.

LARGE SCALE TEXTURES IN NEMATIC POLYETHERS: 1. NEW ASPECTS OF FORMATION+

Hoff M., Keller A., Odell J.A., Percec V.**

University of Bristol, Department of Physics, Royal Fort, Tyndall Avenue, Bristol BS8 1TL, United Kingdom

ABSTRACT: It has been shown previously[1] that nematic polyethers can form large-scale textures, similar to low molecular weight nematic *schlieren* textures but on a scale up to hundreds of microns. Here we demonstrate that their origin is sporadic flow-induced orientation arising due to external strain fields in the isotropic state. Such circumstances may arise during usual sample handling giving rise to effects which are similar to those characteristic of nematic orientation textures but on a larger scale, overlaying the effects intrinsic to the liquid crystal nature. Accordingly, we have a two-tier structure hierarchy, a large-scale one due to external orientation and one within on a finer scale, due to the intrinsic nematicity where the latter conforms geometrically to the former. The recognition of this situation is essential for interpretation of the polarizing optical images in samples which display these features. The effect of molecular weight is also described in terms of chain mobility during relaxation from flow orientation.

INTRODUCTION

In a previous study [1] formation of unusually large birefringent textures in nematogenic polymers has been reported. These textures were found to originate from sporadic flow orientation in the isotropic state. The present study, in two parts, is a resumption of the previous work clarifying and partially amending it. We believe that the presented results are of general interest for liquid crystalline polymers, particularly in revealing textures which may arise as a result of melt processing.

Experimental observations are reviewed in a manner to show the following:

In a liquid crystalline polymer, optical textures are formed to exist on two scales:

1. Large-scale textures (hundreds of microns) induced by multiaxial flow fields in the isotropic state, imposing overlying orientational order over the nematic order on subsequent cooling.

+ *Mol.Cryst.Liq.Cryst.*, **241**, 221 (1994)

**Department of Macromolecular Science, Case Western Reserve University, Cleveland, OH 44106-2699, USA

2. Fine-scale texture (a few microns) intrinsic to nematic molecular order, these must conform to the above overlying flow-induced order creating interesting textures.

In the present paper (Part I) we distinguish between the two separate effects within their overall combination and describe the finding of the conditions which lead to formation of either one. In Part II we shall pursue the structural analysis of the compounded large and fine-scale texture in their various combinations, in the light of the recognitions reported in this part.

Characterization of the two-level hierarchy is an instructive exercise in analysing polarizing optical effects, deserving a record, particularly as it is applicable to other situations and systems where similar effects may arise.

EXPERIMENTAL

The materials used were random copolymers of mesogenic _-methylstilbene and flexible alkyl spacers linked through an ether oxygen with 5 or 7 methylene units in the 1:1 ratio[3] (Figure 1, further referred to as PHMS). The experiments were performed on grades with various molecular weights having different phase transition temperatures. The respective data are summarized in Table 1; T_{NI} and T_{NC} are the nematic-isotropic and nematic-crystalline transitions, respectively, and were taken as onset peak temperatures from DSC traces recorded at heating and cooling rates of 10°C/min. The molecular weights were measured by GPC.

Toluene-cast films with thickness in the range of 5-100 μm were sandwiched between two glass coverslips. Further preparative procedures were carried out either on the Kofler hot bench or in the Mettler FP82 hot stage. All observations were made in a Zeiss Ultraphot II polarizing microscope between crossed polars. Experimental observations *in situ* were made in a Metüler hot stage. Quenched specimens were prepared on the hot bench.

RESULTS AND DISCUSSION

Formation of large-scale textures

Large-scale textures (Figure 2) first appeared accidentally and were further obtained purposefully[1]. They were found to arise along a variety of experimental routes. The essentials are as follows.

Liquid crystalline polymers are highly orientable even while in the isotropic state. Any accidental flow, as created by, e.g., combined sliding and pressing of a coverslip onto a sandwiched liquid layer (common in microscopy) can produce complex orientation resulting in correspondingly complex birefringent patterns (the "large-scale texture"). When pressure and/or shear ceases the orientation will decay in time. If at the same time the sample is being cooled, the strained and relaxing polymer will pass through the isotropic-nematic transition. The flow-induced order may persist in the nematic region if a sufficiently fast cooling rate (quenching) has been applied, or fully relax before the transition has been reached at slow cooling.

In the first case the isotropic-nematic transition will develop a new fine scale texture. This, however, does not affect the overall appearance of the overlying large-scale pattern as seen between crossed polarisers at low magnification. Orientational order on both levels can be preserved on further cooling into the crystalline (or, alternatively, glassy) state which will freeze in the preexisting birefringent pattern without creating new features of its own at least on the scale of the polarizing microscope.

In the second case, i.e., when the flow-induced orientation has been allowed to relax before reaching the nematic region, the characteristic randomized polydomain texture appears without any trace of the previous large-scale order. This is contrary to ref.1, where a reappearance of large scale textures was erroneously interpreted as if the isotropic-nematic transition itself "developed" a latent image of the preexisting large scale texture. This inference was based on failing to recognize another factor to which we shall now turn.

Stresses arising in the sample after cessation of compression applied to the coverslip will give rise to a radial shrinkage of the still fluid polymer film, initially thinned down by the compression (Figure 3). The shrinkage then creates its own strain field and the corresponding large-scale birefringent pattern. The decompression effect (Figure 3d) can take place either after the orientation due to the primary compression (Figure 3b) has relaxed(*) (Figure 3c) or before; in the latter case, the compression and decompression effects will compound and give rise to large-scale texture as well. Unrecognized this effect could give rise to serious misinterpretations, hence our justification for looking into the matter in some length.

To illustrate this Figure 4 shows a circularly symmetrical strain pattern which arises under compression by a sharp tip while in the isotropic state. The pattern with Maltese cross brushes coinciding with the directions of the polarisers. Obviously, squeezing of the coverslips causes the melt to flow out from the pressure centre as demonstrated in Figure 3b. This gives rise to local orientation (compression-induced

(*)This case must have pertained in ref. 1

flow). The largest polarizibility was radial, i.e., birefringence of the pattern was positive in terms of spherulite nomenclature(*).

Figure 4 represents the simplest strain pattern in a real situation. However, in most cases the compression is not centred on a single point and also the coverslips can slip past each other causing the polymer to shear. Such a complex procedure then will bring about a multiaxial, multicentered diverging (or converging) flow field, generating the typical large-scale textures which originally attracted our attention in ref. 1. If these patterns are allowed to decay, still under compression, they may reappear, as stated in the foregoing, on subsequent decompression. This is often accompanied by bubble formation (Figure 3d) and leads to textures such as in Figure 5. The bubbles may act as local centres of the reverse flow during uneven shrinkage.

The large scale textures are a striking manifestation of high orientability of liquid crystalline polymers even in the isotropic state. Moreover, the orientation patterns correspond to vector flow fields which, just like the director fields intrinsic to liquid crystallinity, display their own disclinations on the correspondingly larger scale. In ref. 1 some of these patterns were already classified in accordance with the Frank notation[4]. Further analysis will be provided in Part II.

Fine-scale texture and its relation to the large-scale texture

As already indicated, as soon as a sample has passed into the nematic region, the true fine nematic texture develops within the large-scale orientation, creating a two-tier structure with corresponding long and short-range order. The two are not independent; the nematic arrangement must conform to the preexisting flow-induced order and the appearance of the large-scale effects (e.g., the dark brushes) is influenced by their substructure, this will be discussed in Part II.

Figures 6 and 7 provide examples of the two-tier hierarchy, large dark brushes and fine nematic striations and mottles are apparent.

Figures 6 a and b show the effect of relaxation on the large scale when a sample is held in the nematic region. The existing flow-induced orientation gradually decays (the dark brushes fade) while the fine nematic texture becomes more apparent. We can now explain retrospectively the "grainy" background described in ref. 1: namely, it corresponds to a texture of genuine nematic nature formed at an advanced stage of relaxation of the strain field created previously in the isotropic state.

(*)In terms of molecules, positive birefringence normally indicates radial molecular orientation. Although large polarizibility across the chain can produce positive spherulites even with tangential chain arrangement (e.g. Nylons), with radial flow the presumption of radial chain orientation seems justified.

Figure 7 shows an example of textures within a bubble interior. The accidental presence of bubbles was found useful for studying the effect of film thickness on relaxation of the long-range order; it is immediately apparent that decay of the large-scale orientation is much slower in the thinner film within the bubble (the brushes in surrounding regions decay much faster). This may be due to higher chain mobility in the thicker film compared to the thin parts[5].

The effect of molecular weight

The phenomenon of large scale texture formation was observed with each of the grades summarized in table 1, irrespective of their molecular weight. Even the lowest molecular-weight grade employed (PHMS1) having only a few repeating units per chain, was found to form large scale textures using the above procedure. However, the long-range order could not be successfully preserved at room temperature because of the low T_{NC} of this oligomer. As relaxation is generally faster with lower molecular-weight polymers preservation of textures in these materials requires higher quenching rates.

It follows from the above that the ability of polymers to form large scale textures is not confined to the highest molecular weights as reported in ref. 1 (Figure 11). All molecular weights can give it but the time scale of the treatment sequence, such as in Figure 3, must be shorter for the lower molecular weights. This of course means that the effects in question will be more readily observable for high molecular weight material in accord with ref. 1.

CONCLUSIONS

In summary, the large-scale textures result from multiaxial strain fields in the isotropic state, frozen in by crystallization or vitrification. The strain fields may arise through both compression and subsequent decompression during the usual sample preparation. These considerations are generally applicable to all orientable materials and apply particularly to liquid crystalline polymers because of their ready orientability even in the isotropic state. These effects may be the source of serious misinterpretations and are of relevance to structures arising during processing.

The fine substructure arises due to nematic self-ordering within the large-scale texture to which it conforms geometrically. The precise nature of this two-tier texture is determined by the interplay between the relaxation of the long-range orientation and the formation of the fine nematic texture.

The formation of the large scale textures was not found to be molecular weight limited.

ACKNOWLEDGEMENTS

Sponsorship of this work by the US Army European office, London (Grant N° DAJA 45-89-C-0021) is gratefully acknowledged. The authors wish to thank Dr. J.L. Feijoo, Simon Bolivar University, Caracas for useful discussions on this study.

REFERENCES

1. Feijoo JL, Ungar G, Keller A, Odell JA, Owen AJ, Percec V, Mol. C iq. Cryst. 196, 1 (1991)
2. Donald AM, Viney C, Windle AH, Polymer 24, 155 (1983)
3. Shaffer T, Percec V, Makromol. Chem. Rapid Commun. 6, 97 (1985)
4. Frank FC, Farad. Discuss. Chem. Soc. 25, 19 (1958)
5. Kwiatkowski M, Hinrichsen G, J. Mater. Sci. 25, 1548 (1990)

Table 1: Molecular parameters and phase transition temperatures of the polymer PHMS 5/7.

Grade	M_w	M_w/M_n	T_{NI}[°C]	T_{NC}[°C]
PHMS1	1980	1.1	62.8	16.2
PHMS2	16000	2.1	134.5	57.6
PHMS3	24400	2.3	158.1	76.2
PHMS4	31600	2.6	158.8	72.2
PHMS5	51800	2.9	159.8	68.0

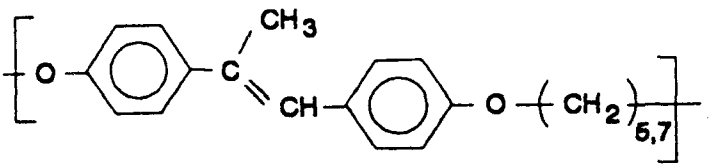

FIGURE 1 Chemical formula of PHMS 5/7.

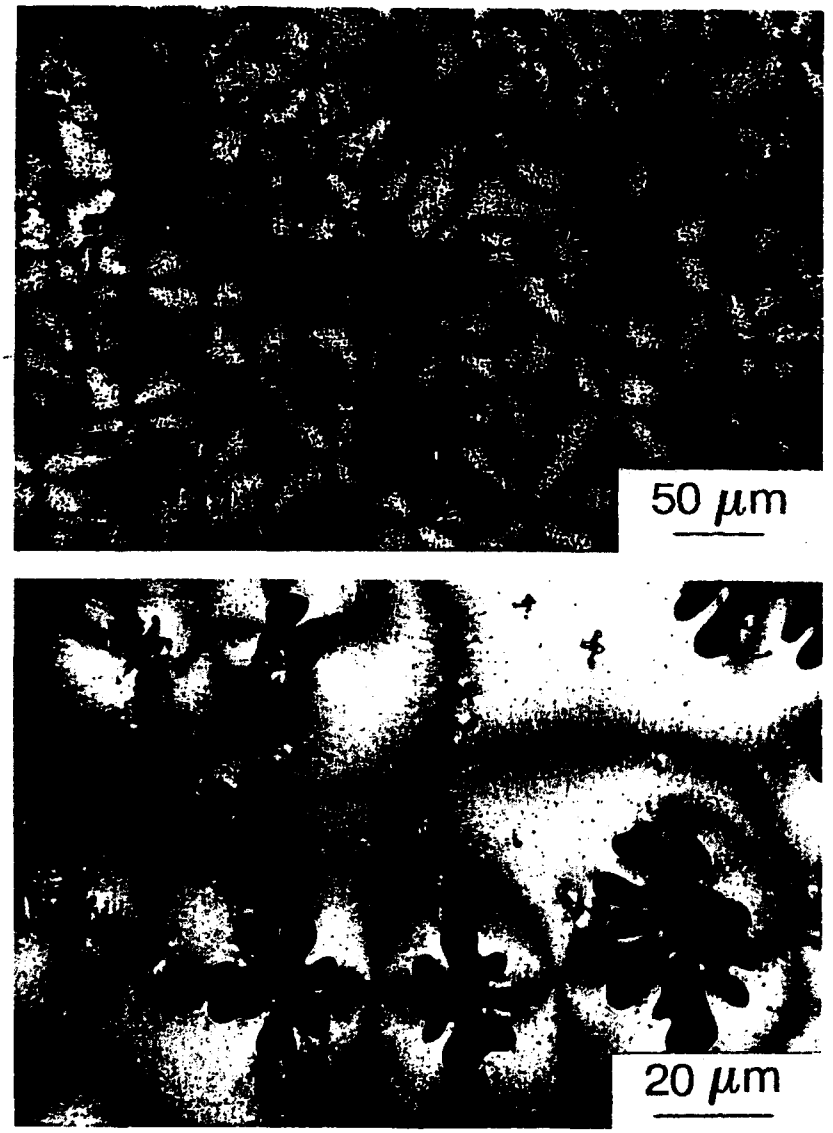

FIGURE 2 Typical examples of large scale textures showing a variety of disclinations in PHMS5 as seen in the polarizing microscope between crossed polars.

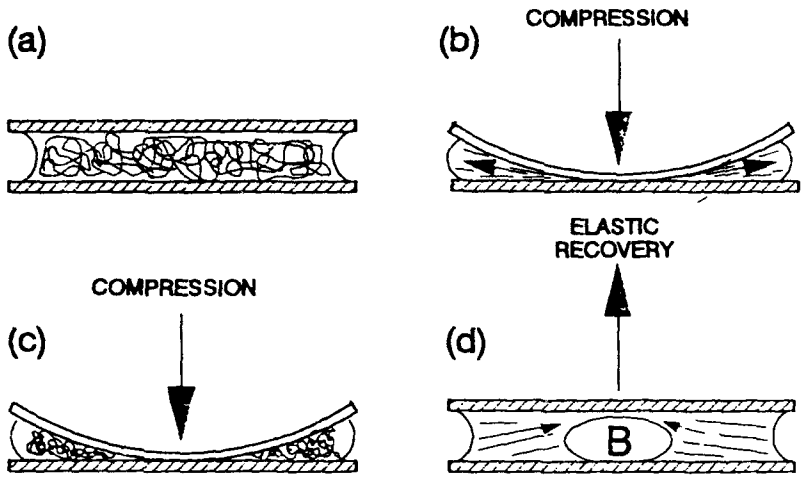

FIGURE 3 Scheme of single stages of the experimental procedure: (a) before compression in the isotropic state, (b) after compression (polymer oriented by flow directed radially out of the pressure centre), (c) under compression (stretched chains relax) and (d) after pressure removal (polymer re-oriented by flow directed radially back to the centre). Arrows inside the film show the direction of flow, B denotes possible formation of vacuum bubbles.

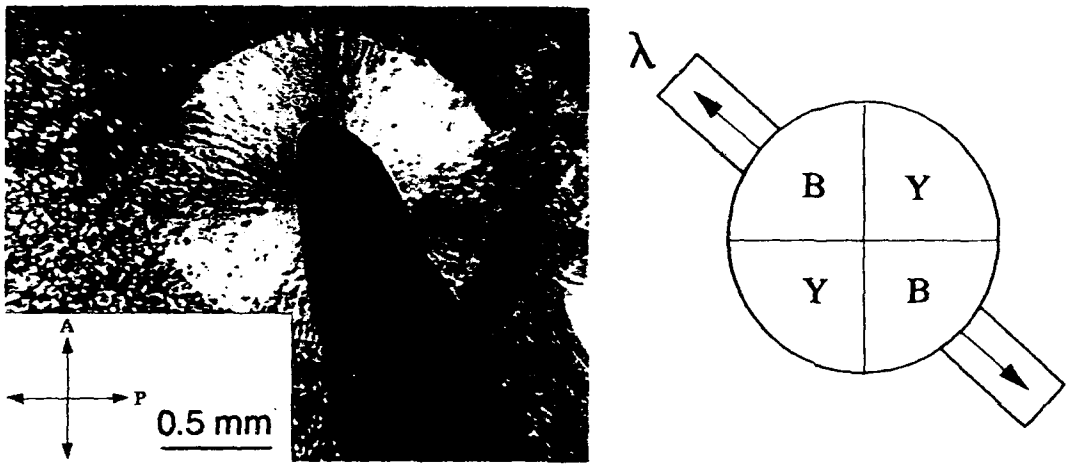

FIGURE 4 Circular Maltese cross pattern in PHMS 5 under compression by a sharp tip in the isotropic state. Optical micrograph between crossed polars (left) and a scheme showing colours (B—blue, Y—yellow) in separate quadrants with a unit wavelength retardation plate inserted (right). Flow direction radial from the centre of the cross.

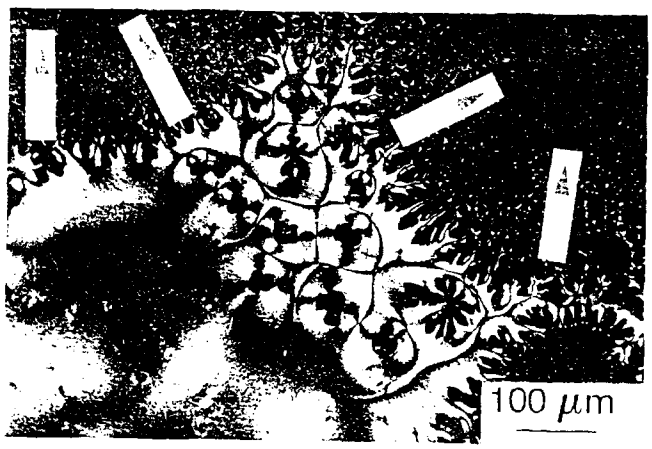

FIGURE 5 Low magnification optical micrograph of a quenched sample showing centre point of expansion. Arrows denote average directions of flow after pressure removal. PHMS content 40% by weight.

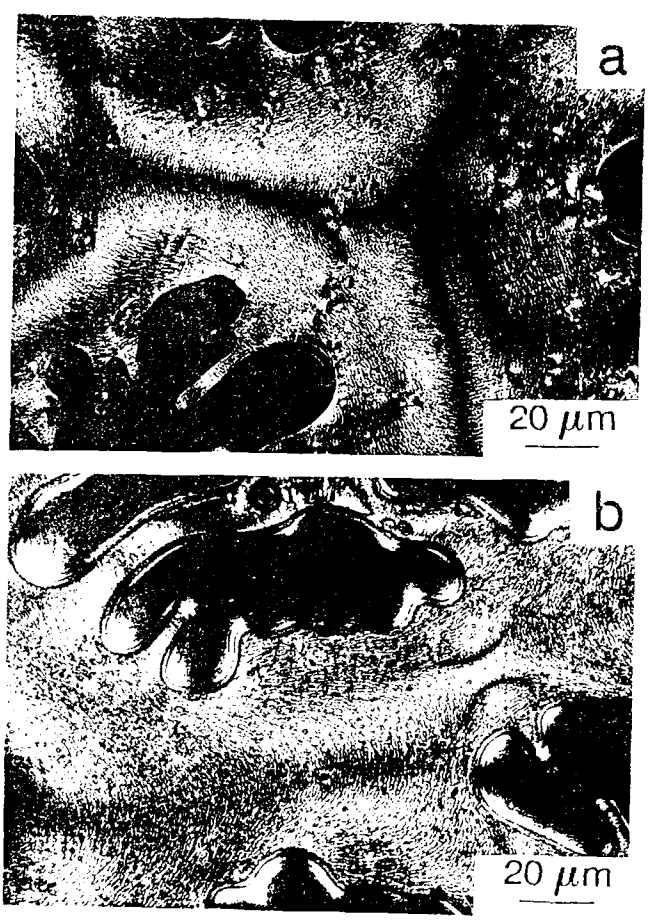

FIGURE 6 Details of extinction brushes due to relaxation in the nematic state. Holding time 15 s, quenched into ice/brine.

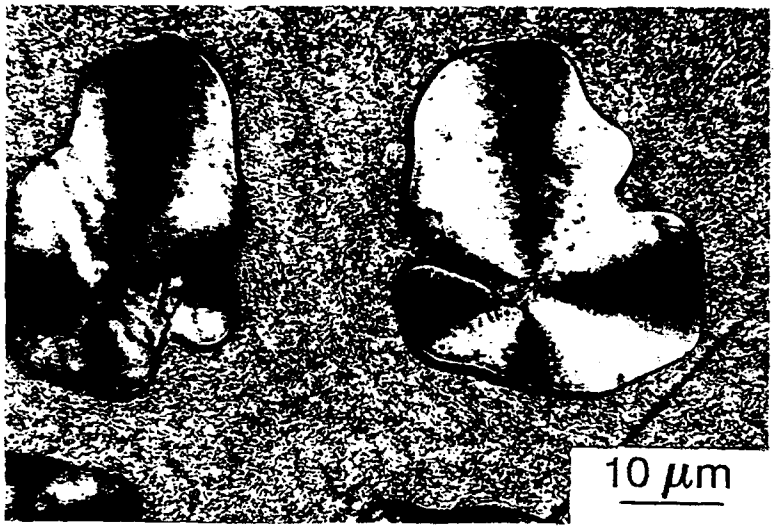

FIGURE 7 Examples of bubbles showing slower relaxation in thinner film within bubble interior

LARGE SCALE TEXTURES IN NEMATIC POLYETHERS: 2. NEW ASPECTS OF ORIENTATIONAL ORDER AND STRUCTURE HIERARCHY

+

Hoff M., Keller A., Odell J.A., Percec V.**

University of Bristol, Department of Physics, Royal Fort, Tyndall Avenue, Bristol BS8 1TL, United Kingdom

ABSTRACT: The flow-induced large-scale textures arising in thermotropic nematic polymers presented in Part I of this study have been further explored. Optical and scanning electron microscopy and light diffraction are employed to interpret the nature of these textures. It was found that on a large-scale, molecular arrangement similar to vector fields around disclinations in ordinary nematics, is created due to superposition of radial flow fields. On a fine scale, there are several stages of relaxation of the internal nematic substructure from the highly oriented state; first, a banding appears due to periodic variations of the local director along the long-range orientation, subsequently relaxing gradually to a polydomain texture. It is shown that interaction of these two processes on the long and fine scales is responsible for the range of complex textures. Once recognized for what they are, these textures can be interpreted without misconceptions, which may otherwise arise due to actual simplification of the polarizing optical analysis.

INTRODUCTION

Thin films of thermotropic nematic polyethers have been shown to form large-scale textures[1,2] induced by flow in the isotropic state and having dimensions as large as 1 mm or more. Between crossed polarisers, they show features typical of the disclinations in nematic *Schlieren* textures; the molecular director fields can be described in terms of their strength[3]. Formation of these textures appears to be a common feature for thermotropic nematic polymers[2].

In our previous studies, coexistence of a long-range orientational order due to the sporadic multidirectional flow in the isotropic state and a finer substructure (short-range orientational order) due to self-ordering in the nematic region has been reported[1,2]. The latter was found to conform to the long-range orientation. The interaction between the large and fine scale structures will be the main subject of this

+ *Mol.Cryst.Liq.Cryst.*, **241**, 231 (1994)

**Department of Macromolecular Science, Case Western Reserve University, Cleveland, OH 44106-2699, USA

study. As we shall see, such structures may be important arising in typical processing conditions. Recognition of the cause of such textures should help to avoid possible misinterpretations of molecular behaviour of liquid crystal polymers on orientation, relaxation and their relation to phase transformations.

EXPERIMENTAL

The materials used were random copolymers of _-methylstilbene and methylene spacers, identical to those in the first part of this study[2]. Therein, chemical structure, molecular weights and transition temperatures of these polymers were summarized and so were sample preparation and experimental procedure leading to large scale texture formation.

Optical analysis of the textures was conducted on samples quenched to room temperature placed on the Zeiss Ultraphot II polarizing microscope. Light diffraction patterns were obtained by inserting a Bertrand lens into the optical path.

To prepare samples for scanning electron microscopy, the glass coverslips from melt-processed samples were first removed by repeated quick cooling of specimens in liquid nitrogen and their subsequent heating to room temperature. The polymer surface was then etched using permanganic method pioneered by Olley and Basset[4]; the samples were immersed in the mixture $H_2SO_4/H_3PO_4/KMnO_4/H_2O$ (compounded in the ratio 13/5/15/40 mg) for 10 minutes, successively rinsed in diluted H_2SO_4, 30% H_2O_2 and H_2O and dried with acetone. Finally, they were coated with aluminium and studied in the scanning electron microscope JEOL 840.

RESULTS AND DISCUSSION

The results described in this section were mostly obtained on a polymer with M_W=51,800 (PHMS 5, see table 1 in Part I of this study[2]) with a few experiments done also on lower molecular weights.

Long-range orientational order

In Figure 1a, an image of the S_{+1} texture(*) between crossed polars is shown with positive birefringence in terms of spherulite nomenclature (Figure 1b). Highest

(*)To describe symmetry of the large-scale textures, we used the customary notation of disclination strength determined by a common test on rotation direction of the extinction brushes with respect to

polarizibility in the radial direction, coinciding in our case with the flow direction, implies also radial molecular orientation.

The same analysis of the S_{-1} textures (Figure 2) proved their characteristic symmetry; on rotation, the sign of birefringence changed every 45 deg (Figure 2b-d). This reflects the corresponding alteration of tangential and radial orientations around an S_{-1} disclination as manifested by the colour changes with a first-order red plate inserted into the light path.

Analogous to nematic textures, large-scale textures of +1/2 and -1/2 strength were also observed (cf ref. 1) and textures of opposite signs were found to combine sharing one extinction brush (Figure 3).

Short-range orientational order

The nature of short-range order in the underlying fine subtexture (arising in the nematic state) was found to depend on the molecular weight and on the time of holding the polymer in the nematic state before its solidification by further cooling(2). Both dependences reflect the degree of relaxation from the initial oriented state (to be discussed further below).

Low orientation - "grainy" structure

As already stated(1) the basic elements of the fine substructure are intrinsic to the nematic structure. When no previous flow-induced long-range orientation has been locked in, or it has fully relaxed, only the usual grainy nematic texture is seen. When the long-range order has almost relaxed the grains appear superposed on the remnants of the long-range arrangement; large-scale extinction brushes become apparent in addition to the fine structure (Figure 4).

The latter case just corresponds to an advanced stage of relaxation when the fine structure takes on the seemingly random grain appearance. However, the extinction brushes demonstrate that there remains a certain anisotropy which, averaged over a local area, coincides with the long-range orientation. Obviously, the local director conforms to the overlying order.

High orientation

Anisotropy at the early stages of relaxation of the long-range order is much higher and even the short-range director largely coincides with the long-range orientation. Therefore, no fine structure is visible (Figure 2, bottom, in ref. 2) except

---

rotated polarizers, even though molecular origin of these textures is external preorientation rather than dislocation.

perhaps within the extinction brushes themselves where even the minutest deviation of the local director from the long-range orientation becomes noticeable; any departure within a dark brush leads to localized light transmission which is sensitively detectable.

Intermediate orientation - banded structure

The most characteristic feature of the intermediate stage of relaxation in the nematic state, is a fine banded structure (Figure 5). Periodic banding is a familiar effect in uniaxially oriented sheared nematic systems, where it appears after cessation of the external orienting influence as a consequence of relaxation from the oriented state. It corresponds to a short-range periodic orientation variation[e.g.,5,6] the origin of which is not fully understood and is currently the subject of intensive attention. Here we maintain that the presently observed banding is basically an identical effect where the banding has conformed to the local orientation produced by preceding flow in the isotropic state. It corresponds to a short-range periodic orientation variation with respect to the long-range orientation. The bands are more or less orthogonal to the long-range director and help to define the vector field of the large-scale texture (see Figure 3).

To illustrate graphically the combined effect of banding and large-scale texture, we select from the various large-scale patterns the S_{+1} director field with circular symmetry (the left side of Figure 3a and Figure 5a). Once understood this treatment can be readily extended to other symmetry patterns.

Figure 6 shows schematic patterns of the extinction lines in the case of spherical symmetry (such as S_{+1}) for hypothetical sinusoidal orientation variation of the short-range director with 3 successively increasing angles _ (corresponding to the deviation of the short-range director from the long-range orientation). The explicit shape of these patterns depends on the geometry of the periodicity (zigzag, sinusoidal or any other director trajectory, to be dealt with in a separate study) but an overall feature is common to them all: the shape of the extinction lines reflects the underlying arrangement of the short-range director. Specifically, the radial distance between the extremities of the zigzag extinction line corresponds to the full period of the periodically varying orientation path of the short-range director, while the azimuthal spread of the extinction lines within an extinction brush (2_) corresponds to the maximum deviation (_) of the short-range director from the radius (long-range orientation). It is further apparent that at azimuths larger than _ there is no extinction and the underlying periodicity remains between crossed polarisers invisible. In a real

low resolution image, the extinction lines, where visible, will merge into a simple extinction cross.(*)

Extension of the above to the S_{-1} disclination long-range field will now be evident and will not be separately examined here. An example of it showing the underlying extinction lines at high resolution is given by Figure 7. The fine lines create a zigzag pattern just as for the S=+1, however, the curvature of the lines in S_{-1} field is convex (as opposed to concentric with S_{+1} symmetry) with respect to the centre.

The presence of periodic banding was further examined by optical diffraction in the microscope. Diffraction patterns provide a representative quantitative measure of the structure already recognized in real space, namely, banding gives rise to V_H diffraction maxima which are equatorially placed with respect to the appropriate radial direction[5,6]. In our case, this is illustrated by Figure 5 where different areas in the S_{+1} and S_{-1} textures were selected for diffraction. As seen, the light diffraction maxima occur along azimuths perpendicular to the radii and change orientation accordingly when moving from one selected area to another. The spacing derived from the angular position of the maxima were between 0.5 - 1.3 μm, in good agreement with direct measurement on the image.

The above defined orientation in the diffraction pattern, however, is seen to deteriorate towards the centre of the large-scale texture and gradually change into the mottled structure at its centre. Here the diffraction pattern has four intensity maxima (not easily discernible due to closeness to the central beam) along both equator and meridian, typical of the usual unoriented nematic polydomain structure[8,9]. Detailed analysis of the light scattering patterns is beyond the scope of this study and will be given elsewhere.

Scanning electron micrographs of etched surfaces revealed features which correlate with the polarizing optical image. Figure 8 shows an area containing S_{+1} and S_{-1} large-scale disclinations containing corresponding concentric and convex banding with a spacing of approximately 1 - 2 μm. Thus, the quenched polymer must contain structural elements resistant to etching (probably crystallites), an inference which follows from similar observations reported elsewhere[6,11,12].

Higher magnification revealed a fine structure within the bands (Figure 9). Even if there is considerable irregularity, the 1-2 μm vertical banding is recognizable,

---

(*)Zigzag extinction lines, in place of uniform Maltese extinction crosses, have been described previously by one of us in some polymer crystal spherulites [7] and interpreted in the same way as presented here. From the point of view of polarizing optics the two systems, namely the present liquid crystals and the crystalline spherulites are identical as both conform to the same geometry on the scale in question. However, the two systems are intrinsically different; the spherulites are the products of crystal growth, while the liquid crystalline system is a continuum under the constraints arising during various stages of relaxation.

with a zigzag fibrous substructure of about 0.1 μm, perpendicular to the banding. It may appear tempting to associate these zigzag fibrils with the short range director trajectory. However, such correspondence has not proved satisfactory: the angle between the fine striations and the banding, itself perpendicular to the long-range orientation, is far to small and is closer to the complement of the angle to be expected if the fine striations represented the short-range director. It is suggested therefore that we are seeing crystal lamellae which, as known, can be perpendicular to it[10] The actual relation between the fine crystal structure and the liquid crystal banding will be further discussed elsewhere. At this stage, we shall not pursue this issue further, beyond stating that the morphological equivalents for the optically visible structure have been identified on both large and fine scale.

Hydrodynamic origin of large-scale texture formation

In the light of the above analysis of structure hierarchy in the large-scale textures, we can now discuss their origin on a more general hydrodynamic basis.

We have already shown that the appearance of the overall texture reflects the multidirectionality of the flow before quenching; it is justifiable to assume that the long-range orientation follows the flow directions. More or less pronounced symmetry within the large-scale disclinations indicates that there also must have been some analogous symmetrical flow fields present in the isotropic state. Based on the optical orientation analysis (Figures 1,2) and banding arrangement (Figure 5) of the S_{+1} and S_{-1} textures, we can now show what is the Hydrodynamic origin of such symmetries. In Figure 3b, the arrangement of banding in the textures from Figure 3a is schematically illustrated. The lines in Figure 3c perpendicular to the bands represent the long-range director field and, consequently, the streamlines of the frozen flow field. The radial and fourfold symmetry of the flow field in S_{+1} and S_{-1} texture, respectively, is seen.

The S_{+1} radially symmetrical field represents what is called, in terms of hydrodynamics, sink flow, in the centre of which the fluid velocity during a flow process remains zero.

The combination of two such flow sinks with radial symmetry can then produce a hyperbolic flow field in the centre of which there is also a singularity with zero fluid velocity. This kind of flow field analogous to that realizable in polymer melts and solutions in a four-roll mill or between two opposed sucking jets[13,14], is in our case represented by the S_{-1} textures.

If the flow was dominated by the shear component (rather than the extensional component) the low fluid velocity around the flow singularities would be

accompanied by little preferential long-range orientation. This would account for the presence of macroscopically random grain structure and associated non-anisotropic light diffraction (Figure 5) in the centres of the symmetrical textures as discussed above.

CONCLUSIONS

The origin of the large-scale director fields similar to those intrinsic to the nematic textures is due to combinations of flow fields of different kinds present in the isotropic state.

The underlying fine structure formed in the nematic state reflects consecutive stages of relaxation from the highly oriented to the random nematic state. At each stage the fine structure conforms with the overlying long-range order in a rational, analysable fashion. This recognition, beside leading to the more correct interpretation of complex effects, also simplifies the optical analysis of banded structures in liquid crystals: namely in a circular symmetrical arrangement of the large-scale director we have all orientations of the orienting field with respect to the polarizers simultaneously present. This obviates the need of step-by-step stage rotation as needed for the analysis of uniaxially oriented specimens, by providing an image of the overall extinction features.

ACKNOWLEDGEMENTS

Sponsorship of this work by the US Army European Office, London (grant No DAJA 45-89-0-0021) is gratefully acknowledged. The authors wish to thank Dr. J. L. Feijoo, Simon Bolivar University, Caracas for useful discussions on this study.

REFERENCES

1. Feijoo JL, Ungar G, Keller A, Odell JA, Owen AJ, Percec V, *Mol. Cryst. Liq. Cryst.* **196**, 1 (1991)
2. Hoff M, Keller A, Odell JA, Percec V (Part I)
3. Frank FC, *Farad. Discuss. Chem. Soc.* **25,** 19 (1958)
4. Olley RH, Bassett DC, *Polym. Commun.* **23**, 1707 (1982)
5. Donald AM, Viney C, Windle AH, *Polymer* **24,** 155 (1983)

6. Liu X, Shen D, Shi L, Xu M, Zhou Q, Duan X, *Polymer,* **31**, 1894 (1990)
7. Keller A, *J. Polym. Sci.* **17**, 291 (1955)
8. Shiwaku T, Nakai A, Hasegawa H, Hashimoto T, *Macromolecules* **23**, 1590 (1990)
9. Rojstaczer SR, Stein RS, *Macromolecules* **23**, 4683 (1990)
10. Hudson SD, Thomas EL, Lenz RW, *Mol. Cryst. Liq.Cryst.* **153**, 63 (1987)
11. Bedford SE, Windle AH, *Polymer* **31**, 616 (1990)
12. Chen S, Jin Y, Hu S, Xu M, *Polym. Commun.* **28**, 208
13. Mackley MR, *J. Non-Newt. Fluid. Mech.* **4**, 111 (1978)
14. Mackley MR, Keller A, Phil. *Trans. Roy. Soc. London.*, **278**, 29 (1975)

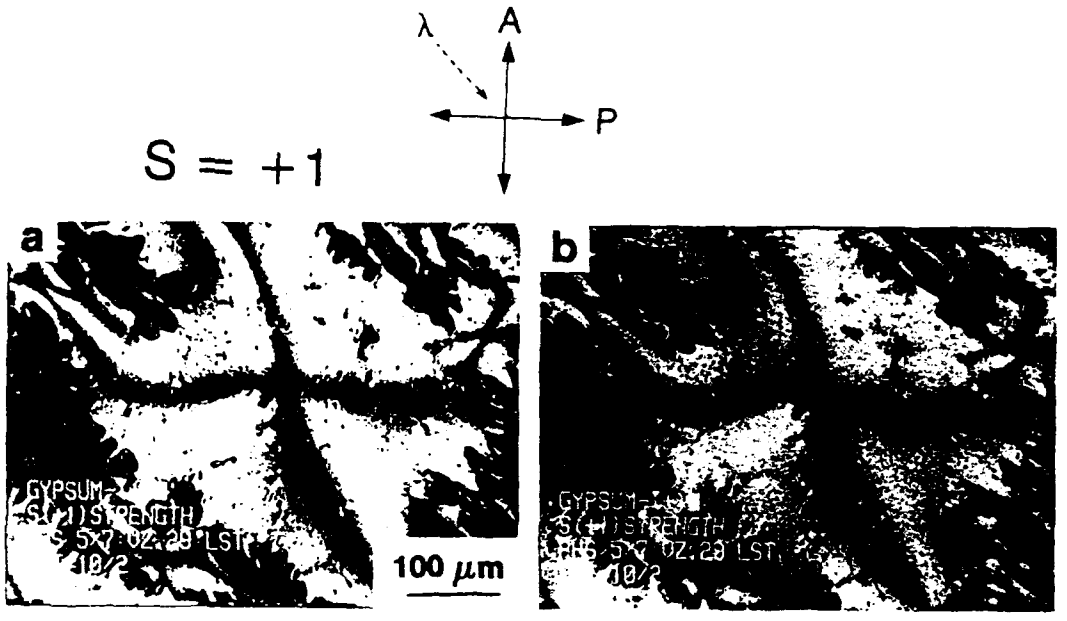

FIGURE 1 S_{+1} texture in the PHMS5 polymer (quenched) as seen between crossed polars without (a) and with a unit retardation plate (b). *A*, *P*, denote the directions of analyser, polariser and the retardation plate. See Color Plate XII.

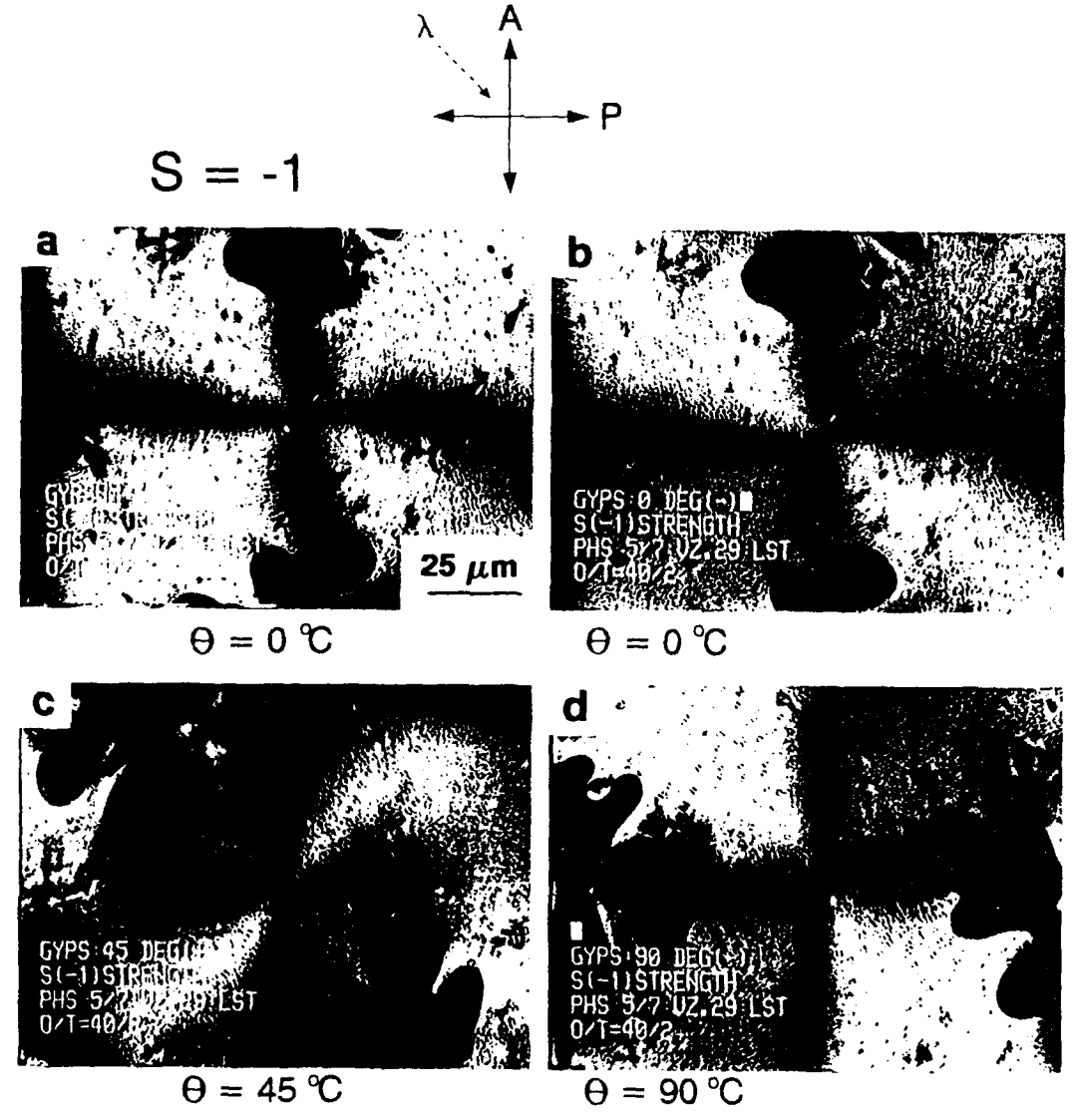

FIGURE 2 S_{-1} texture in the PHMS5 polymer (quenched) as seen between crossed polars without (a) and with a unit retardation plate at various angles of sample rotation (b, c, d). Symbols as in Figure

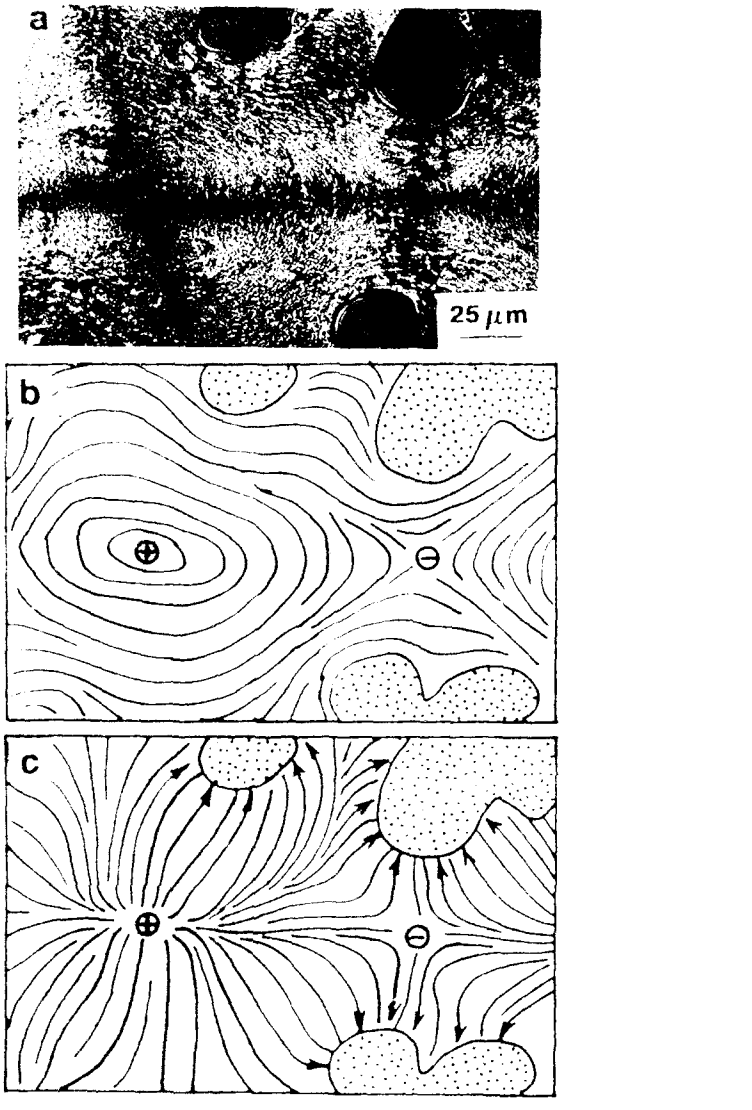
a
25 μm
b
⊕
⊖
c
⊕
⊖

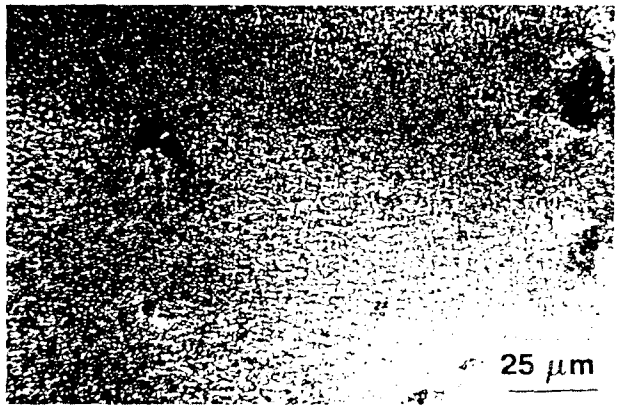
25 μm

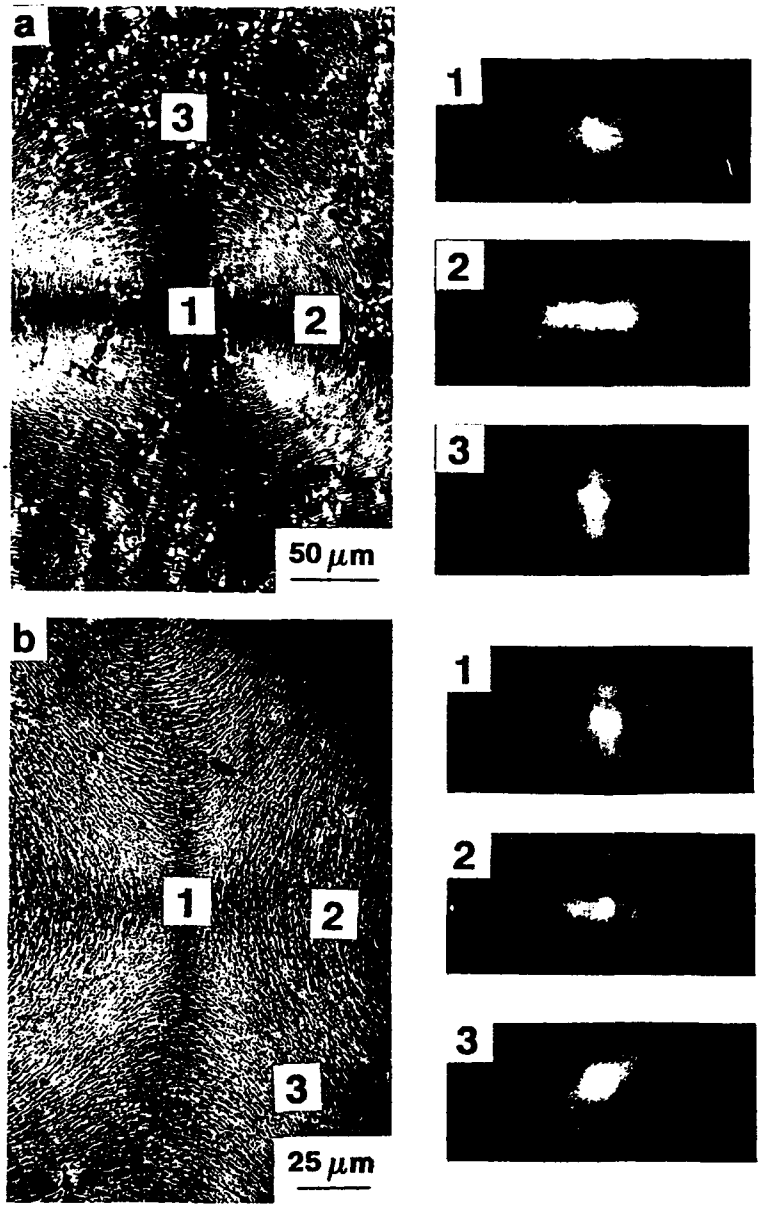

FIGURE 5 Optical micrographs of (a) S_{+1} and (b) S_{-1} textures and light diffraction patterns from particular areas. Polymer PHMS5 (quenched), diffraction in $V_{//}$ position with respect to band orientation. Crossed polars orthogonal.

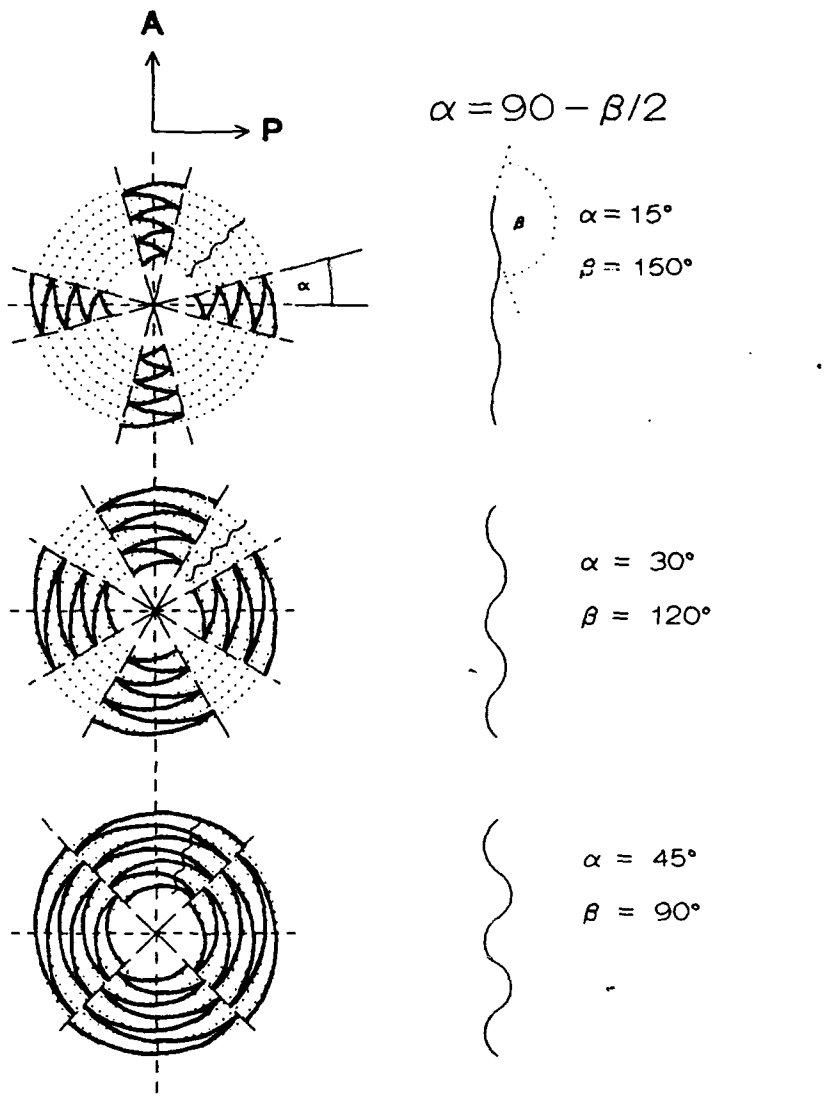

FIGURE 6 Diagram illustrating traces of minimum birefringence intensity (extinction lines, denoted by the heavy lines) in circularly symmetrical fine banding (S_{+1} texture) between crossed polars (A, P) for a sinusoidal periodicity of the director orientation. Symbols discussed in the text.

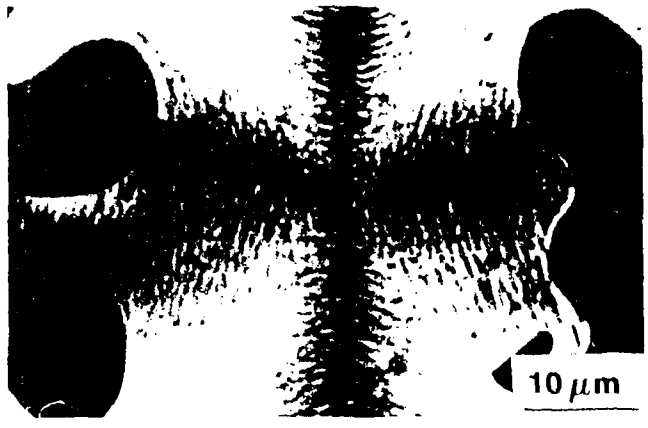

FIGURE [illegible] Zigzag type extinction lines within dark brushes of an S = texture. Optical microscope, crossed polars, polymer PHMS9 (spherulites).

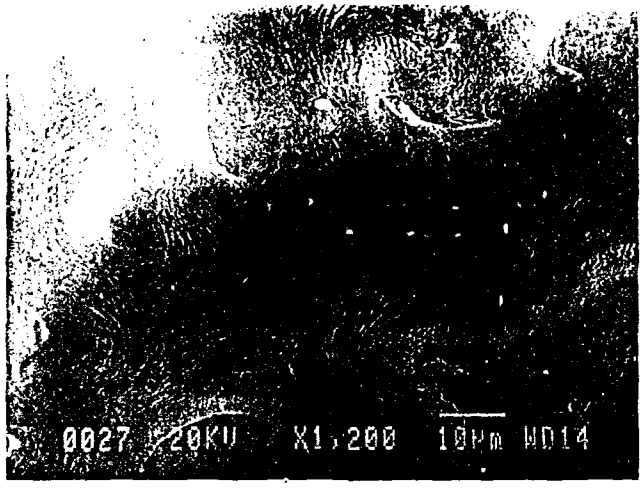

FIGURE [illegible] Scanning electron micrograph of bands in large scale textures. Polymer PHMS9 (spherulites), [illegible] and S = symmetry apparent.

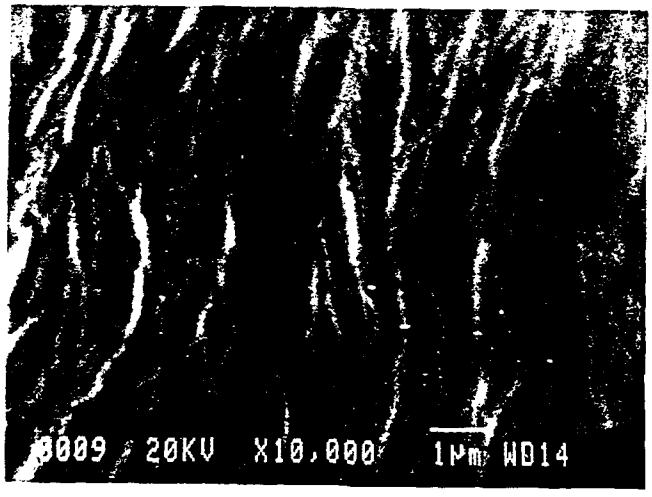

FIGURE [illegible] Zigzag lamellar arrangement in bands as seen in scanning electron microscope. Polymer PHMS[illegible]

CRYSTALLIZATION-INDUCED BAND FORMATION IN NEMATIC POLYETHERS+

M. Hoff, A. Keller, J. A. Odell, V. Percec**

University of Bristol, H.H. Wills Physics Laboratory, Tyndall Avenue, Bristol BS8 1TL, United Kingdom

SYNOPSIS

The effect of the nematic-solid phase transition on texture of both crystallizable and amorphous nematic polymers was studied using polarizing and electron microscopy and light scattering. We found that crystallization, unlike vitrification, can lead under certain conditions to formation of banding which has so far been reported only as induced by external flow. To achieve banding on crystallization, nematic domains must acquire sufficient size by previous annealing. Crystallization brings about directionally non-uniform volume changes and corresponding excess free-volume energy to which we attribute the presently observed effect.

INTRODUCTION

In the past decade close attention has been paid to banded textures formed in liquid crystalline nematic polymers during relaxation of chains previously oriented by external flow [1-4]. Although the precise mechanism of band formation has not yet been explained satisfactorily, it is generally believed that the bands, a periodical arrangement of the molecular director, form to minimize excess elastic energy of the system[2,5-8]. There are two principle sources of the elastic energy that could drive the effect[9]: the molecular elasticity due to distortion of molecules from their equilibrium arrangement and the elasticity of the texture (particularly splay). In a recent work by we observed the equivalent banding effect as due to localized orientation in strain fields which can arise unintentionally in the course of normal sample manipulation[10]. The same work also indicated a connection between the

+ *Polymer*, **34**, 1800 (1993)

**Department of Macromolecular Science, Case Western Reserve University, Cleveland, OH 44106-2699, USA

banding and the intrinsic nematic domains in the unoriented state, hence the influence of texture in addition to purely molecular features.

In this study we will show how banding can arise in nematic polymers spontaneously without previous orientational treatment, when passing through the nematic-crystal transition, and suggest another possible mechanism leading to its formation.

MATERIALS AND EXPERIMENTAL

The polymers used in this study were random aromatic copolyethers of mesogenic _-methyl stilbene and flexible alkyl spacers with 5 and 7 methylene groups in the 1:1 ratio (PHMS 5/7) and random copolyethers of mesogenic 1-(4-hydroxy-4'-bisphenyl)-2-(4-hydroxy phenyl butane) with spacers containing either 10 (TPB 10) or 14 (TPB 14) methylene units. The TPB 10 grade is amorphous, i.e. it exhibits during heating only glass-nematic (T_g) and nematic-isotropic (T_{NI}) transitions whereas PHMS 5/7 and TPB 14 are crystallizable exhibiting also a crystalline-nematic transition (T_{CN}). Chemical formulae of the polymers are shown in Figure 1, DSC heating traces obtained on the Perkin-Elmer DSC 7 instrument in Figure 2, and their molecular weights are listed in Table I. All the polymers used show pronounced shear-induced banding effect.

Thin films (10-20 μm) solvent-cast onto a coverslip were placed in the Linkam TMS 91 hot stage, annealed in the nematic state in an inert atmosphere and subsequently cooled to either the crystalline or the glassy state. *In situ* microscopic observations were carried out with a Zeiss Ultraphot polarizing microscope and light scattering patterns were obtained by inserting a Bertrand lens into the optical path.

To prepare samples for transmission electron microscopy (TEM), we used 2-stage replication from the polymer surface etched in a permanganic etchant[11]. The Pt-Pd replicas were studied in the Philips EM 301 microscope.

RESULTS

In situ observations during annealing of the polymers in the nematic state have confirmed what has already been reported elsewhere; the nematic domains grow with time up to a certain maximum size[12]. An increase in the orientation correlation length was confirmed by simultaneous recording of light scattering; the maxima in typical four-quadrant V_H patterns shifted towards smaller scattering angles, as shown

in Figure 3. The maximum domain size was found to be affected by the annealing temperature, higher temperatures, i.e. closer to T_{NI} leading to larger maximum-sized domains. This is documented in Figure 4 by a plot of the angle of the maximum scattering intensity against annealing time for TPB 10 and TPB 14. Up to this point, no substantial differences were found in the behaviour of the polymers which were crystallizable (on appropriate cooling) and those which were not.

On cooling, the crystallizable polymers were found to change their textures dramatically after passing through the nematic-crystalline transition; apparently spontaneous pronounced banding appeared within the, by now, enlarged domains. This was accompanied by the appearance of wide-angle light scattering maxima due to a much smaller band spacing (Figure 5). No spontaneous flow could be detected either during the annealing or the cooling stage. To achieve the banding effect, domains had to be sufficiently enlarged; smaller domains (shorter annealing times or lower tempeartures) led to less pronounced banding and, finally, below a certain domain size, the bands did not form at all. The same procedure applied to the amorphous TPB 10, here cooled to well below T_g (42 ^oC) did not lead to band formation; there were no changes in texture or light scattering pattern in comparison with those observed before cooling, regardless of the domain size.

The cooling rate was observed to have only little effect on band formation, but has not yet been fully evaluated. At present, we can only say that banding appears at any cooling rate investigated, i.e., in the range between quenching and 0.01 deg/min. The banding which arises at very low cooling rates does however look somewhat less pronounced (Figure 6).

The annealing temperature had an effect through its influence on the domain size; the lower the annealing temperature (increasing difference T_{NI}-T) the smaller is the domain size which is reached at a comparable annealing time (see Figure 4) and correspondingly less pronounced is the banding.

The alternation of narrow extinction lines and broader light bands (straighter in TPB 14 than in PHMS 5/7, Figure 5) indicate the same kind of periodic variation in director orientaiton as with sheared polymeric nematics[1]. For PHMS 5/7, TEM micrographs of etched samples revealed that there were two levels of supermolecular structure. In Figure 7a, overall topology is shown at a lower magnification, corresponding to the optical texture from Figure 5b; column-like domains containing smoothly packed curved structural elements (corresponding to curved bands in Figure 5b) are separated by corrugated boundaries. Higher magnification revealed a zigzag morphology within individual bands (Figure 7b, magnified area denoted in Figure 7a).

The banding itself was conspicuously revealed by electron micrographs also of the TPB 14 polymer (Figure 8a,b) where the boundaries are seen to protrude from the

surface. However, the permanganic etchant employed proved inadequate for revealing any fine structure in TPB 14 (etched and unetched samples did not show any difference in TEM). Analogously processed amorphous TPB 10 displayed no banding, exhibiting only a more or less smooth topology (Figure 8c).

DISCUSSION

The salient feature in the present observations is the appearance of a banded structure, similar to that seen in flowing or deformed systems after removal of the external orienting influence, but in this case arising apparently spontaneously, without external interference with the system. It is clear that the effect sets in only when sufficiently enlarged domains are allowed to crystaliize.

It is evident further that vitrification does not lead to the same effect as crystallization. The nematic-crystal transformation, as a thermodynamic first order transition is accompanied, unlike vitrification, by a decrease in volume. In separate domains with local anisotropy in molecular orientaion one may expect the volume change to be highly anisotropic as well. In fact, as the chains acquire closer lateral packing and better alignment in crystals, the domain will contract perpendicular to the chain direction and expand along it. As adjacent domains have different orientations within an overall randomly oriented sample, expansion will be frustrated, a situation which can then lead to periodic buckling which could be manifested as banding. Convincing precedents of such buckling under essentially equivalent circumstances have been found in polyethylene shish-kebab crystals expanding on further crystallization while embeded in a matrix[13] and in macroscopic nylon fibres surrounded by a contracting medium[14].

On a more general basis, volume changes will produce an excess free-volume energy contributing to the energies due to texture elasticity (splay, bend, twist). In the nematic continuum, the latter is localized in disclinations, the concentration of which decreases with increasing domain size[15]. In the early stages of annealing, the concentration of the disclinations will be sufficient to localize also the excess free volume created by crystallization. Distances between neighbouring disclinations are small so the net longitudinal expansion of the crystallizing chains per domain will be small, insufficient to cause buckling. Domain growth causes the disclination-to-disclination distance to increase and the net expansion per domain will then be accompanied by band formation. The relieved free volume and the respective excess free-volume energy will then remain localized at the band boundaries. As can be seen from Figure 8b, protruding material between the bands indeed indicates an excess

volume (hence lower interior density) which then squeezes out material to above the ambient sample plain, here, as seen, in a periodic manner.

It is not obvious whether factors such as above could play any part in the more usual band formation in oriented systems such as are seen to arise in the nematic state without the intervention of crystallization. Nevertheless, when crystallization is known to occur the present new phenomena will certainly need to be taken into account.

Recently, after completion of the present work, similar observations, namely of band formation on domain growth without external orienting influence, has come to our notice also from another source using a different liquid crystal forming polymers[16,17]. Hence the effect seems general. We have no information as to any attribution of this effect to crystallization (as done here by ourselves) in this parallel work.

CONCLUSIONS

A new source of banding has been discovered which does not involve external flow. This arises on crystallization of sufficiently enlarged domains. We propose that the effect is connected with non-uniform volume changes within the crystallizing material which may cause buckling of the directionally constrained polymer. In general, this draws attention to the role of volume changes and to that of excess free volume in particular as a source or contributing factor to band formation in the nematic polymers.

ACKNOWLEDGEMENT

Sponsorship by the US Army European Office, London (grant No DAJA 45-89-0-0021) is gratefully acknowledged.

REFERENCES

1. Donald A.M., Viney C., Windle A.H., *Polymer* 1983, **24**, 155

2. Horio M., Ishikawa S., Oda K., *J. Appl. Polym. Sci. Appl. Polym. Symp.* 1985, **41**, 269

3. Marruci G., Grizutti N., Buonaurio A., *Mol. Cryst. Liq. Cryst.* 1987, **153**, 263

4. Wang J., Bhattacharaya S., Labes M.M., *Macromolecules* 1991, **24**, 4942
5. Zachariades A.E., Navard P., Logan J.P., *Mol. Cryst. Liq. Cryst.* 1984, **110**, 93
6. Nishio Y., Yamane T., Takahashi T., J. *Polym. Sci. Polym. Phys.* 1985, **23**, 1053
7. Ernst B., Navard P., *Macromolecules* 1989, **22**, 1419
8. Maffettone P.L., Grizutti N., Marruci G., *Liq. Crystals* 1989, **4**, 385
9. Gleeson J.T., Larson R.G., Mead D.W., Kiss G., Cladis P.E., *Liq. Crystals* 1992, **11**, 341
10. Hoff M., Keller A, Odell J.A., Percec V., to be published in *Mol. Cryst. Liq. Cryst.*
11. Olley R.H., Bassett D.C., *Polym. Commun* 1982, **23**, 1707
12. Feijoo J.L., Ungar G., Owen A.J., Keller A., Percec V., *Mol. Cryst. Liq. Cryst.* 1988, **155**, 187
13. Grubb D.T., Keller A., *Colloid. Polym. Sci.* 1978, **256**, 218
14. Dale W.C., Baer E., *J. Mater. Sci.* 1974, **9**, 369
15. Shiwaku T., Nakai A., Hasegawa H., Hashimoto T., *Polym. Commun.* 1987, **28**, 174
16. Chen S., Qian R., China - UK Bilateral Conference on Polymer Science, April 1992, Beijing, China, Abstracts p. 18
17. Qian R., Chen S., *Makromol. Chem. Macromol. Symp.* 1992, **53**, 345

Table I: Molecular weights of the polymers TPB 10, TPB 14, and PHMS 5/7 as determined by GPC

Grade	M_w	M_n
TPB 10	62,600	31,600
TPB 14	84,000	40,800
PHMS 5/7	30,200	14,500

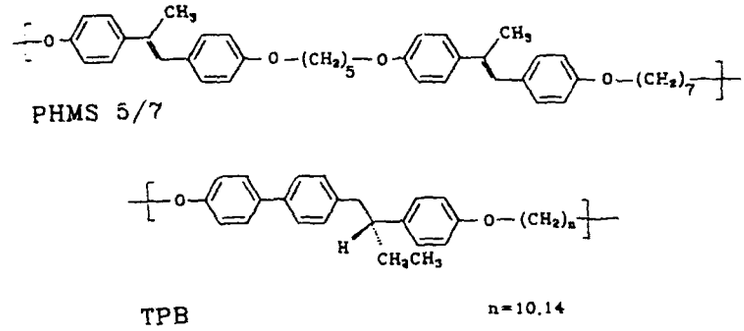

Figure 1 Chemical formulae of the polymers used

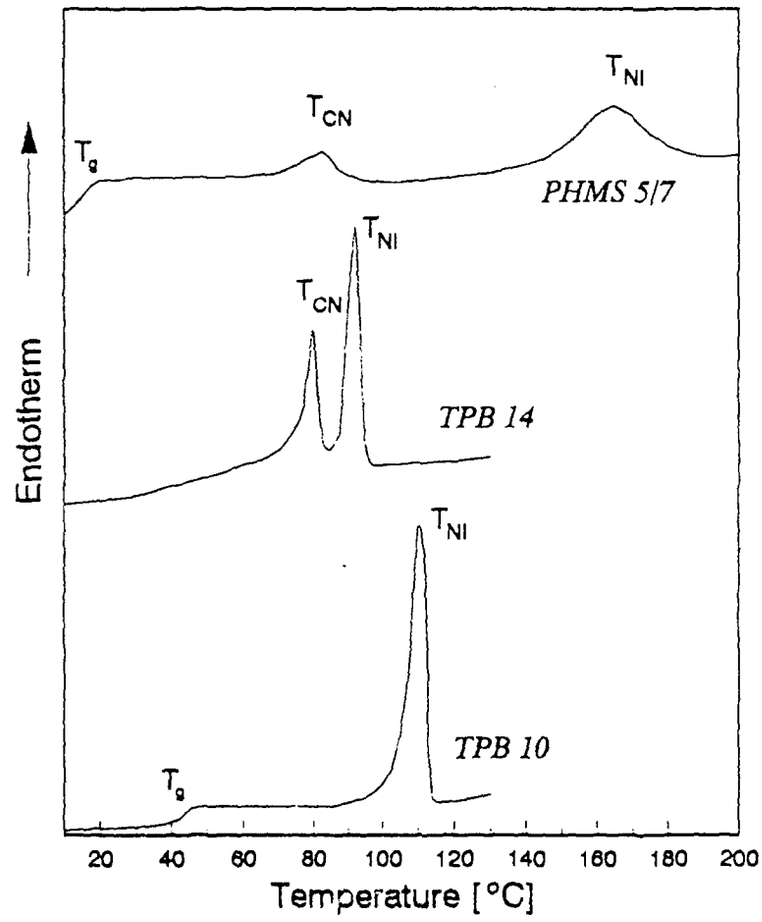

Figure 2 D.s.c. heating traces of the polymers used. T_g, T_{CN} and T_{NI} are the glass–nematic, crystalline–nematic and nematic–isotropic transitions, respectively

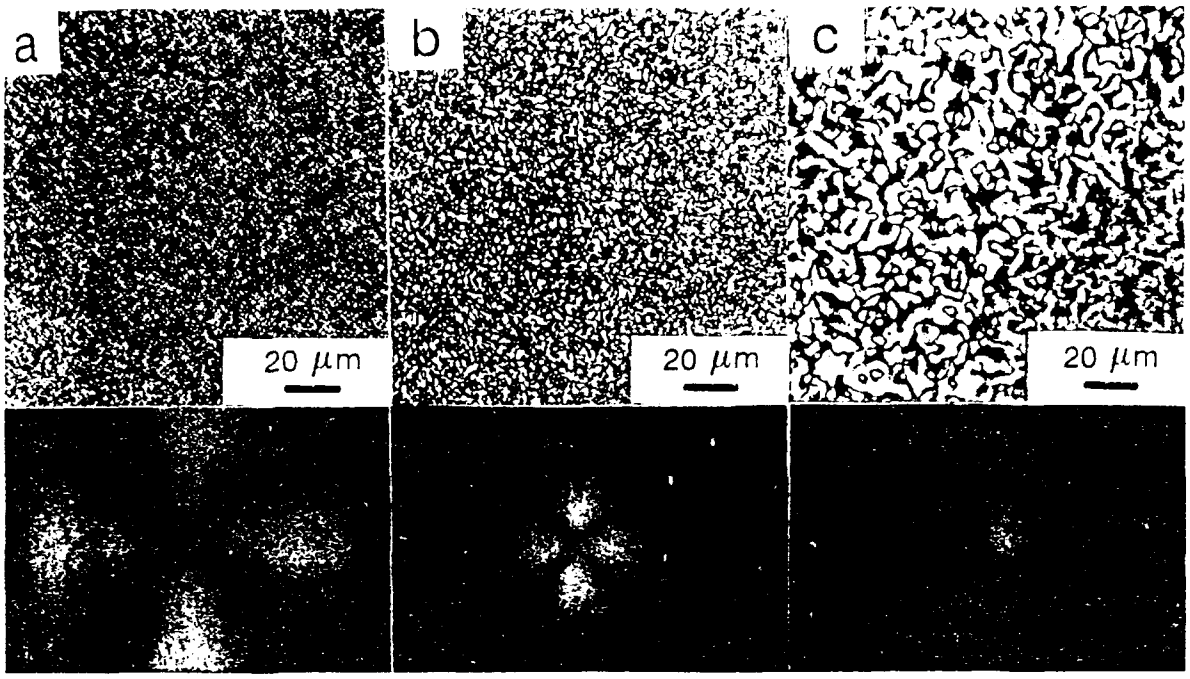

Figure 3 Effect of annealing in the nematic state on the texture and light scattering of TPB 14. Polymer (a) just heated up to 90 °C and annealed [illegible] min at 288°C, observed polars.

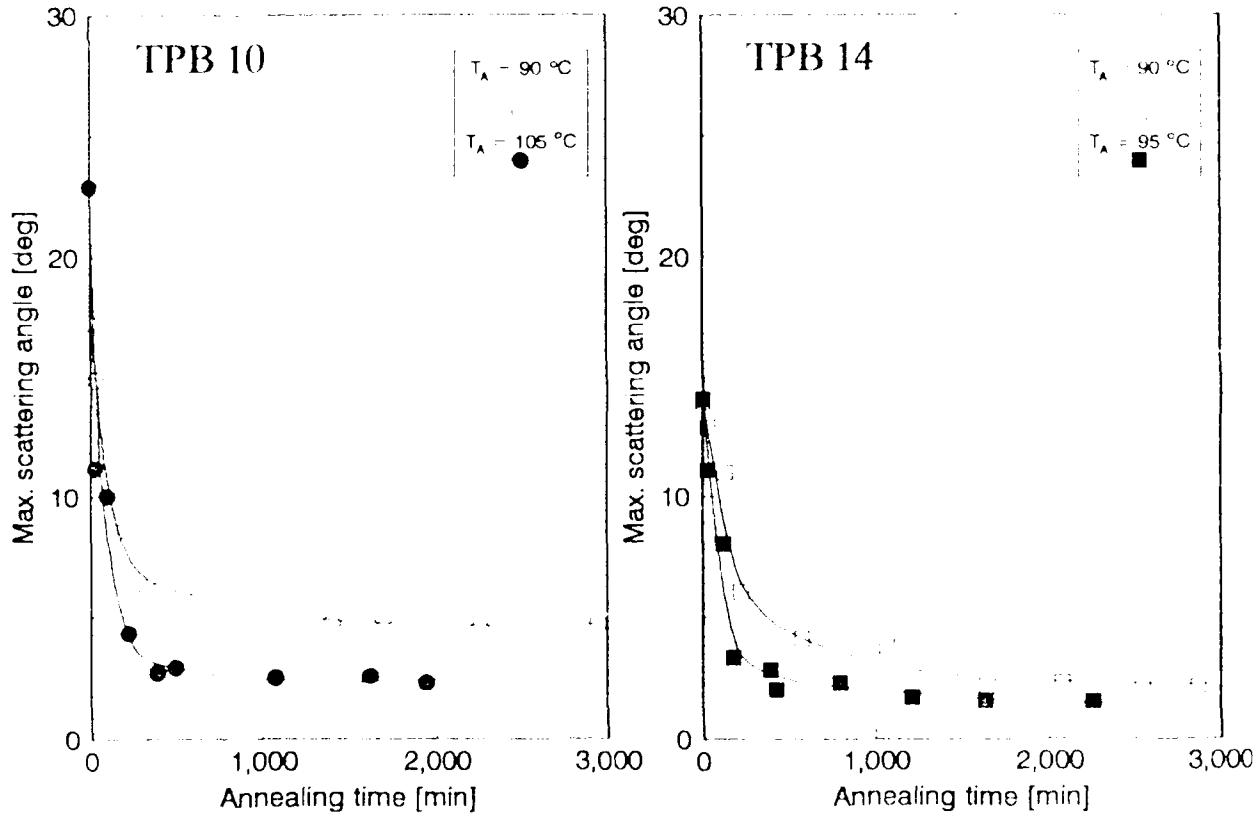

Figure 4 [illegible]

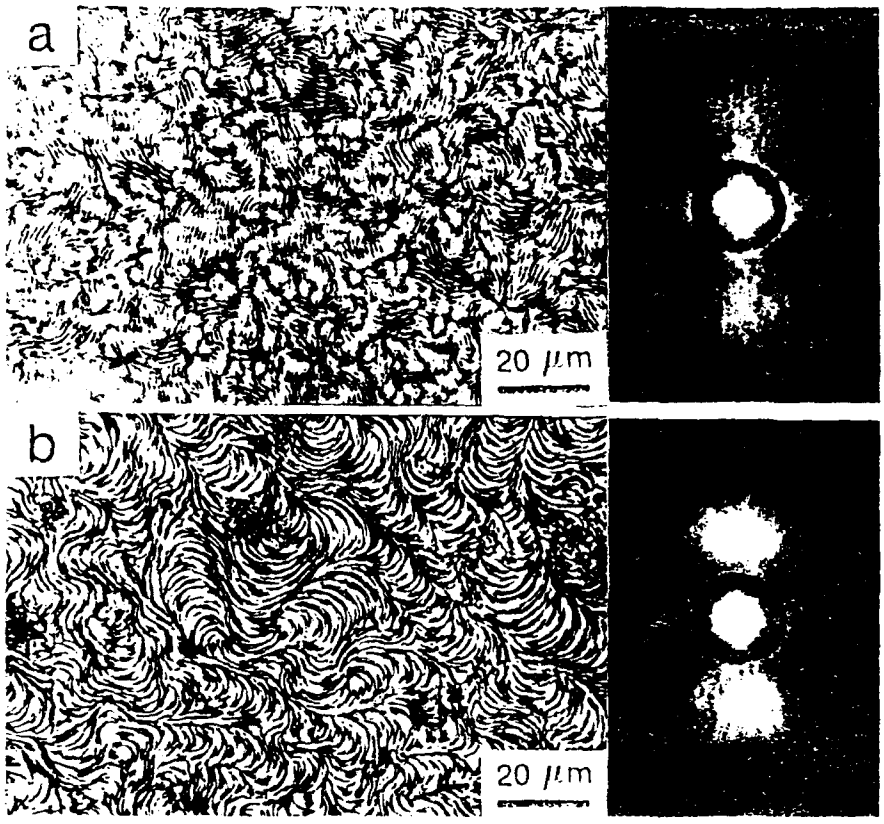

Figure 5 Optical micrographs and $V_{\parallel}$ light scattering patterns of the crystallizable polymers quenched after annealing (3000 min) close to T_{NI} below their crystallization temperatures. (a) TPB 14, (b) PHMS 5-7, crossed polars. The centres of the prints were exposed longer to envisage more intense scattering at the small-angle areas

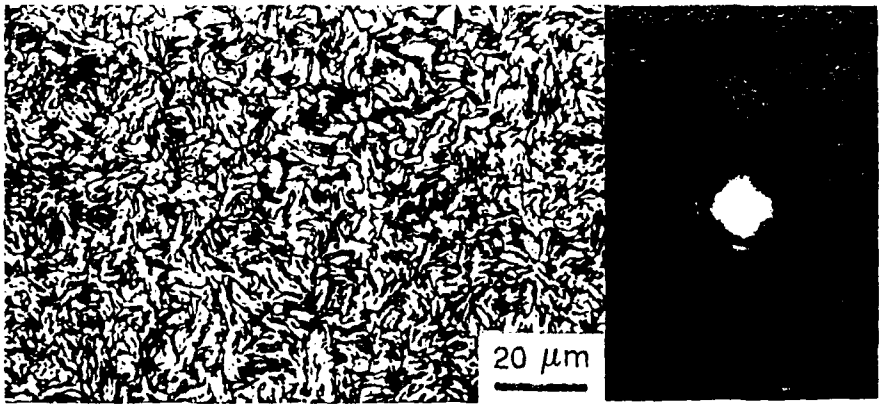

Figure 6 Optical micrograph and $V_{\parallel}$ light scattering pattern of TPB 14 annealed at 90°C for 2260 min and cooled to room temperature by the rate 0.01°C min^{-1}. The centre of the print was exposed longer to envisage more intense scattering at the small-angle areas

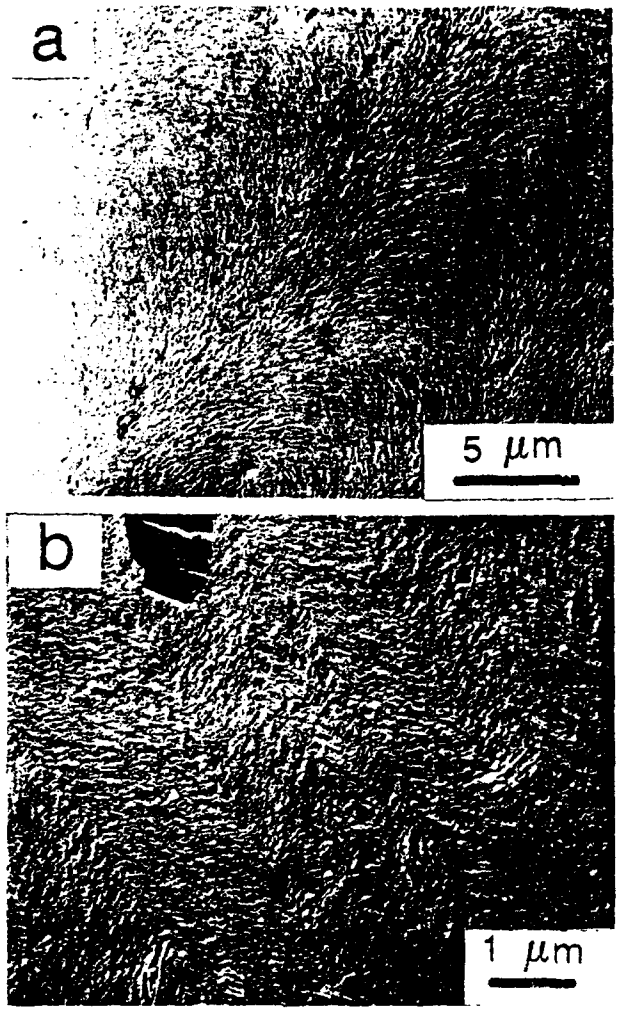

Figure 7 Banded morphology of PHMS 5/7 annealed close to T_{NI} and quenched into the crystalline state. TEM, Pt–Pd replica at low (a) and high (b) magnification

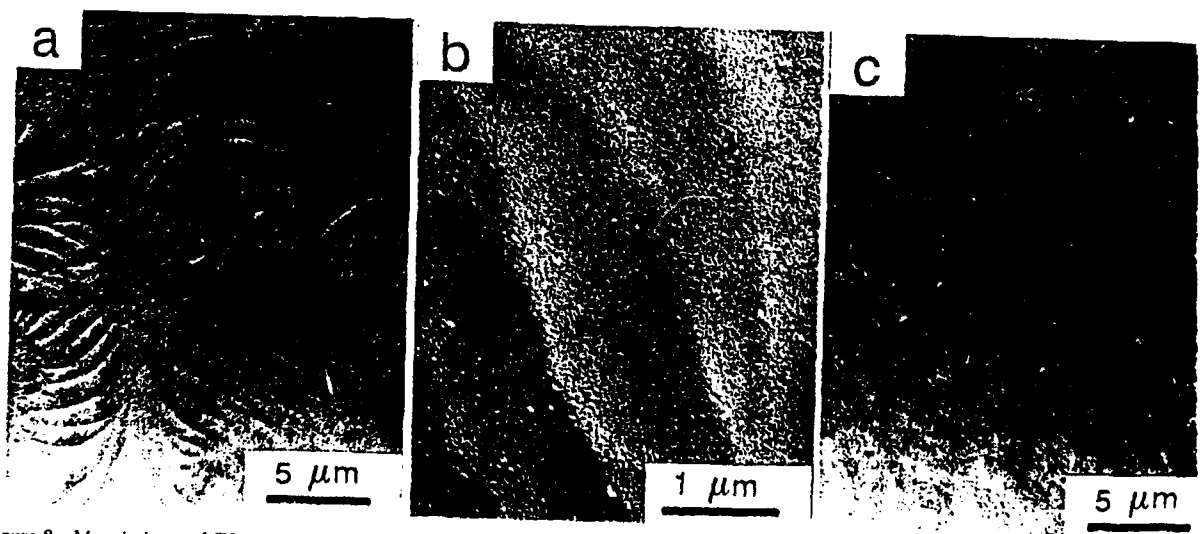

Figure 8 Morphology of TPB polymers annealed close to T_{NI} and quenched to the crystalline or glassy state (a), (b) Banding in crysta TPB 14; (c) smooth surface of glassy TPB 10. TEM, Pt-Pd replica

ATOMIC FORCE MICROSCOPY OF THE BANDED STRUCTURE OF LYOTROPIC POLYMERS*

H. Fischer, M. J. Miles, and J. A. Odell
H. H. Wills Physics Laboratory, University of Bristol, Tyndall Avenue, Royal Fort, Bristol, BS8 1TL, U. K.

INTRODUCTION

A common feature during disorientation of liquid crystalline polymers after cessation of flow is the appearance of a transverse banded texture, underlying a periodical variation of orientation. This effect is attributed to the early stages of disorientation and is thought to be co-operative[1]. The mechanism is still rather obscure, but it has been speculated that it arises from the reduction of stored elastic energy together with the requirement to minimise splay during disorientation. Some investigations have been performed on the system Poly-p-phenylene-benzbisthiadiazole (PPTA) / sulphuric acid (H_2SO_4) [2-4] and on systems with Poly-g-benzyl-L-glutamate (PBLG), Hydroxypropylcellulose (HPC) or thermotropic nematic melts[5-9]. Mostly it is reported that banded textures are displayed as part of the relaxation behaviour after a shear application. The dimensions are dependent on the stress, the film thickness and the relaxation time. The appearance of the bands is also dependent on the film thickness and the application time of the stress. With a decrease in thickness, an increasing induction period is necessary to obtain the banded structure after the end of the shear application. Mostly the bands show sharp zigzags as the direction of the orientation of the macromolecules [2-5,7] although sinusoids with a 3-dimensional disorientation (one component out of shear plane) have also been reported. The micromorphology of the disorientation is thought to reflect the mechanism for banding - minimization of splay would favour a zig-zag trajectory. We report the first experiments to investigate the bands formed during the relaxation process of lyotropic polymers using atomic force microscopy (AFM). This relatively new technique provides information about the surface structure of materials. It should be possible to obtain information about the three-dimensional structure of the bands and also of the orientation of single molecules.

* *Macromol.Rapid Communications*, accepted for publication

EXPERIMENTAL

The experiments have been performed on oriented samples from solutions of poly-*p*-phenylene-benz-bis-thiozol (PBZT) in orthophosphoric acid (OPA) and HPC in water. Also, additional experiments have been done using polarization microscopy (POM) and transmission electron microscopy (TEM) of thin sheared films. A 9 % solution of PBZT in OPA has been used as described elsewhere[1]. In the investigation of the band formation, the high sensitivity of PBZT solutions to moisture in the air was an advantage, since it enabled precipitation at the very early stages of relaxation (after 2-5 seconds) during the preparation of thin films on glass surfaces. The experiments were carried out at a temperature of 100 °C in order to obtain a relatively low viscosity and to exclude water as a nonsolvent as much as possible. Almost immediately after shearing the sample, the formation of an orange crystal solvate was observed. The films were rapidly precipitated in water and washed several times in distilled water and a mixture of water and ethanol (50 %) to wash the solvent out, and dried on the glass surface for the POM and TEM investigations and on a fresh mica surface for the AFM experiments. HPC samples were obtained using the same method with a 60 % solution of HPC in distilled water without the precipitation procedure. In this case it was sufficient for a preservation of the banded structure to shear the sample in a dry atmosphere. For the TEM investigations, thin films were transferred to copper grids. AFM Images were recorded on a Digital Instruments (Santa Barbara, California) Nanoscope III atomic force microscope operated in the contact mode. The cantilever with integral pyramidal tip had a nominal spring constant of 0.06 N/m. The force used for each sample was the lowest for which stable feedback conditions could be obtained without the use of filters in the feedback circuit. The PBZT was imaged in air (force ~100 nN) and under a non-solvent, n-propanol (force ~8 nN) in order to reduce capillary forces on the tip. The HPC was also imaged in air (force ~100 nN) and under a non-solvent, hexadecane (force ~10 nN). Typical scan times were ~40 s. In each case, the sample was oriented in the AFM such that its shear direction was not close to either the fast or slow scan directions. Image processing consisted of plane fitting only.

RESULTS AND DISCUSSION

The shear direction is indicated in each figure. Figure 1 shows a TEM image of PBZT. The corresponding AFM image of PBZT at low magnification is shown in Figure 2. The shear direction is easily visible. At higher magnification, it is possible

to observe the structure of the bands. The direction of the bands is strictly perpendicular to the shear direction (Figure 3). The width of the bands was found to decrease with increasing shear rate. In the samples investigated, the band width is very uniform and has a value of about 0.6 mm. An analysis of the bands is shown in Figure 4. The spectrum shown documents the uniformity of the bands. The profile provides new information on the band structure. The bands have a three-dimensional structure at the surface. This has been observed also with TEM (see Figure 5). The profile is approximately sinusoidal. It appears, that the molecular director is going through a sinusoidal trajectory of the macromolecules. The thickness of the bands was calculated from the optical and electron microscopy pictures to be about 0.7 μm (see Figure 5). The AFM pictures showed a difference in height of about 50 nm across the bands.

The variation in forces on the cantilever during the scanning of the PBZT specimen in air caused serious instabilities in the feedback control, requiring a higher set force. In case this force instability originated from a capillary force associated with an adsorbed liquid layer on the specimen surface, the PBZT specimen was also imaged under n-propanol, a non-solvent, to eliminate the liquid surface on the tip and cantilever. Although this improved the stability somewhat, the high resolution that might be expected from such a rigid specimen could not be attained. Some pull-on force still gave unstable conditions. The origin of this force for this sample is not known, but it may be associated with an adsorbed layer of solvent leaching from the specimen and not removed by the washing procedure. It was found that if the force was not continually adjusted to the minimum value that could be sustained, then the tip caused some surface modification of the specimen. However, by carefully monitoring the applied force, it could be kept within a range of values which avoided major instabilities and surface modifications.

Similar structures have been observed in the case of banded structures of HPC (see Figures 6 and 7). Here it was possible to obtain a better resolution in the AFM pictures. In Figure 7, fibrillar features of dimensions of about 0.3 μm spacing are clearly visible. They follow the main chain trajectory and are in principle similar to the fibrils observed in the TEM pictures of the PBZT solutions. Here also a strongly three-dimensional banding, perhaps forming an elliptical helix, was observed.

The imaging of HPC in air also suffered from force instabilities which could be attributed to an adsorbed water layer. Successive images scanned in air exhibited progressive disruption of the surface which, in the initial stages emphasized the underlying orientation present. It was not possible to use a propanol environment for scanning as this is a solvent for HPC. Instead, the non-polar liquid hexadecane was used. This was effective in decreasing the instabilities of the capillary force and

allowed images to be obtained at lower set point values. The consequent disruption of the surface structure was considerable reduced, allowing several scans to be made in a given area before any significant surface damage was detected.

CONCLUSIONS

We have shown, that AFM can be a complementary technique to optical microscopy and TEM for examination of the banded texture of liquid crystalline polymers. In particular, it yields higher resolution and 3-D information, *i.e.*, the out of plane component. It seems that for the 2 systems examined here, the banding is sinusoidal in both planes, but of unequal amplitude, resulting in an elliptically-helical fibrillar structure. This is perhaps rather difficult to understand in light of the proposed mechanism (minimization of splay) which would favour a zig-zag morphology with the splay confined to very narrow defect regions in the disorienting liquid crystal.

REFERENCES

1 Marucci, G. and Maffetone, P. L., *Macromolecules*, **22**, 4076 (1989)

2 Odell, J. A., Ungar G. and Feijo, L. J., *J.Polym.Sci.Polym.Phys.Ed.*, **31**, 141 (1993)

3 Chen, S., Jin, Y., Qian, R. and Cai, L., *Macromol.Chemie*, **188**, 2713 (1987)

4 Chen, S., and Qian, R., *Macromol.Chemie*, **191**, 2475 (1990)

5 Roche, E. J., Allen, J. R., Galara, V. and Cox, B.,*Polymer*, **30**, 1779 (1989)

6 Wang, J., Bhattacharya, S. and Labes, M. M., *Macromolecules*, **24**, 4942 (1991)

7 Fincher Jr., C. R., *Mol.Cryst.Liquid Cryst.*, **155**, 559 (1988)

8 Ernst, B. and Navard, P., *Macromolecules*, **22**, 1419 (1989)

9 Viney, C., Donald, A.H., and Windle, A.H., *J. Mat. Sci.*, **18**, 1136 (1983).

FIGURE CAPTIONS

Figure 1: Bands of PBZT observed in the POM, the arrow indicates the shear direction.

Figure 2: A low magnification view of PBZT in the AFM. The shear direction is indicated by an arrow.

Figure 3: A higher magnification view of PBZT in the AFM showing the structure of the bands.

Figure 4: A sectional analysis through the banded texture along the shear direction.

Figure 5: A TEM picture of a thin film of PBZT after a relaxation time of about 5 seconds, showing the banded texture. The arrow indicates shear direction.

Figure 6: Bands of HPC observed in the POM; the arrow indicates the shear direction.

Figure 7: AFM image of banding in HPC in air.

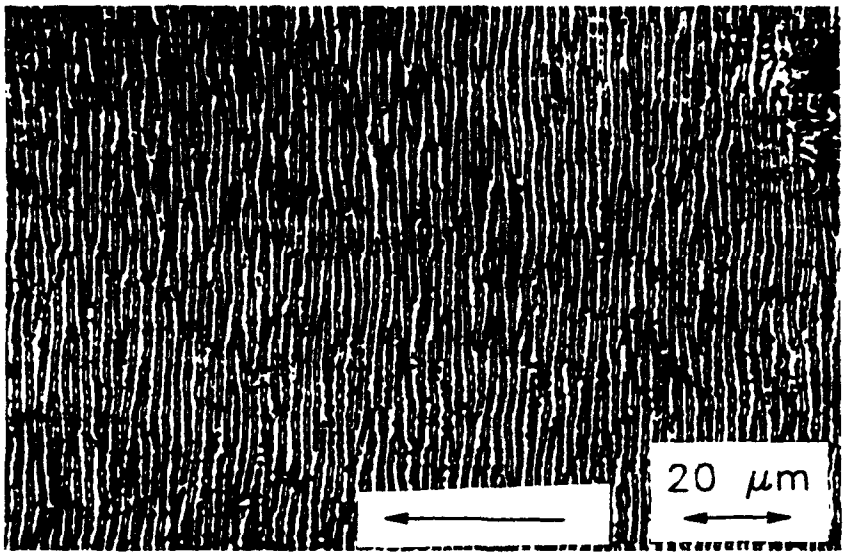

Figure 1

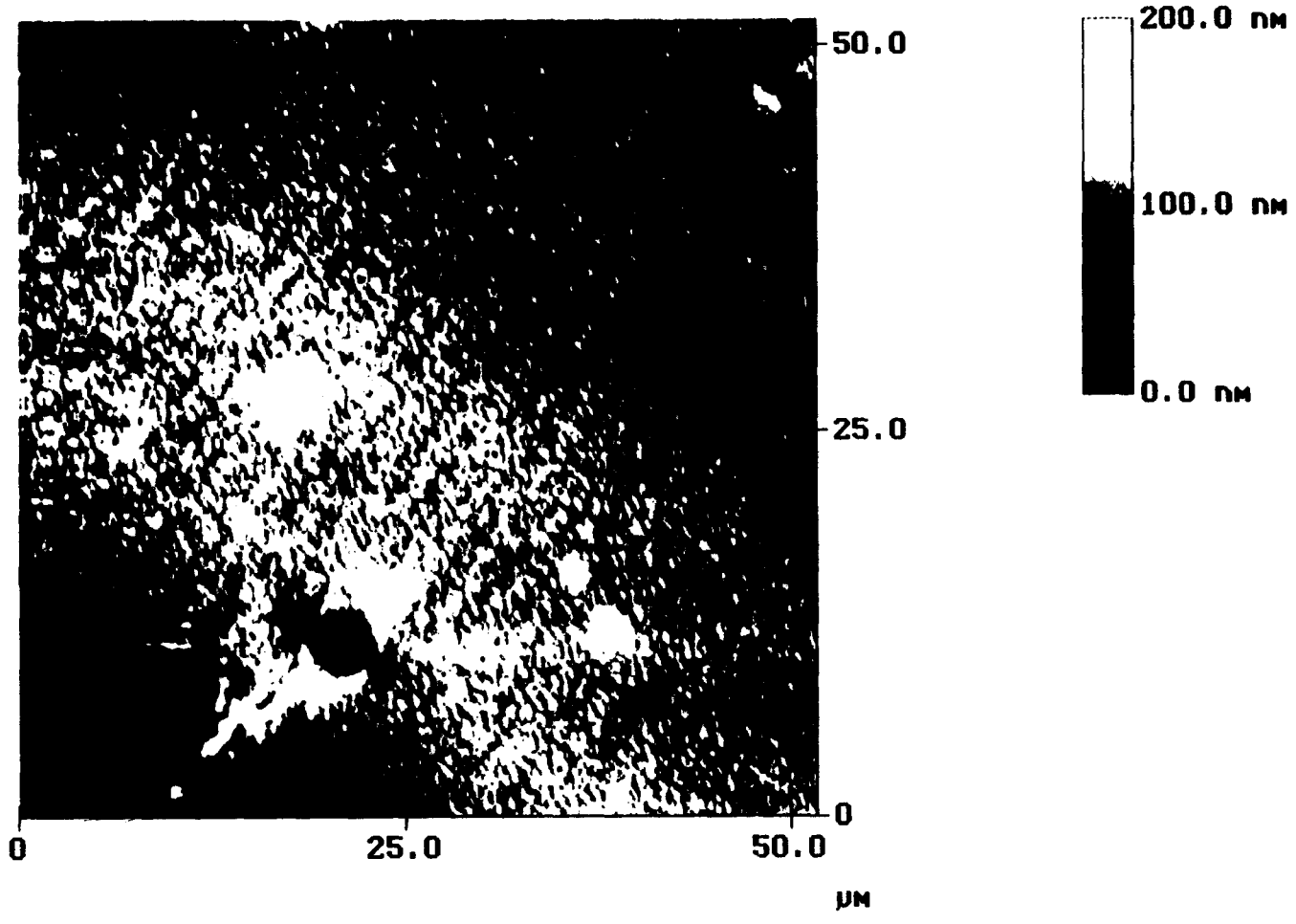

Figure 2

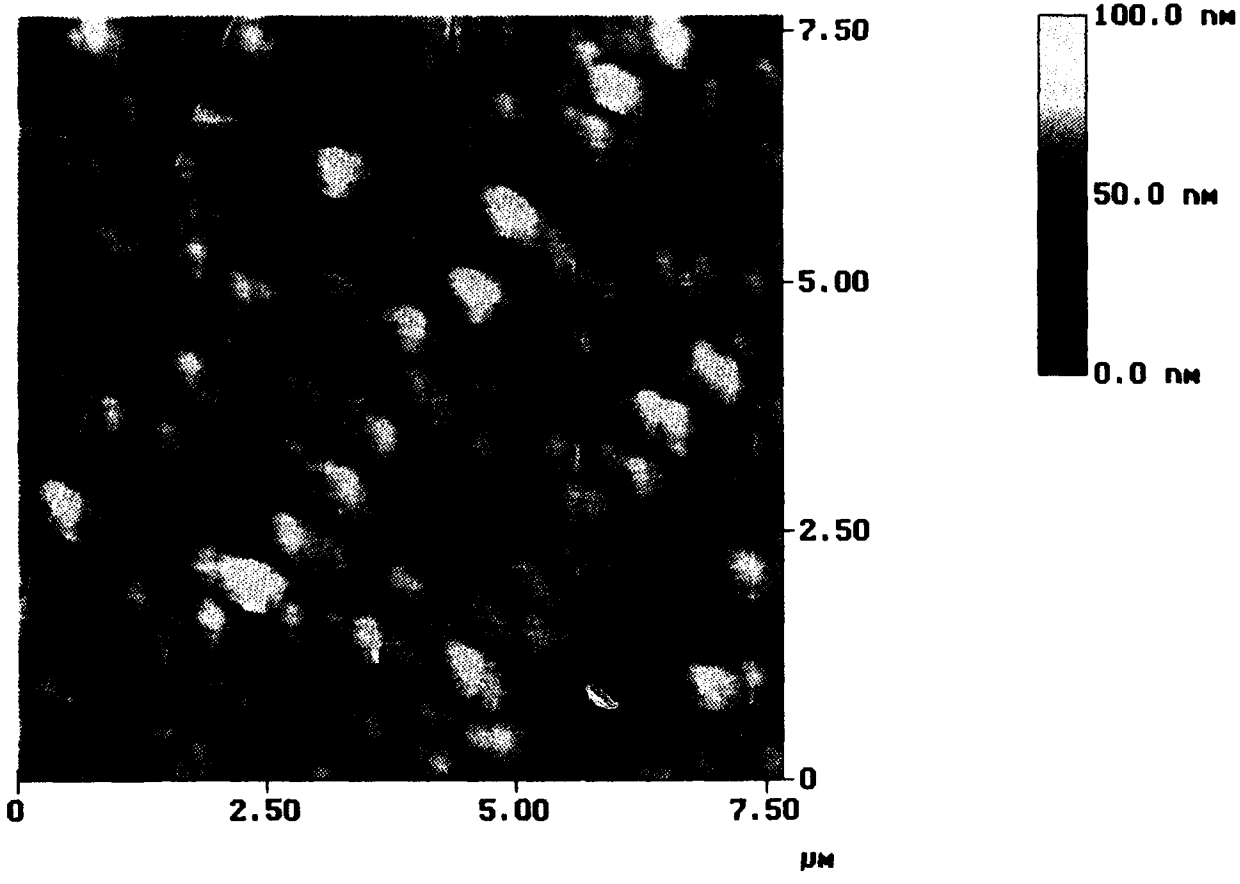

Figure 3

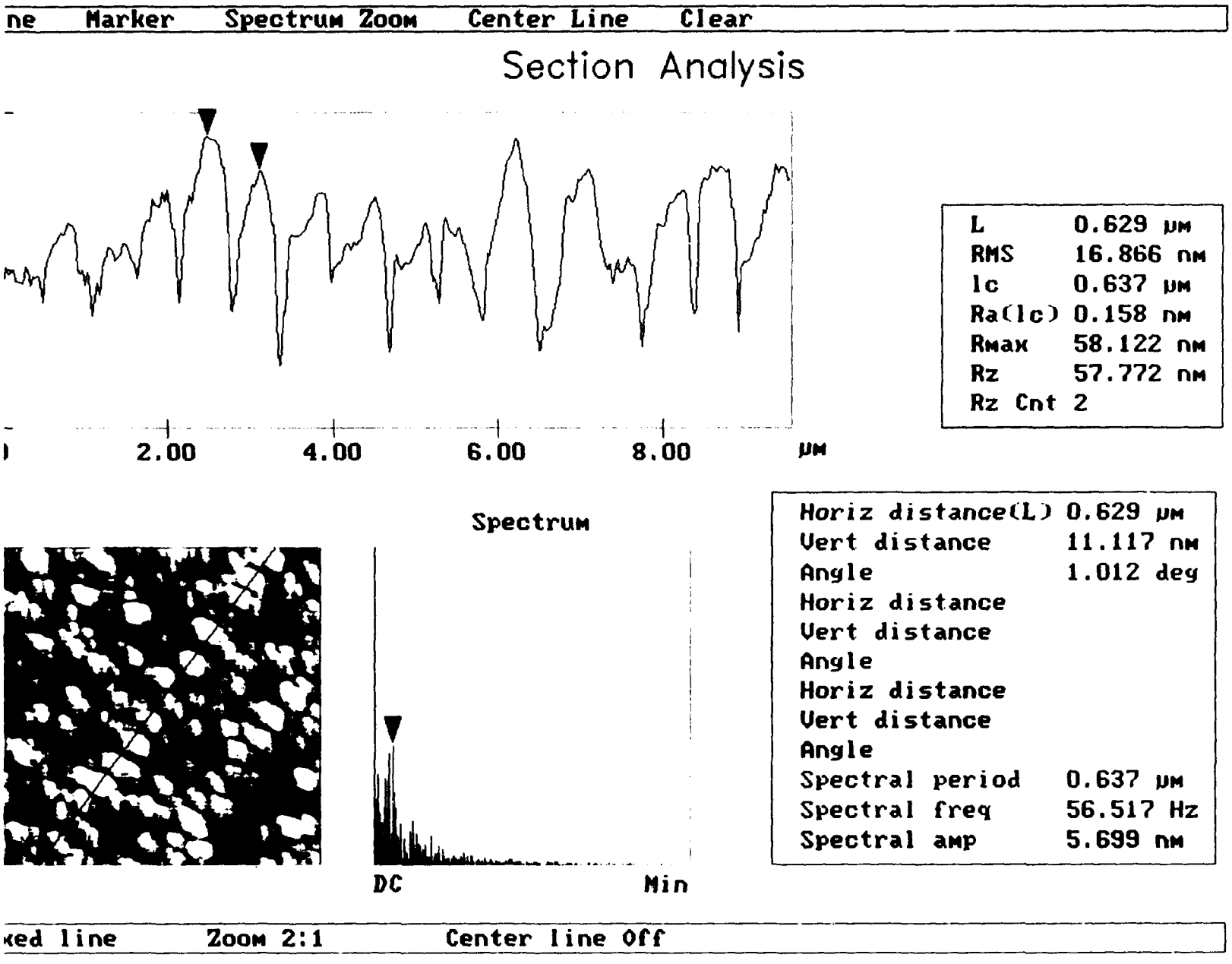
ne Marker Spectrum Zoom Center Line Clear
Section Analysis
2.00
4.00
6.00
8.00
µm
L 0.629 µm
RMS 16.866 nm
lc 0.637 µm
Ra(lc) 0.158 nm
Rmax 58.122 nm
Rz 57.772 nm
Rz Cnt 2
Spectrum
DC
Min
Horiz distance(L) 0.629 µm
Vert distance 11.117 nm
Angle 1.012 deg
Horiz distance
Vert distance
Angle
Horiz distance
Vert distance
Angle
Spectral period 0.637 µm
Spectral freq 56.517 Hz
Spectral amp 5.699 nm
ked line Zoom 2:1 Center line Off

Figure 4

Figure 5

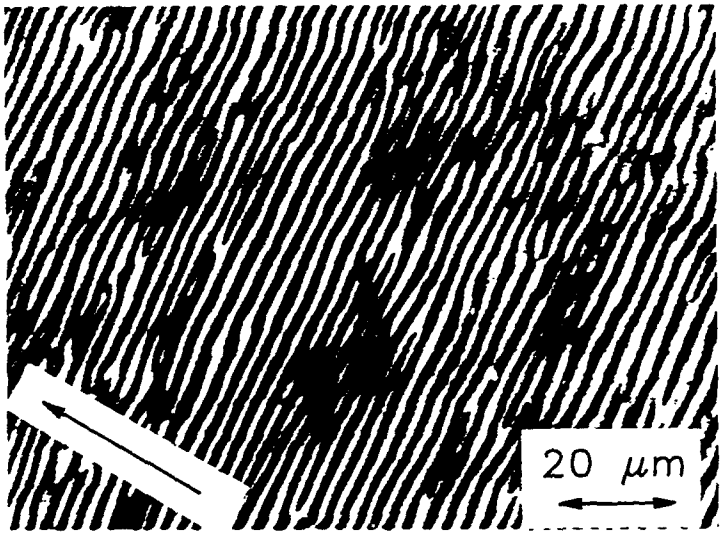

Figure 6

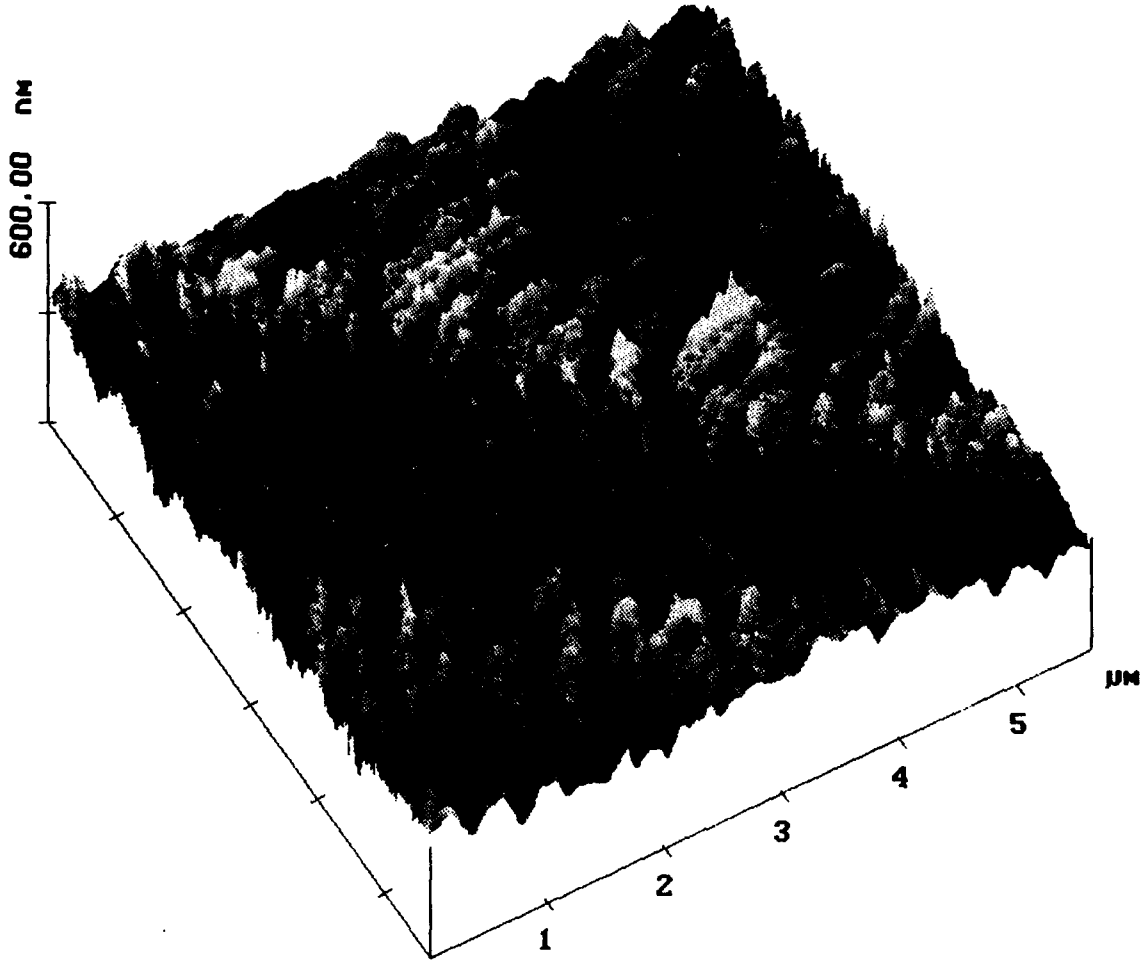

Figure 7

SECTION 2: RHEOLOGY AND FLOW-INDUCED LIQUID CRYSTAL PHASE TRANSITIONS IN THERMOTROPIC POLYETHERS.

Thermotropic materials have many potential advantages, they can have excellent thermal and mechanical stability, have good mould filling behaviour, and can achieve high orientation during processing resulting in high modulus and strength, albeit at the expense of anisotropy. They are also, of course, highly tractable materials, lending themselves to all forms of melt processing.

Most polymers which promise commercial success are based upon co-polyesters (e.g. Vectra). These materials are, however, not ideal for studying thermotropic behaviour *per se*, since at the high temperature required to process them they trans-esterify and change whilst being investigated. In this regard the novel co-polyethers of Percec have great advantages: they melt at accessible temperatures, enabling the whole phase behaviour from crystal, nematic and isotropic to be studied. Further they can be fractionated to yield controlled model materials on which to test our understanding of rheology and phase behaviour.

In this report we investigate the rheology of such copolyethers in both the nematic and isotropic state, verifying the often assumed reduced viscosity of the nematic state. Further, using fractionated materials we study the rheology as a function of molecular weight, establishing scaling laws for comparison with existing theories. We then go on to see how the applied flow-fields affect the phase behaviour and demonstrate that the nematic-isotropic phase boundary can be significantly raised in temperature, in accordance with the predictions of some theories.

Rheology and Flow-induced Liquid Crystal Phase Transitions in Thermotropic Polyethers*

D.P. Heberer, J.A. Odell, and V. Percec+

H.H.Wills Physics Laboratory, University of Bristol, Tyndall Avenue, Bristol BS8 1TL

+Case Western Reserve University, Cleveland, Ohio

ABSTRACT: This work investigates the interdependance of the phase behaviour, viscosity, temperature , molecular weight, and shear rates of thermotropic liquid crystalline polyethers. The viscosity of the isotropic and nematic phases are quantitatively compared; a positive variation in viscosity with respect to temperature is found, with the isotropic viscosity being about an order of magnitude higher than the liquid crystalline viscosity. The dependance of viscosity upon molecular weight of well defined fractions is investigated in both the liquid-crystal and isotropic phases. Variations in the viscosity due to temperature changes affects the isotropic phase more than the liquid crystal phase. No evidence for a negative first normal stress difference is seen. Finally, it is shown how the phase diagram of the material can be altered by shearing the material in the isotropic phase. This is evident by the onset of a shear thinning region at temperatures slightly above Ti which can be attributed to the formation of shear induced liquid crystallinity.

INTRODUCTION

The rheology of liquid crystalline polymers is characterized by a number of unusual phenomena: high shear thinning behavior, low extrudate swell and often negative normal forces have been reported [1]. These rheological properties provide distinct advantages for processing in comparison to random coil isotropic melts, and processing in the liquid crystalline state can result in high molecular alignment and high modulus and mechanical nisotropy in the solid artefact, even at low shear-rates.These properties are thought to originate in the ease of alignment of liquid-crystalline domains providing an easy shear direction in the fluid.

For lyotropic systems this behaviour is quite well documented and understood. Generally, the viscosity of a thermotropic liquid crystal polymer is assumed to be higher in the isotropic state than in the liquid crystalline state. Thus, the viscosity of a polymer liquid crystal decreases with decreasing temperature. The majority of

* *J. Mater. Sci.*, accepted for publication

rheological data on thermotropic liquid crystals has been published on random aromatic copolyesters [2,3], although some reports deal with copolyesters containing flexible methylene spacers [4,5]. The positive variation of viscosity with respect to temperature was not found for these materials, although in some instances the isotropic state could not be attained prior to sample degradation or transesterification.

The explanations of the rheological behavior of liquid crystals have concentrated predominantly on the effect of shear on the domain texture (and hence director) of the liquid crystal. A rheooptical study by Onogi and Asada [6] led them to propose a mechanism to account for the shear viscosity of polymer liquid crystals. A plot of the logarithm of the viscosity versus the logarithm of the shear rate shows three distinct regions. Region I encompasses low shear rates where the material is shear thinning and flow occurs by the relative motion of the liquid crystal domains without a net orientation of the directors. In Region II the viscosity is nearly constant and the increased shear rate breaks down some of the domains which then act as a solvent for the remaining domains. Lastly, in Region III, the material is again shear thinning and the texture becomes a continuous monodomain structure oriented in the shear direction.

A molecular theory due to Doi [7] applies a Maier - Saupe type potential to the isotropic model to successfully describe many aspects of liquid crystal behavior. The theory accounts for the discontinuity in viscosity between the isotrpic and liquid crystalline , it cannot however address the problems of strong flows or polydomain textures encountered in real processing conditions.. The Doi theory has been modified, however, to account for a polydomain structure of a sample under high shear rates by averaging the response of many individual domains [8,9]. These modified theories have met some success in explaining the behaviour of lyotropic systems. They specifically predict that the effect of flow would be to move the phase transition boundary between isotropic and liquid crystal states, the flow orientation favouring the ordered liquid crystal state. in lyotropics this would produce aliquid crystal transition at lower concentrations under flow, in the thermotropic case it would produce a liquid crysatl phase at a higher temperature.

The verification of these theories in thermotropic systems has been difficult because of the degradation and transesterificationof the aromatic liquid crystals at high temperatures. Liquid crystal polyethers with flexible spacers in the backbone do not undergo transesterification reactions and have transition temperatures well below their degradation temperatures. These materials are therefore excellent candidates for rheological studies of polymer liquid crystals. This report will focus on several aspects of polymer liquid crystal rheology which have not yet been reported in the

literature. In particular the interdependance of the phase behaviour, viscosity, temperature , molecular weight, and shear rates are presented.

EXPERIMENTAL

Material

The polymers used in this study had the structure

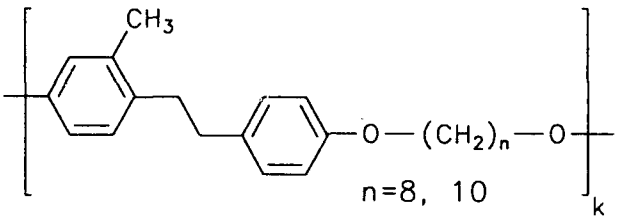

The polymer was a 50/50 mixture of flexible sequences consisting of eight and ten methylene units. There was a random placement of head to tail linkages of the mesogen and the flexible spacers.

The polymers were previously studied by simultaneous synchrotron X-ray analysis and differential scanning calorimetry in previous work [10]. The polymer was found to be an enantiotropic liquid crystal that exhibited a stable nematic phase at temperatures between 96 and 112 °C.

Fractionation

The material used in the determination of the phase behavior performed earlier had a Mn of 39,000 and a Mw of 74,000 (Polydispersity=1.90). In order to better determine the effects of molecular weight on the phase transitions and the rheological behavior, the original material was fractionated into narrower molecular weight fractions. The fractionations were conducted according to the successive fractionation procedure [11] at 38 °C with toluene as the solvent and methanol the nonsolvent. The collected fractions were dried overnight in a vacuum oven at 75 °C. The molecular weights were determined relative to polystyrene standards in chloroform at 40 °C. The molecular weights of each fraction are listed in Table 1 and the corresponding GPC traces are shown in Figure 1 (fraction #3 was omitted since it was not used in the experiments because of its low yield).

It is evident that the molecular weight distributions of the fractions have been reduced relative to the original material, but some overlap of the traces occurs for each fraction. Nevertheless, the fractionation must be considered a success because a high

and a low molecular weight tail have been removed in each successive fractionation. A comparison of molecular weights of samples before and after the rheological measurements indicated that no appreciable change in molecular weight occurred during the experiments.

Differential Scanning Calorimetry

The effect of the molecular weight on the phase transitions was investigated by DSC. As an example of the phase behavior of the MBPE-8/10 fractions Figure 2 illustrates the cooling and subsequent reheating curves of fraction #2 (recorded at 10 K/min). The MBPE 8/10 polymers underwent two transitions on cooling from the isotropic melt; the first was the isotropic to nematic transition occurring at 112 °C, and the second was the crystallization of the nematic phase at a lower temperature. The crystal melting endotherm was shifted to slightly higher temperatures on reheating while the onset of the liquid crystal to isotropic transitions occurred at the same location. All molecular weight fractions exhibited identical phase behavior; apparently the molecular weight was above a limiting value and had no effect upon the transition behaviour.

Rheology

The rheological determinations were conducted on a Rheometrics RMS-800 rheometer using the cone and plate fixture. The cone had a radius of 12.5 mm and an angle of 0.014 rad. A constant cone and plate separation of 10 um was used in all experiments. All experiments were allowed to reach thermal equilibrium prior to measurement and were conducted in a nitrogen atmosphere to limit sample degradation. Start-up experiments were conducted to determine the strain required to reach a steady state viscosity and all viscosities were determined in the plateau region. As an example, figure 3 shows the stress as a function of time for fraction #1 on start up and cessation of shear. In all samples the viscosity initially overshoots, going through a pronounced peak. The strain at which this peak occured was around 1-2 and was invariant with molecular weight and strain-rate. A steady-state value for the viscosity was only attained after approximately 30-180 seconds depending upon molecular weight. A corresponding delay time was used before measurement for the frequency sweep experiments. The viscosities were recorded as the material was constantly and continuously sheared only in the clockwise direction (no reversal of direction was used).

The torque values recorded at the lowest strain rates were near the limitations of the rheometer. To determine the point at which the data became meaningful the baseline torque (the torque recorded with no sample) was subtracted from the recorded values. The experimental data reported were those which were larger than the lower limit of the rheometer. The torque was then converted to viscosity data

using the appropriate equations. The shallow angle of the cone and the small cone and plate separation made the normal force measurements sensitive to small fluctuations in temperature. The thermal expansion and contraction due to the heater switching on and off created a background noise which made normal force measurements even more difficult. Even so, no evidence was seen of negative normal stresses. The oscillatory shear experiments were conducted with the cone and plated geometry with a strain of 1%. The rheometer was calibrated according to standard procedures prior to the measurements. Visual observation of the sample confirmed the occurrence of the phase transitions.

The previous shear history of the nematic phases was removed by heating the sample into the isotropic phase (this treatment was shown to remove shear history in reference 5). This was repeated for each measurement. The time required for thermal equilibrium also provided for the total relaxation of the material prior to measurements.

RESULTS

The start-up stresses shown in fig.3 were typical across all samples and strain-rates. The stress overshoots by around 60% before settling back to a steady-state value. As mentioned above, the time required for the achievement of the steady-state stress was a function of molecular weight, high molecular weights require longer times. The settling times were 180, 45, and 30 seconds for fractions #1, #2, and #4 respectively, when using a strain rate of 1 s-1. These values were not strongly dependant upon strain rate. These settling times are significantly longer than those recorded on a liquid crystal polyester which contained 10 methylene spacer units [5]. The peak of the overshoot, however, occured at essentially the same time for all samples, it varied with strain-rate in such a way that it occurred at a constant value of total fluid stain of about 100-200 %.

Figure 4 illustrates the steady state viscosity as a function of shear rate for fraction #2 at five temperatures: the two lowest temperatures (103 and 108 °C) were within the nematic phase, the two highest temperatures (118 and 140 °C) represent the behavior of the isotropic phase, and the remaining temperature (113 °C) is slightly above the isotropic to liquid crystal transition temperature. The viscosity of the nematic liquid crystal did not vary significantly with temperature, as evident by the nearly superimposed curves for 103 and 108 °C. For both temperatures there was a plateau region at low shear rates followed by a shear thinning region at higher shear rates. The viscosity of the isotropic phase was around one order of magnitude higher

than the viscosity of the nematic phase (113 °C compared to 108 °C). The viscosity of the isotropic phase, however, decreased with increasing temperature (as shown by a comparison of 118 and 140 °C) in a manner typical of flexible polymers, such that the low shear-rate viscosities at 103 °C and 140 °C were approximately equal.

The behaviour of the isotropic phase at temperatures only slightly above Ti was dramatic. At low shear rates there was an initial plateau in the viscosity, but as the shear rate increased the viscosity quickly decreased as the material became shear thinning. The shear rate required for the onset of shear thinning decreased as the temperature decreased. The transition occurred at 0.1 s-1 at 118 °C but fell to 0.01 s-1 at 113 °C . The viscosity at 113 °C decreased and became similar to the viscosity of the liquid crystal phase at the highest shear rates. The viscosity at 118 °C also decreased with increasing shear rate, but it never equalled the liquid crystal viscosity with the strain rates used. There is no evidence of a shear thinning region in the behavior observed at 140 °C.

Figure 5 shows the viscosities of fraction #4 at the same shear rates and temperatures as shown for fraction #2. Generally, the behavior was similar to fraction #2. The plateau and shear thinning regions of the nematic liquid crystal state appeared, and again there was little change in the viscosity with temperature between 103 and 108 °C. The isotropic phase exhibited 2 shear thinning regions. The first being a steep decrease in viscosity at low shear rates and the second a more gradual decrease at higher shear rates. In the first region the viscosities at 140 and 118 °C are approximately equal, but as the shear rates increased the viscosity at 140 °C was reduced relative to the viscosity at 118 °C. Over most shear rates at these temperatures, again it was clear that the isotropic phase had a larger viscosity than the nematic phase. The largest difference in the behavior between fraction #2 and fraction #4 concerns the viscosity recorded at 113 °C, just above the isotropization temperature. The viscosity behaviour at 113 °C for fraction #4 was very similar to that seen for the nematic phase at 103 and 108 °C, throughout the strain rate range. in fact the viscosity about 30% lower than that recorded at 103 and 108 °C This is in contrast to fraction #2 where the viscoty of the isotropic phase at 113 only approached that of the nematic phase beyond a shear rate of 1 s-1.

The variation of the viscosity with molecular weight is displayed in the following two diagrams. In Figure 6 the viscosity of the nematic phase at 103 °C as a function of shear rate is shown for the three molecular weight samples. Fractions #2 and #4 exhibited the plateau and shear thinning region as previously mentioned, but the plateau region was absent for fraction1. The most dramatic observation in Figure 5 is the change in the viscosity with molecular weight. The viscosity increased by approximately 2 orders of magnitude with a 2.5 times increase in the molecular

weight (fraction #4 to fraction #1 respectively). Comparing the low strain rate plateau viscosities of fraction #2 and #4, would suggest a dependance of viscosity upon molecular weight to about the power of 3.5. Inclusion of the lowest shear rate results for fraction #1 (as a lower bound, since it has not reached a plateau) suggests an even higher dependance of viscosity upon molecular weight, around M 5. The data at the highest shear rates for fraction #1 is suspect because the sample began to flow out from between the cone and plate either because of centrifugal or elastic forces.

A more complete illustration of the effect of molecular weight on the viscosity of the isotropic phases is illustrated in Figure 7. This is a replotting of the data already presented for fractions #2 and #4. It is evident that the viscosity, regardless of the phase, is roughly an order of magnitude higher for fraction2 at a given temperature. Qualitatively, the change in the viscosity with molecular weight was greater in the isotropic phase than the nematic phase.

On cessation of steady shear the stress takes a considerable time to decay away. Fig. 3 shows an illustrative example for fraction#1 at 103 °C. This relaxation can be well described by a double exponential where the characteristic relaxation times depend upon molecular weight. At 103 °C the relaxation fast and slow relaxation times for fraction #1 are 2s and 100s,whilst for fraction #4 they are considerably longer at 5s and 1000s. In each case the slower time scale corresponds with the onset of banding in the optical texture and with the timescale for the relaxation of <P2> as assesssed by X-ray diffraction 14 . Stress relaxation in the isotropic state occurs much more rapidly and is complete on a time scale of a few seconds, comparison with X-rays shows that the orientational order completely relaxes on this time-scale [14].

The final figure (8) compares the oscillatory shear behavior of fraction #4 in the isotropic and nematic phases. The results were similar for each case; with increasing shear rates G' and G" increased (resulting in an increase in tan(delta)) and the complex viscosity decreased. An amplitude of strain of 1% was used for these results.

DISCUSSION

The low transition temperatures of the MBPE 8/10 polyether made it possible to investigate the rheological behavior of both the anisotropic liquid crystal phase and the isotropic phase without sample degradation. The nematic liquid crystal phase was found to have a quite different flow behaviour to the isotropic phase; most notably the viscosity of the liquid crystal phase was much lower than the isotropic phase even

though its temperature was lower. The positive temperature dependence of the viscosity with temperature has been explained by the ordered alignment of the molecules in the liquid crystal phase which allows for easier movement relative to the random isotropic melt. This behaviour has been confirmed in a number of reports [4,5] and has even been used to determine the phase diagram of a commercial main chain polyesteramide [12]. The viscosities of both the liquid crystal and isotropic phases decreased as the temperature increased as expected for polymer melts. The effect of temperature was more pronounced on the isotropic phase: a change of five degrees from 113 °C to 118 °C resulted in a ten-fold drop in the viscosity for fraction #2 (see Figure 4) while the same temperature change within the nematic state (103 and 108 °C) produced only negligible changes. The viscosity values used for 113 and 118 °C were those at the lower shear rates, before the onset of shear thinning which was due to a phenomenon discussed below.

The isotropic phase (at temperatures >> Ti) exhibited near Newtonian behaviour, whilst the liquid crystalline phase exhibited two different flow regions. From Figure 4 one can see that there is a plateau in the viscosity at low shear rates followed by a shear thinning region at higher shear rates. This Newtonian plateau and shear thinning behavior has been observed in lyotropic systems, most notably PBLG [13] and PBZT [20]. This behavior is typified by a Region II to III transition as predicted by the theory of Onogi and Asada. Thus, if this were the case then the polymer would have been converted from a polydomain material into a monodomain structure, with a regular ordering of the directors about the shear direction. The ordering of the MBPE 8/10 polymer under shear has been determined through synchrotron X-ray experiments [14]. The orientation is found to be quite high corresponding to a <P2> value of 0.85. The plateau regions are absent in fraction #1; but because of the shift in the plateau to lower shear rates upon going from fraction #4 to fraction #2 we could expect the plateau to occur at shear rates lower than those used. If this were indeed Region II, then the larger molecular weight would be expected to undergo deformation of domains at lower shear rates because of the greater entanglement density and longer relaxation times of the higher molecular weight.

We might ask why we did not observe a Region I (polydomain) shear thinning behaviour at the lowest shear rates? The shear rates used may not have been low enough, or perhaps the yield stress that occurs during start up (see Figure 3) corresponds to Region I.5 The yield stress and the higher viscosities at the lower shear rates indicate that some stress is needed to induce alignment and therefore facilitate flow. The initial stress could break down some of the domains but still leave a polydomain structure intact which concurrently breaks down in the Region II to III

transition at higher shear rates. this would be in good agreement with the rheooptic results of Onogi and Asada6 and with results on PBLG [22] and thermotropic systems [23].

The start-up instabilities can also be accounted for by a numerical extension to Doi's molecular theory due to Larson [9], this does not require the breakup of domains. This theory predicts a transition in the motion of the mesogens from continuous tumbling, through a damped oscillation around the flow direction, to a steady-state high orientation as shear-rate is increased. At high shear-rates start-up transients very similar to those we observe are predicted to occur at fixed low strains independent of the precise strain-rate.

The sharp drop in the viscosity with increasing shear rates of the isotropic melt at temperatures only just above Ti to values similar to those of the liquid crystal phase indicates that shear induces a liquid crystal like state from the isotropic phase. The alteration of a phase diagram by shear has been previously observed where flow has been found to decrease the concentration required to form a lyotropic liquid crystal [13] and also it was both predicted [16] and found experimentally to extend the nematic region to higher temperatures [17]. The reasons for the extension or alteration of the phase diagram by shear is that in addition to the thermodynamic order present in the liquid crystal or the isotropic melt, there is also a contribution from mechanical forces. A decrease in viscosity could result from either a local ordering of the polymers due to volume restrictions (the normal thermodynamic consideration) or from shear induced orientation of the molccules. The shear forces affect the Brownian motion of the molecules and leads to an increase in the stiffness of the molecules. The effect is more pronounced in semirigid polymers where flow fields increase the persistence length [13,18]. Thus, in a system whose mesogen is based upon conformation isomerism, the effect could be expected to be quite large.

We are now in a position to discuss why the shear thinning behavior is not observed at temperatures far from Ti and why the behavior is dependent upon the polymer molecular weight. The key lies in the response time of the material to the shear flows in comparison to the relaxation rates of the molecular species. The relaxation time will decrease with both increasing temperature and decreasing molecular weight. Therefore, in order to observe the shear thinning behavior one would have to use increasingly higher shear rates as the temperatures were increased or the molecular weight decreased. This is observed in Figures 4 for fraction #2 which show that the shear rate at which the shear thinning region begins shifts from 0.01 s-1 to 0.1 s-1 for 113 and 118 °C respectively, and that no shear thinning regions are observed at 140 °C. Since the relaxation times are a strong function of the molecular weight (maybe the sixth power [7]) the effects of molecular weight should

also be significant. This is apparent in the comparison between the behaviour of fraction #2 and #4; the isotropic phase of fraction #4 does not exhibit shear thinning at any temperature or shear rate.

Relaxation is essentially complete in a few seconds above the isotropization temperature. This presumably reflects the strong entropic driving force towards disorder in the isotropic state. This is entirely consistent with the observed molecular disorientation from X-ray synchrotron diffraction experiments [14].

The molecular weight also affects the magnitude of the viscosity, as illustrated in Figures 7 and 8. The viscosity of both the liquid crystal and isotropic phases increased as the molecular weight increased. In the MBPE 8/10 system, the viscosity of the liquid crystalline phase was found to scale to the power of M3.5 to M5. The molecular weight dependence of viscosity in the isotropic phase is not as clear since only two data point are available, but the results show that fraction #2 is around 10 times the viscosity of fraction#4 over most of the shear rate range and at both 118 and 140 °C. This corresponds to an approximately viscosity scaling dependence of M4, this is broadly in line with the expectation for the scaling of viscosity for an isotropic entangled melt M3.4 and with the predictions of reptation theory [21].

The lack of great differences observed in the oscillatory behavior could be either a temperature effect or it could be due to the low strain of 1% used in the experiment. This strain is much lower than that required to overcome the start-up effects (100-200%) and so may not be been large enough to create structural changes within the material. It has been shown that the strain amplitude does not affect the liquid crystal state oscillatory properties but it did affect the isotropic melt results, however those authors used much larger strains than that used here [19]. Further investigations at a variety of strains and temperatures would be required before making definite conclusions about the MBPE 8/10 system.

CONCLUSIONS

This work has increased the knowledge of the rheological properties of thermotropic liquid crystals in several ways. First, the viscosity of the isotropic and nematic phases have been quantitatively compared; the material had a positive variation in viscosity with respect to temperature, with the isotropiv viscosity being about an order of magnitude higher than the liquid crystalline viscosity. Secondly the dependance of viscosity upon molecular weight has been investigated in both the liquid-crystal and isotropic phases. The variations in the viscosity due to temperature changes affected the viscosity of the isotropic phase more than the liquid crystal

phase. No evidence for a negative first normal stress difference wsa seen. Finally, it was shown how the phase diagram of the material can be altered by shearing the material in the isotropic phase. This is evident by the onset of a shear thinning region at temperatures slightly above Ti which was attributed to the formation of shear induced liquid crystallinity.

ACKNOWLEDGEMENTS

Sponsorship of the US Army European Office, London is gratefully acknowledged. We are grateful to Prof. Andrew Keller for helpful discussions.

FIGURE CAPTIONS

1. GPC traces of the original and subsequent fractions (Y axis arbitrary).
2. DSC trace of fraction #2 recorded on heating (dotted line) and cooling (solid line) at 10oC/min.
3. The stress as a function of time at the start up and cessation of shear for fraction1
4. The viscosity as a function of shear rate and temperature for fraction #2.
5. The viscosity as a function of shear rate and temperature for fraction #4.
6. A comparison of the steady state shear viscosities of the three molecular weight fractions in the nematic state at 103oC.
7. A comparison of the viscosities of fraction #2 and fraction #4 as a function of shear rate at four temperatures.
8. The oscillatory shear behavior of fraction #4 at 140oC (isotropic state) and at 105oC (nematic state).

REFERENCES

1. Chapter 13, Rheology of Thermotropic Liquid Crystal Polymers, pages 424-440 from the book Melt Rheology and it Role in Plastics Processing.
2. K. F. Wissbrun, *Br. Polymer Journal,* **12**(4), 163 (1980).
3. F. N. Cogswell, *Br. Polymer Journal*, **12**(4), 170 (1980).
4. J. R. Tuttle, H. E. Bartony, Jr., and R. W. Lenz, *Polm. Eng. Sci.*, **27**, 1156 (1987).

5. K. F. Wissbrun and A. C. Griffin, *J. Polym. Sci., Polym. Phys. Ed.*, **20**, 1835 (1982).

6. S. Onogi and T. Asada, in Rheology, edited by G. Astari, G. Marucci, and L. Nicholais, Plenum, New York, 1980, Vol. 1, 127-147.

7. M. Doi, *J. Polym. Sci., Polym. Phys. Ed.*, **19**, 229 (1981).

8. G. Marucci and P. L. Maffetone, *Macromolecules*, **22**, 4076 (1989).

9. R. G. Larson, *Macromolecules*, **23**, 3983 (1990).

10. G. Ungar, J. L. Feijoo, A. Keller, R. Yourd, adn V. Percec, *Macromolecules*, **23**, 3411 (1990).

11. Fractionation, Encyclopedia of Polymer Science.

12. J. M. Gonzalez, M. E. Munoz, M. Cortazar, A. Santamaria, and J. J. Pena, *J.Polym. Sci., Polym. Phys. Ed.*, **28**, 1533 (1990).

13. G. Kiss and R. S. Porter, *J.Polym. Sci., Polym. Phys. Ed.*, **18**, 361, (1980).

14. D.P. Heberer and J.A. Odell -to be published.

15. K. F. Wissbrun, *Faraday Disc. Chem. Soc.*, **79**, 161 (1985).

16. G. Marucci and A. Cifferri, *J. Polym. Sci., Polym. Lett. Ed.*, **15**, 643 (1977).

17. S. L. Wunder, S. Ramachandran, C. R. Gochanour, and M. Weinberg, *Macromolecules*, **19**, 1696 (1986).

18. G. C. Alfonso, E. Bianchi, A. Cifferri, S. Russo, F. Salaris, and B. Valenti, *J. Polym. Sci., Poly. Symp.*, **65**, 213 (1978).

19. P. Driscoll, T. Masuda, and K. Fujiwara, *Macromolecules*, **24**, 1567 (1991).

20. J.A. Odell J.L. Feijoo and G. Ungar, *J. Polym Sci. B Polymer Physics*,. **31**, 141-155, (1993)

21. M. Doi and S.F. Edwards "Theory of Polymer Dynamics" Clarendon Press, Oxford (1986)

22.J. Mewis and P. Moldenaers, *Mol. Cryst Liq. Cryst*,. **153**, 291 (1987)

23. G.G. Viola and D.G. Baird, *J.Rheol.* **30** ,601 (1986)

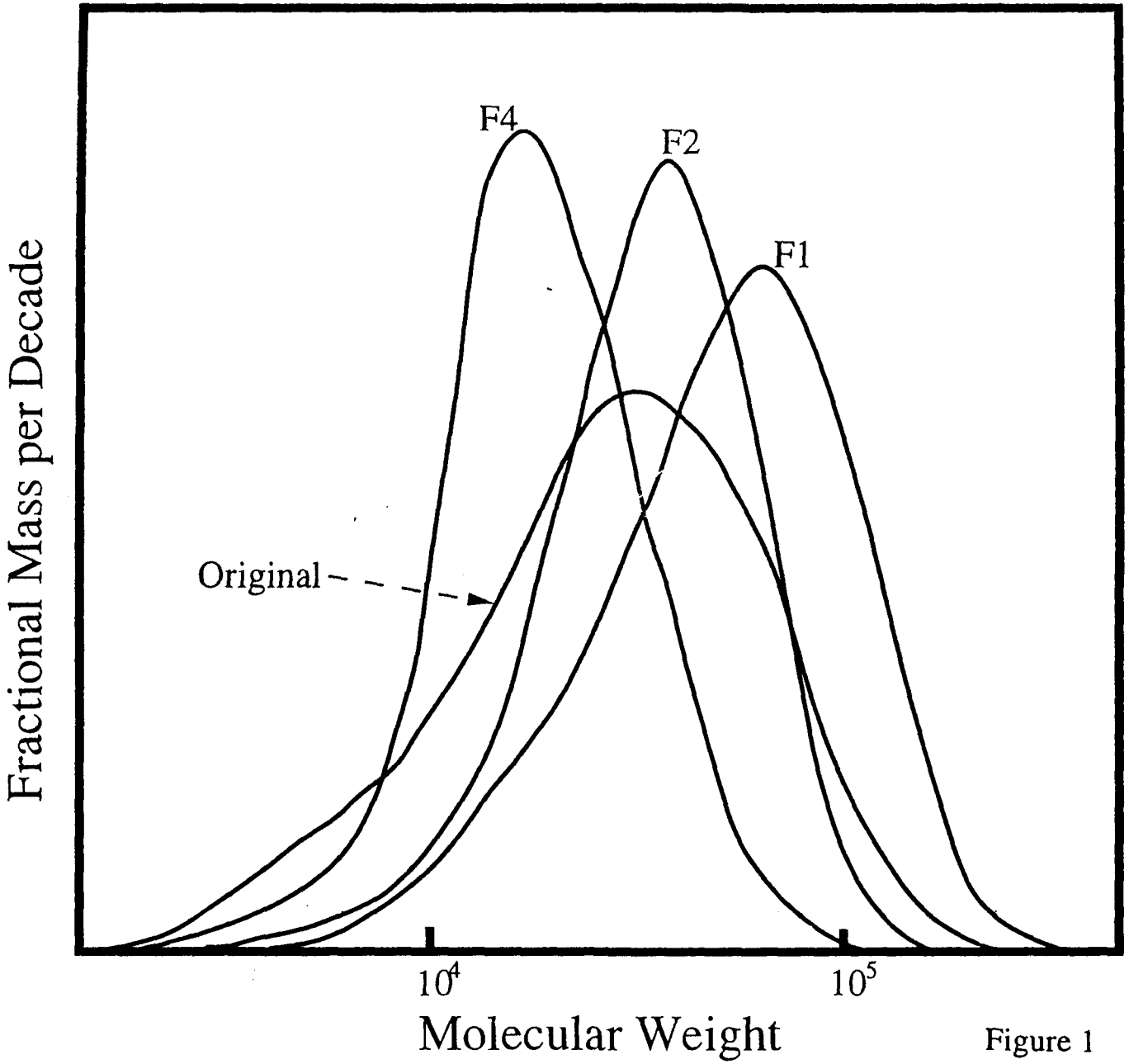
F4
F2
F1
Original
Fractional Mass per Decade
10^4
10^5
Molecular Weight

Figure 1

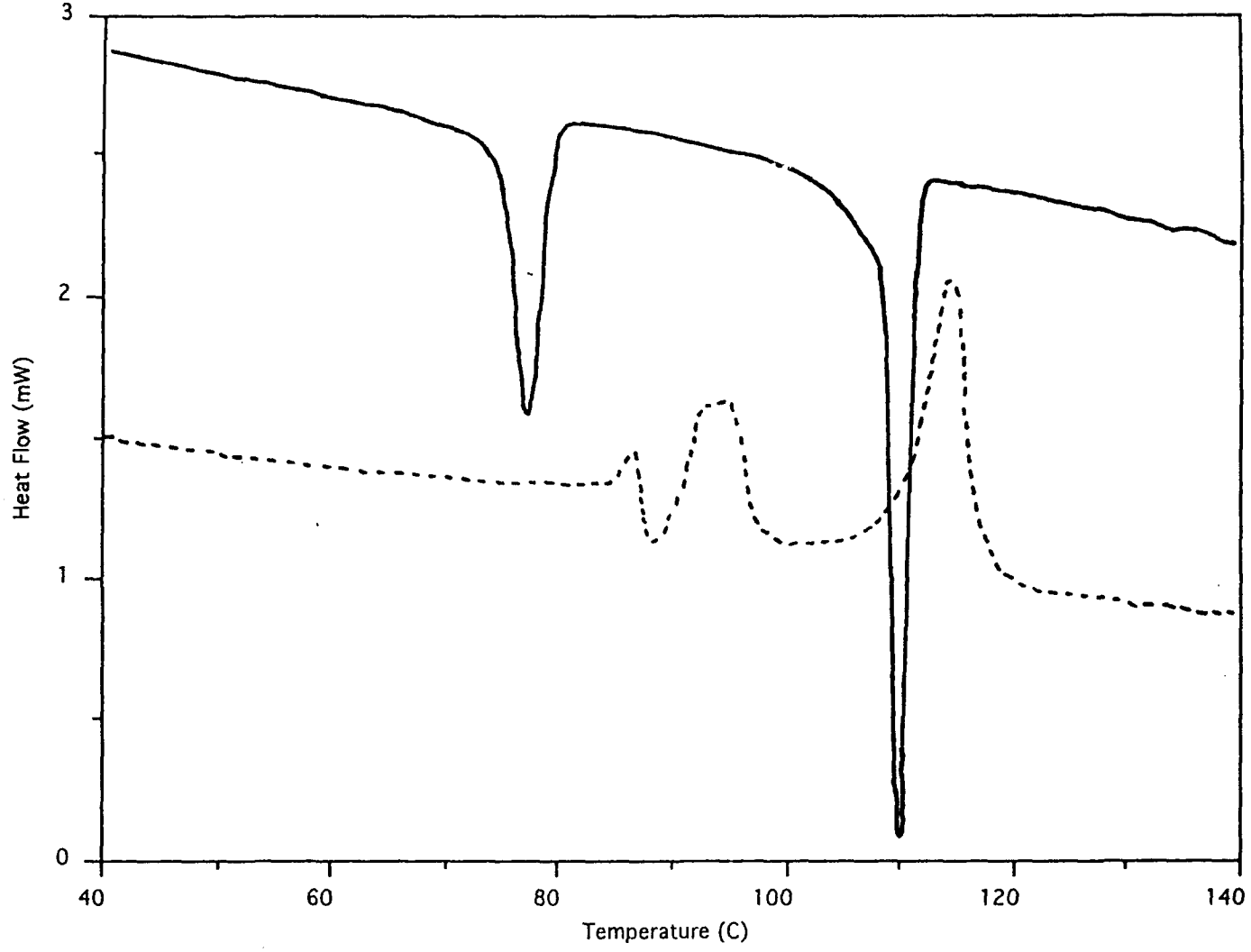

Figure 2

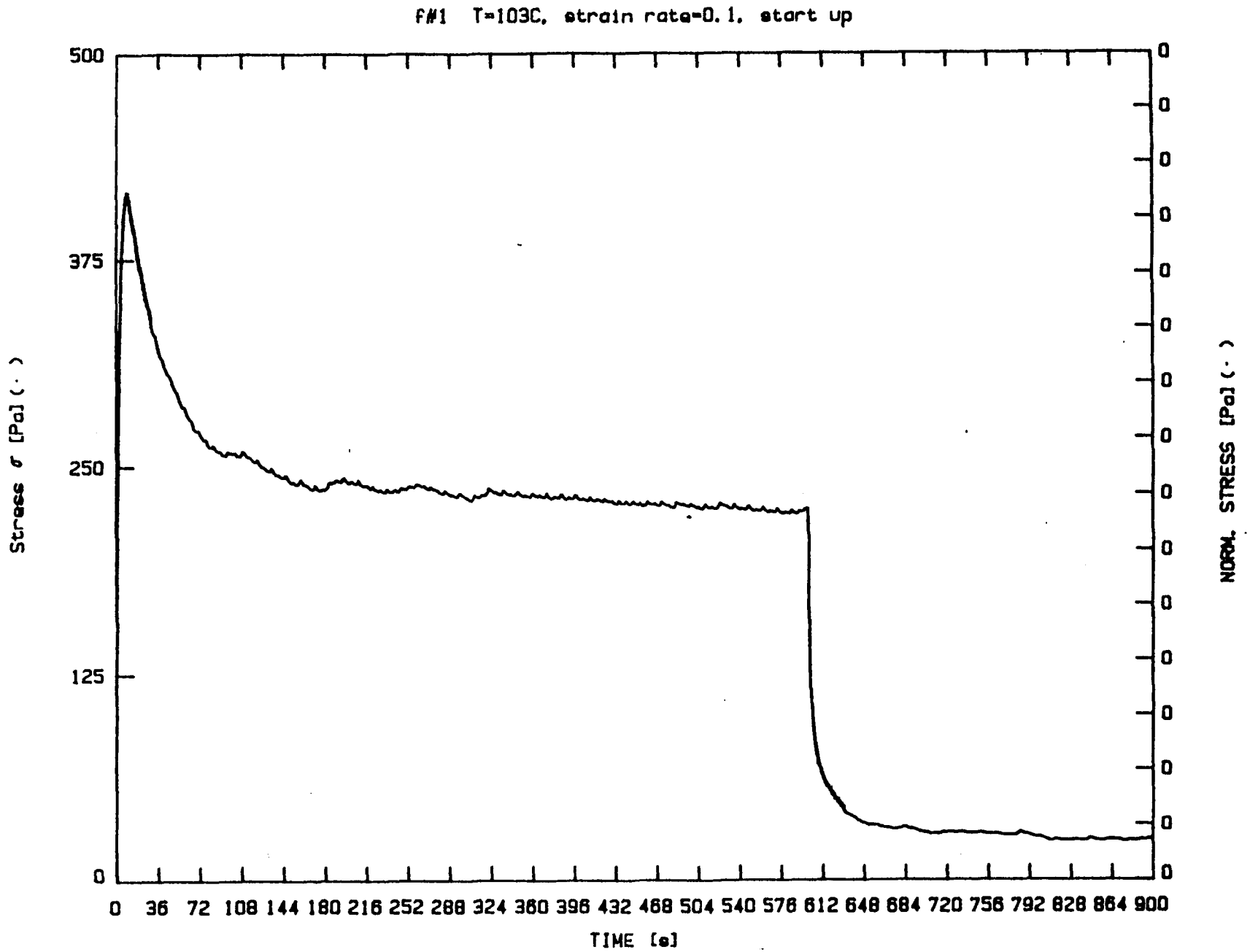
fM1 T=103C, strain rate=0.1, start up
500
375
250
125
0
Stress σ [Pa] (·)
0 36 72 108 144 180 216 252 288 324 360 396 432 468 504 540 576 612 648 684 720 756 792 828 864 900
TIME [s]
NORM. STRESS [Pa] (·)

Viscosity vs. Strain Rate

MBPE F#2 MW=55K

Baseline Torque Subtracted

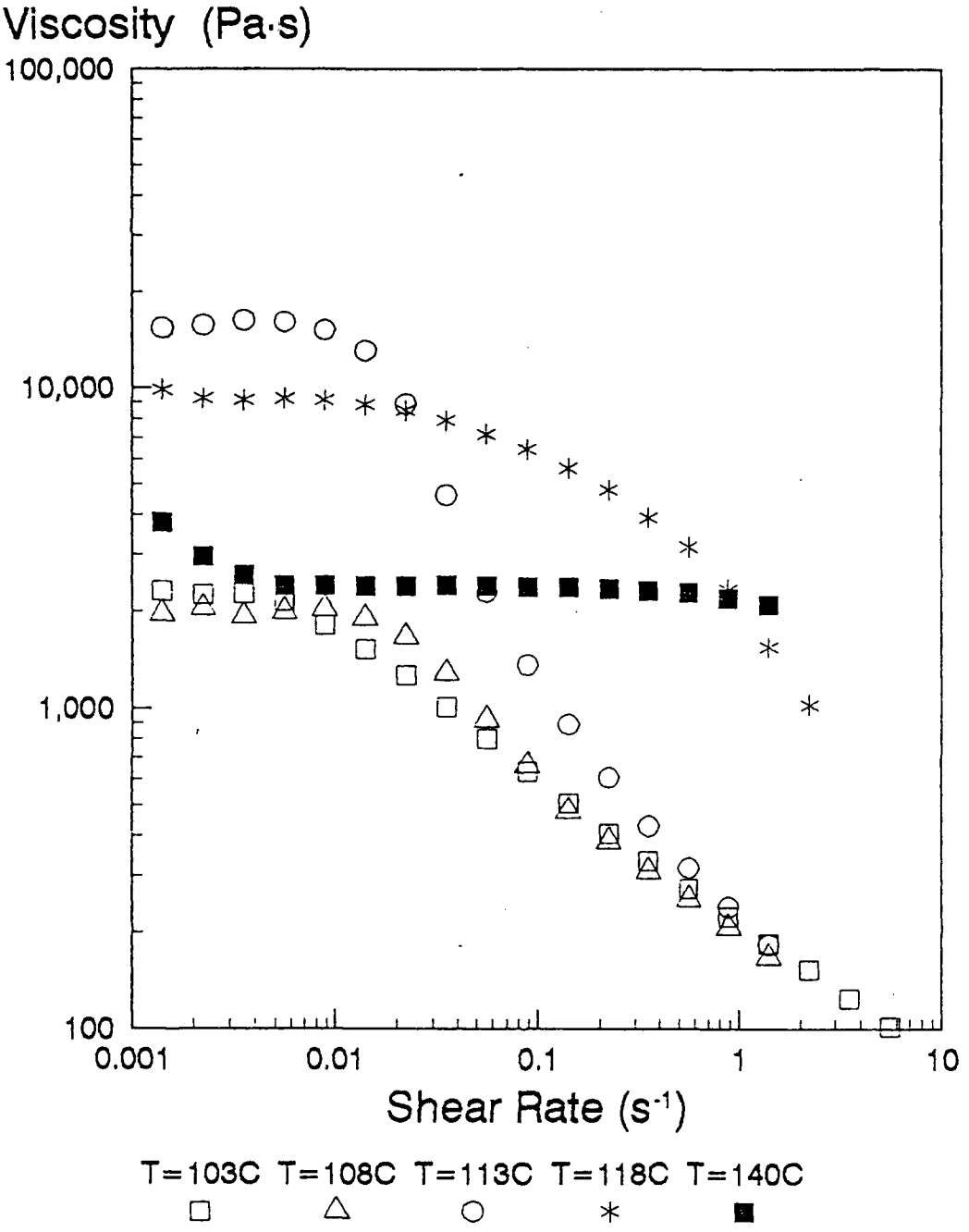

Raw Data Worksheet: \mbpe\rheom\f2torque.wk1
Grpah Name: f2torqc

Figure 4

Viscosity vs. Strain Rate

MBPE F#4 MW=32K

Baseline Torque Subtracted

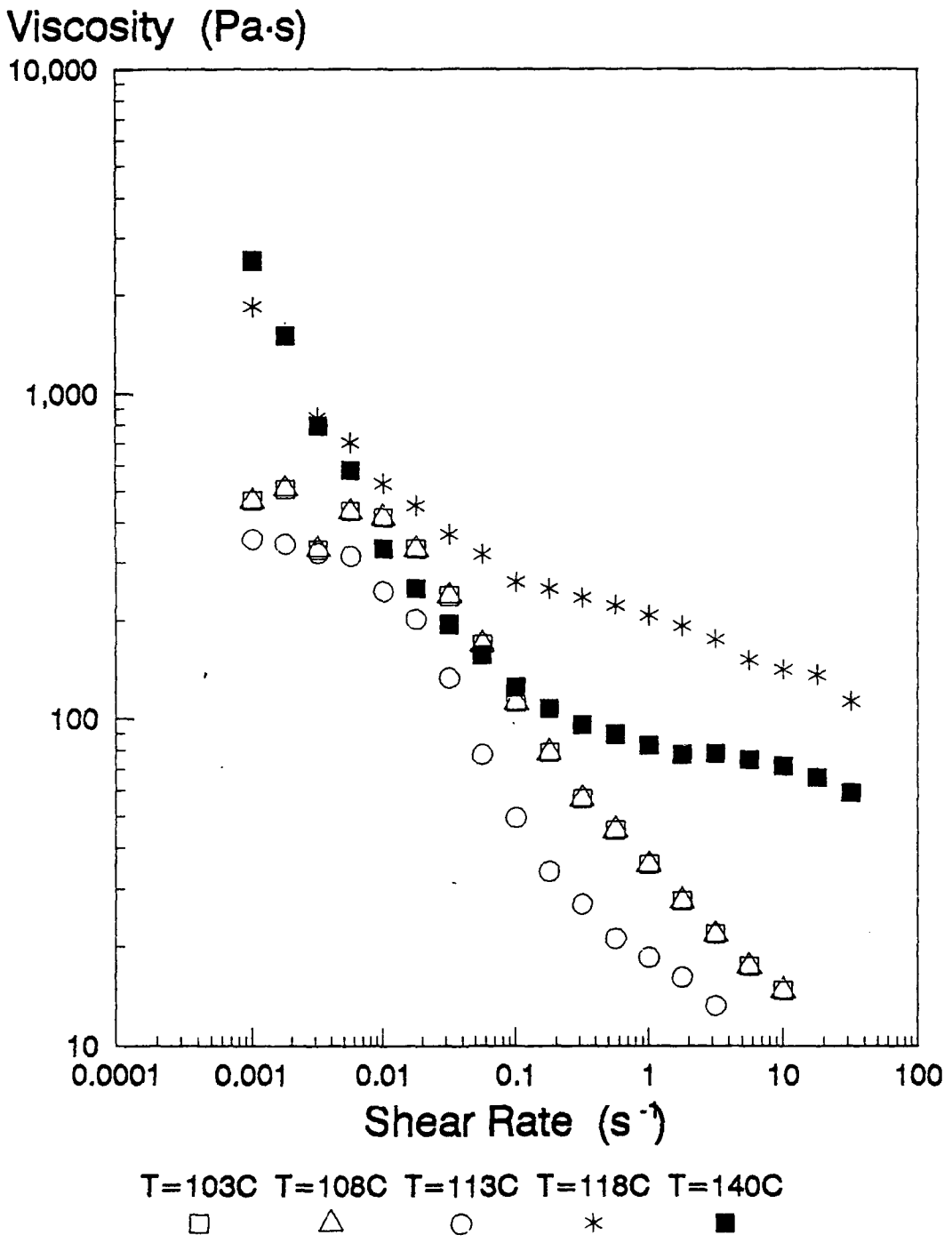

Raw Data Worksheet: \mpbe\rheom\f#4torqu.wk1
Graph Name: \mbpe\rheom\f4torq.drw
54torqd.

Figure 5

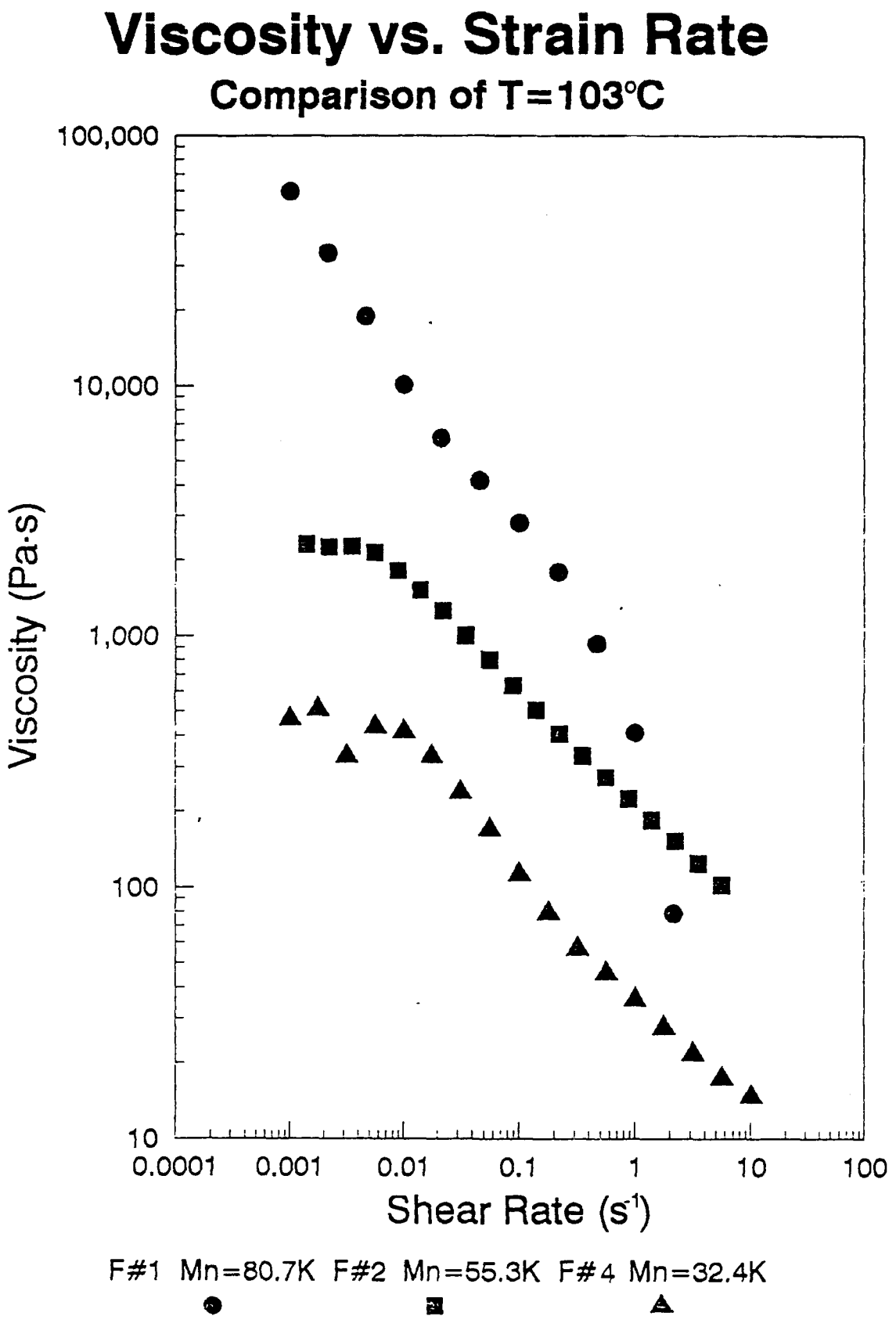
Viscosity vs. Strain Rate
Comparison of T=103°C
100,000
10,000
1,000
100
10
Viscosity (Pa·s)
0.0001
0.001
0.01
0.1
1
10
100
Shear Rate (s-1)
F#1 Mn=80.7K F#2 Mn=55.3K F#4 Mn=32.4K

Figure 6

Viscosity vs. Shear Rate

F#2 vs. F#4

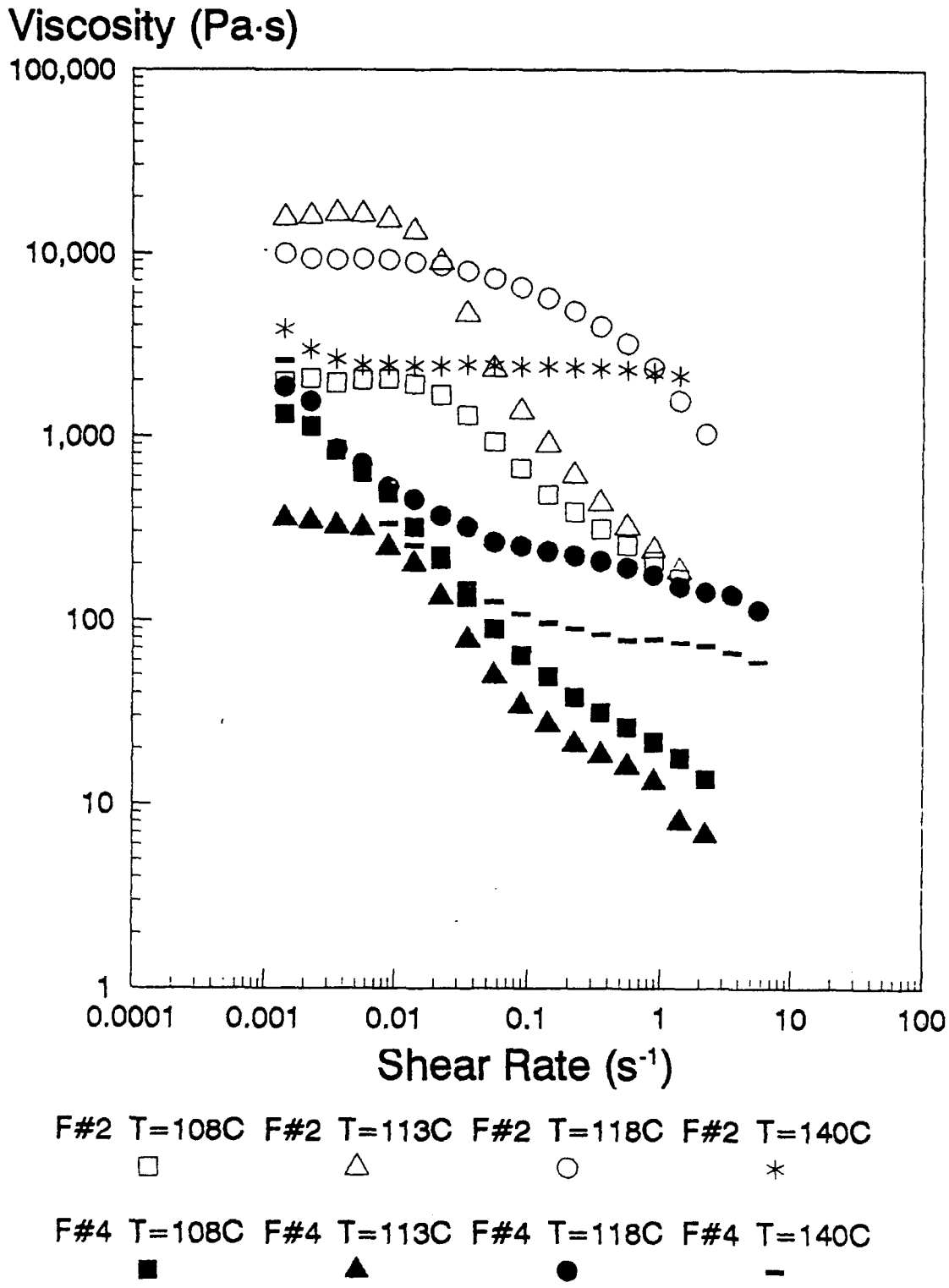

Figure 7

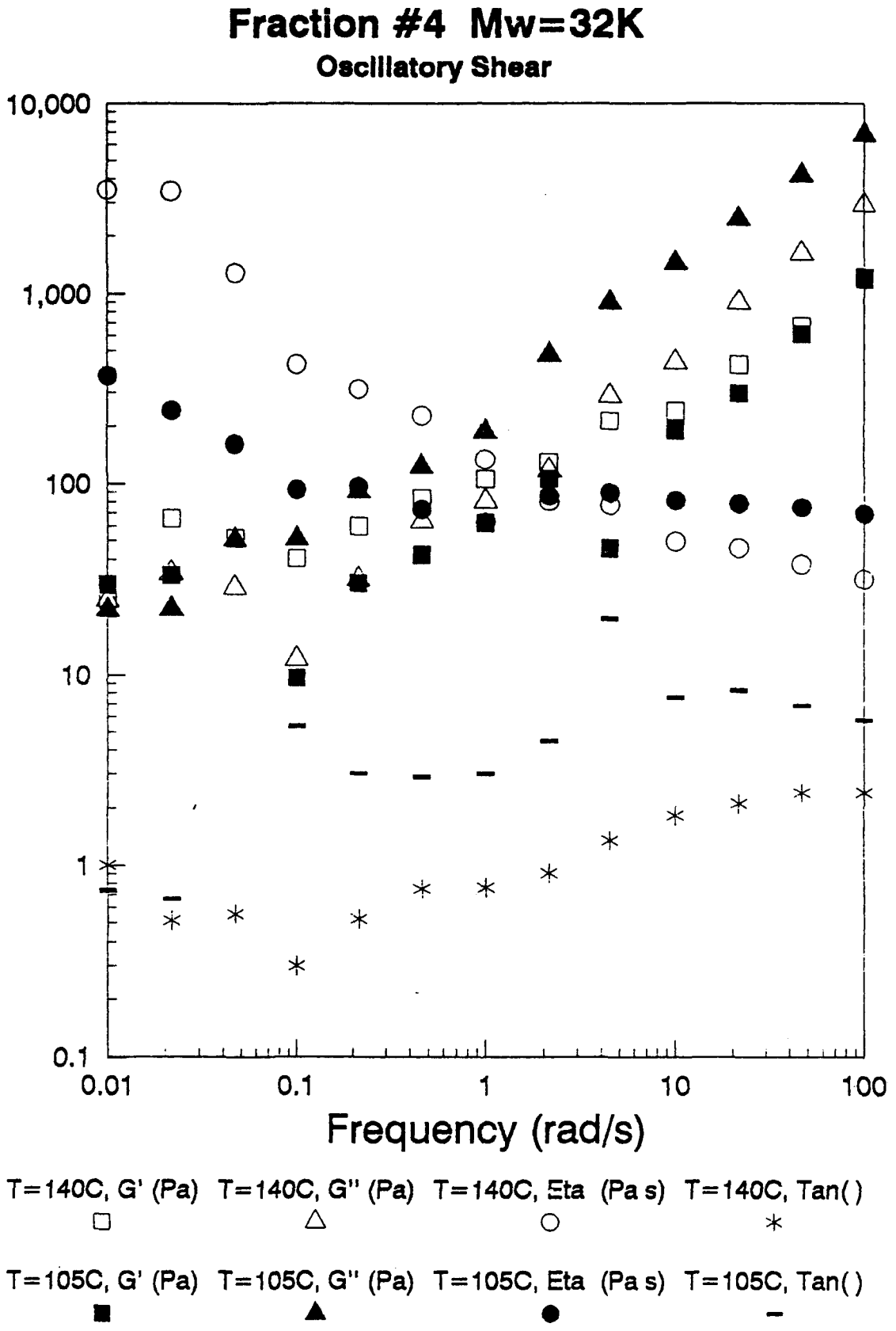
Fraction #4 Mw=32K
Oscillatory Shear
10,000
1,000
100
10
1
0.1
0.01
0.1
1
10
100
Frequency (rad/s)
T=140C, G' (Pa)
T=140C, G'' (Pa)
T=140C, Eta (Pa s)
T=140C, Tan( )
T=105C, G' (Pa)
T=105C, G'' (Pa)
T=105C, Eta (Pa s)
T=105C, Tan( )

Figure 8

SECTION 3: MORPHOLOGY

The purpose of this section was to create a link between the morphology of liquid crystalline (LCP) and crystalline polymers. The topic addressed was the morphology that results when an LCP crystallises; specifically does the liquid crystalline state leave a mark on the resulting crystal morphology, and if so, in what way is this manifest? The issue is both of fundamental and of applied interest. From the fundamental point of view it is a basic and intriguing question in view of the fact that in the LCP state, at least in its nematic variant, the chains are envisaged to be essentially in an extended chain configuration while in the usual semi crystalline polymer the chains are folded giving rise to a lamellar morphology. Chain folding arises due to kinetic reasons because from an isotropic melt, where the chains are in a random conformation, crystallization can proceed faster by chain folding than by chain extension, which nevertheless leads to a state of greater thermodynamic stability. Once, however, the chains are in an overall extended conformation, as envisaged for the nematic type LCP state, there would seem little reason why the chain should fold up on crystallization. It is therefore the more surprising that claims for lamellar crystal morphologies, indicative of chain folding, feature in current literature on LCP-s. Addressing this problem is therefore of basic importance. At the same time many technological LCP-s are, at least partly in the crystalline state in the from used as structural materials, hence their properties should be basically affected by the underlying morphology. The present investigation was motivated by the combination of the above scientific and technological considerations. Even if we did not reach down to the molecular issues themselves within the scope of the present studies, we laid down the basic thermodynamic and kinetic framework for continuing studies in this direction. In fact we can assert that the present work has been a prerequisite for productive future investigations along these lines.

Interrelation between crystallization and liquid crystal formation; a calorimetric and polarizing microscopical study on a monotropic system.

D. Heberer*, A. Keller

H.H. Wills Physics Laboratory,University of Bristol, Tyndall Avenue, Bristol, BS8 1TL

V. Percec

Department of Macromolecular Science, Case Western Reserve University, Cleveland, Ohio, USA

* Present address: Morton International, Woodstock, Illinois, U.S.A.

ABSTRACT: The crystallization of the monotropic liquid crystal forming polyether poly n nonyl 4 4' biphenyl 2 chloroethane was investigated using DSC calorimetry and polarizing optical microscopy. The principal theme was the nature of crystallization from the nematic liquid crystalline state which in the monotropic system could be directly compared with the more familiar crystallization from the isotropic melt using one and the same compound. Novel, polarizing optical structures were observed which combine features of both the usual LCP-s (fine "grains") and those of the conventional crystallizeable polymers (spherulites) with differing degrees of prominence of each according to crystallization conditions. It was inferred that in the appropriate temperature range liquid crystal formation and crystallization compete onto which a further competition, that of crystallization directly from the isotropic state and crystallization from the liquid crystal state, which had formed first, is superposed, where the latter (crystallization from the liquid crystal state) can lead to an acceleration of the overall crystallization rate. The above observations together with several further intriguing details, have led to wider generalizations. These, still within the polymer field, prompted us to consider the consequences of incomplete liquid crystal formation which compounds with the usual incomplete crystallization extending the conception of the familiar, amorphous-crystalline ratio so as to embrace also the liquid crystal state. Beyond polymers, the new findings lead to the more general considerations on metastable phases, specifically to their emergence and competition with the phases of ultimate stability. In this respect the present study on a monotropic LCP provides an illustrative example of a more general treatment presented elsewhere[8].

INTRODUCTION

The main objective of the work is to investigate the crystallization of polymers from the liquid crystal (LC) state. As known, in conventional small molecular LC materials the final crystal structure bears little or no relation to the preceding LC morphology:usually a crystallization front is seen sweeping through the sample on crystallization under the normal conditions of microscopic viewing obliterating all liquid crystal texture. In contrast, with polymeric liquid crystals (LCP) of conventional polymeric molecular weight (MW) (degree of polymerization of say 50 or more) the LC texture on the level of the optical microscope is retained unaltered.

The first objective of the present paper is to explore under what conditions can or will crystallization leave its mark on the LC morphology, or alternatively will leave it unaffected. The LC texture itself in a usual LCP is on a fine scale, as seen optically. It is constructed of small birefringent grains delineated by dark (extinguishing) boundaries. Often this texture is only manifest as a fine mottle (so called worm or tight structures [1,2]); by suitable heat treatments sometimes it can be developed to sufficient size to reveal further detail, in which case the familiar disclination network can be identified [3] as delineating what is normally referred to as grains or domains. In either case, by general experience crystallisation does not alter the appearance of this polarizing optical pattern. Of course there must be changes occurring at some level of the structure. Thus, on the level of the electron microscope striations perpendicular to the director directions have been reported, in fact "decorating" the preceding LC texture[4,5]. Such situations are consistent with the familiar lamellae (in their edge-on view in the usual thin films investigated) arising on crystallization. The issue concerning the mechanism by which such lamellae arise, or their structure on the molecular level, has not fully been faced up to: specifically is any chain folding involved (as suggested e.g. in ref. 6), and if so why should this arise in a nematic structure where the chains may be expected to be more or less extended to begin with. Having put the issue of the finer structure on the map, it will not be pursued further in this paper which will remain confined to appearances under the polarizing microscope and to associated heat effects as assessed by differential scanning calorimetry (DSC).

For comparing the crystallization of the same substance from the isotropic and from the LC states monotropic systems present themselves as most appropriate because here both can take place according to the temperature (T) range chosen. As a reminder of the essentials we recall that in a monotropic system (nomenclature quite general, not restricted to LCP's, due to Ostwald) there is only one transformation which leads from

one stable phase to another; all other transformations involve metastable phases, in the sense that such additional phases do not represent states of ultimate stability. In the case of our interest the true, potentially stable phases are the isotropic (L ≡ liquid) and the crystal (C), where, however, an intermediate LC phase can exist as a metastable state. The concept of monotropicity arises because in usual practice the LC state is realised only in one direction, i.e. on cooling from the L state, but not also on heating from the C state which would be the situation if the LC state were the phase of ultimate stability (usually referred to as enantiotropic).

The above use of the term 'monotropic' has further implications which are usually not explicitly spelled out. Consider the phase diagram of a monotropic system of our concern, which in case of a one component system is a T scale (Fig. 1a). The only transition between the ultimately stable phases is L⇔ C with T_m (melting point) as the transition temperature. T_i (isotropization temperature) is that for the L→ LC transition, where LC is metastable in a sense that it is stable w.r. to L but metastable w.r. to C (the situation for an ultimately stable LC phase corresponding to a so called enantiomorphic system is shown by Fig. 1b). In order to get into the LC range at all we need to reach T_i. We can only do this on cooling, i.e. we need to pass through the T_m-T_i range of the crystal stability regime from above without crystallization setting in there. This means that we must be able to supercool L at least by the amount $\Delta T \equiv T_m - T_i$. However, to actually obtain the LC phase this needs to appear at T_i, or not much below, which means that the LC (in contrast to the C) phase is not super-coolable, or at least only to a much smaller extent than the C phase. While this may appear self evident in the the LC field, it is also a manifestation of a wider experience applying to metastable phases in broader generality. It is a consequence of this empirically observed lower supercoolability of metastable phases that such metastable phases, if they exist, appear preferentially in the course of a transformation between two ultimately stable phases an experience expressed by Ostwald's Rule of Stages [7].

A metastable phase (LC in the present case), once arisen, will in the course of time, and/or on further cooling, transform into the phase of ultimate stability. (here C phase). It follows from Fig. 1a that once this happens there will be no reversal to the metastable phase (here LC) on subsequent heating: in this case we go directly into the ultimately stable phase L in keeping with the meaning of monotropicity.

Accounting for phase behaviour in terms of supercooling and supercoolability "relegates" the whole subject (and with it Ostwald's Rule of Stages) to a matter of rates, specifically to a competition between the rates of transformation into different possible

end states (of which only one can be the ultimately stable one). This topic has, in its wi !er generality, been taken up in a different work in this laboratory[8] to which we direct the interested reader. We are referring to it at this place because it provides the wider frame-work for the present study, or conversely, the present work represents a specific illustrative example of the more general scheme laid out there.

EXPERIMENTAL

Materials and Techniques

The material chosen for these experiments was a polyether where the chemical repeat was of the class as shown by the formula below. As seen, it consists of a "pseudo" mesogen chlorobiphenyl ethane linked by an ether linkage to the aliphatic spacer to be referred to in the abreviated form ClBPE-n. For the present experiments in particular n was chosen to be 9 the compound to be referred to as ClBPE-9.

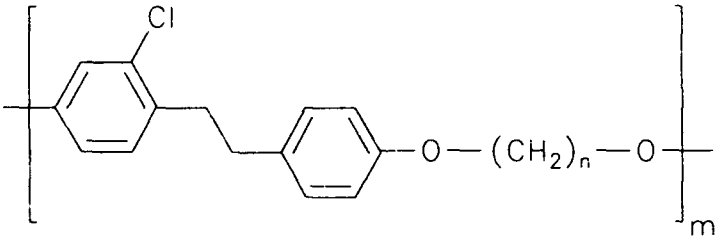

The techniques used throughout were DSC calorimetry and polarizing optical microscopy on thin film samples including observations on heating and cooling through use of a hot stage. Proceedures were standard requiring no further comment.

Phase Behaviour

Basic Experiments

The basic phase behaviour was first explored by DSC calorimetry supplemented by some general observations under the polarising microscope. The initial work consisted of determining the thermal behaviour observed on heating and cooling in the DSC. Figure 2 shows the DSC thermograms recorded on cooling (dashed line) from 130 °C to -20 °C at 10 °C/min and the DSC trace recorded on subsequent reheating (solid line) over the same temperature range with the same heating rate. On cooling there is a

sharp exotherm with an onset temperature T_{ons} = 76 °C, a peak temperature T_p = 73.5 °C, and a heat of transition of 16J/g. With further cooling two more peaks are observed; the first is a small shoulder on the high temperature side of a second, very broad peak. These peaks begin at 59 °C. Upon reheating the sample only a single endotherm with a T_{ons} = 92.5 °C and a T_p = 98.2 °C ($T_p \equiv$ peak value) is evident. The heat of fusion °H of the single melting endotherm is 68.8 J/g, equal to the summation of the heats of transitions for the exotherms observed on cooling. This indicates that the material loses its order in a single melting process despite having obtained it through multiple processes during cooling.

The pattern in Fig. 2 is consistent with monotropic LC behaviour. Specifically, with a metastable LC state appearing only on cooling. Namely, the sharp peak at 73-75 °C should be the liquid → liquid crystal (L→ LC) transition, i.e. T_i. The exothermic peak at lower T (~55 °C) should then correspond to crystallization. The single endotherm appearing at 98.7 °C on heating, being far above all the previous exotherms, is indicative of crystal melting. The fact that there is only one peak is consistent with monotropicity, i.e. that the LC state is not recovered on heating; hence there is no T_i peak.

Observations with the polarising microscope showed the appearance of a fine grained, mottled birefringent structure (such as in Fig. 3) appearing fairly suddenly at close to 76 °C on cooling. This kind of fine grained structure is characteristic of LCP's, hence its appearance concurrently with the sharp exotherm peak consistent with the latter being a T_i transition. This texture does not change on cooling to room temperature (RT) except for some increase in brightness, hence birefringence, in spite of the appearance of exothermic peaks at ~55 °C in the thermograms. This is in keeping with what was said in the Introduction, namely that in LCP's the original LCP textures are usually preserved on crystallization. That in fact the material at RT is crystalline is testified by X-ray diffraction showing sharp rings (Fig. 4) which, even without further analysis, is a finger print of a crystalline material. This texture remains unaffected on subsequent heating up till 98 °C when it disappears completely. This is in accord with the corresponding DSC trace, specifically with crystal melting at 98-99 °C.

Supporting Experiments

The above conclusions in general, and assignment of DSC peaks in particular, have been further substantiated through varying the time scale of the DSC experiments. Figure 5a shows the transition behaviour of ClBPE-9 as a function of cooling rates.

The samples were cooled from 130 °C to -25 °C with cooling rates ranging from 2.5 to 40 °C/min. The samples were subsequently reheated at 10 °C/min to observe the melting behaviour (Figure 5b). Two exotherms are observed for all cooling rates. The higher temperature exotherm exhibits roughly the same onset temperature of T_{ons} = 75 °C (after corrections for thermal lag) and the same heat of fusion of 16/J/g for all cooling rates.

On reheating, the samples previously cooled at rates less than 10 °C/min, exhibit only a single endotherm with a T_p = 95-100 °C. (Figure 5b). Samples cooled with faster rates exhibit a glass transition at 5 °C (this is missing in slowly cooled samples) soon followed by a region of exothermic behaviour: after an initial sharp exotherm (T_p = 25-30 °C) there is a broad endothermic region leading up to crystal melting. As with the more slowly cooled samples there is only a single endotherm, again with peak temperatures between 95-100 °C.

It is apparent that the response of the system to variations in cooling and heating rates is fully consistent with the monotropic behaviour established by Fig. 2. Namely, on fast cooling only L → LC transition takes place with the LC phase formed being quenched into the glass with crystallization having little or no chance to take place on the time scale involved (see 40 °C/min curve Fig. 5a). In contrast, on slow cooling, the low T exothermic peak, which we attribute to crystallization, becomes comparatively more pronounced crystallization now occurring from the LC state. We note further that the exothermic T_i peak shifts to somewhat lower T for the fastest cooling rates (Fig. 5a) while still remaining distinct, both in position and in comparative sharpness, from the small, crystallization peak which is at a lower temperature. We regard this last mentioned observation noteworthy, because it records supercoolability even for the LC state a point to take up significance in the considerations to follow.

Clearly, the three phases L, LC, and C should be distinct also regards their consistency. The small amount of material available, however, did not allow quantative rheological characterization. Even so, some qualitative tests could be conducted by shearing the samples between two coverslips which proved to be highly informative. While in the isotropic state (here 85 °C) the material is extremely viscous and considerable force is required to induce flow. No birefringence was observed during shear. At 72.5 °C, the material acquires the mottled texture and could be sheared easily as the material was displaying pronounced fluidity. As the material flows the birefringence intensity increases greatly. If held isothermally at this temperature the viscosity increases and after several minutes the sample can no longer be sheared. If the sample is cooled from

the isotropic melt directly to 45 °C, the optical texture is again the mottled texture but flow cannot be induced as the sample only fractures when stress is applied. This sample does not gain fluidity until the birefringence is lost at temperatures greater than 98 °C, whereupon the material re-enters the isotropic state.

Thus the qualitative shearing experiments as a function of T are again fully consistent with the assigned phase behaviour (Fig. 1a) where the high viscosity corresponds to the isotropic, fluidity to the LC and absence of shearability (below 45 °C) to the crystalline state.

In conclusion (at this stage): the DSC thermograms, the optical observations, the x-ray diffraction pattern and the qualitative fluidity test are all consistent with the monotropic behaviour according to Fig. 1a. In the light of the above experiments we can now place actual numbers to the transition temperatures; these feature in Fig. 1a.

Polarizing Optical Morphology on Isothermal Crystallization

The fine scale morphology of the LC phase formed on comparatively rapid cooling has already been mentioned (Fig. 3) and also that this was retained on subsequent crystallizatiion. As a next stage we shall follow the formation of the crystal morphology, on the level of the light microscope, under isothermal conditions. For this we shall take phase diagram Fig. 1a as guidance in the choice of T. Two regions are clearly delineated. 1) between T_m and T_i and 2) below T_i. In the latter (i.e. below T_i) there is a further two-fold subdivision as will emerge from the present work: far below T_i (region 2b) we have the familiar fine grained texture, such as obtained on fast cooling (Fig. 3) already referred to as typical for an LCP, while closely below T_i , region 2a, new, unprecedented effects are seen. There is no sharp boundary between 2a) and 2b) yet for the present system operationally it will be fixed at 60 °C.

Crystallization from the isotropic state (region 1) gives rise to the spherulitic morphology that is typical of semicrystalline polymers. Figure 6 shows a spherulite grown isothermally at 80 °C which displays a Maltese cross as well as a concentric banding pattern consisting of 2 sets of concentric rings. Studies using the full-wave retardation plate combined with birefringent measurements on oriented fibres, show that the spherulites are negative and thus the chains are arranged perpendicular to the spherulite radius in a manner analogous to polyethylene. Crystallization from the isotropic state always results in a small number of these large, well formed spherulites.

In region 2 the crystal morphology is more complex and it depends upon how far away from T_i the crystallization occurs. At temperatures very close to but still lower than T_i, region 2a, the crystallites maintain the Maltese crosses but the regular banding pattern is replaced by a mottle texture at approximately 75 °C (see Figures 7 and 14 further below). As the crystallization temperature decreases there is an increasing loss of the Maltese cross extinction effect and the spherulites now exhibit a mottled texture void of both Maltese cross and banding patterns (Fig. 8a). The circular symmetry of the orientation giving rise to the birefringence, however, becomes apparent by viewing through a full wave retardation plate (Fig. 8b). For crystallization temperatures lower than 74 °C two different morphological entities became apparent. Both morphologies have the mottled texture, lack a distinct Maltese cross, and are negative. Figure 9 contains the two morphologies during in-situ crystallization at 72.3 °C . The bright morphology (relative to the liquid crystal background) is labelled as M1 and is readily apparent but in the second morphology M2 is obscured by the surrounding liquid crystal (Fig. 9a). the M2 morphology is very difficult to observe but by using the full-wave plate they can be differentiated from the liquid crystal background (Fig. 9b). The distinguishing features between the two morphologies is the birefringence differences relative to the liquid crystal phase background and also the nature of the crystallite edges after melting away the residual liquid crystal phase (see heating sequence Fig. 9c - 9f later. Here the M1 morphology has an edge that is very rough or jagged and the birefringence intensity change observed upon going from the interior to the exterior of the spherulite is a gradual decrease; in contrast, the M2 morphology has a definite, more distinct boundary). Although the distinct Maltese cross and the regular banding patterns are lost at lower crystallization temperatures, the crystallites still exhibit some preferential orientation with circular symmetry as revealed when viewed with the retardation plate. Both the M1 and the M2 morphologies were found to have negative optical characters. Thus, like the spherulites grown from the isotropic phase the polymer chains are arranged perpendicularly to the radius as usual in semi crystalline polymers.

Below T_c ~70 °C we enter progressively the crystal morphological region defined above as 2b. This is the fine grained structure indistinguishable from the characteristic LC texture (Fig. 2). Here the liquid crystal has transformed into true crystal without any change in the texture on the level of the optical microscope; only the intensity, hence the underlying birefringence, has increased as assessed here by visual impression.

Crystallization Rates

Crystallization rates could be assessed both by calorimetry (DSC) and by observing the evolution of the morphology microscopically.

For the DSC determinations the development of the crystal endotherms (as assessed on heating) was registered as a function of crystallization time (t_c) at preselected constant temperatures (T_c). The heat of transition observed then provides a measure of the degree of crystallinity after a given t_c, which, if followed as a function of time, then provides a measure of the rate of crystallization at a given T_c. Fig. 10 is an example of the development of the melting endotherms formed at T_c = 72.7 °C as a function of crystallization time t_c. This crystallization temperature represents crystallization from the liquid crystal state since it is several degrees below T_i. At short t_c the heating traces reveal a pronounced endotherm located at around 80 °C, i.e. several degrees above the crystallization temperature. The peak is fully developed even after short-crystallization times and we interpret it as representing the isotropization of the liquid crystal phase.[1]

In addition, there is a mere trace of a further endotherm at the much higher temperature of 98 °C. This we interpret as corresponding to melting of crystals. As the crystallization time is increased the liquid crystalline peak decreases in magnitude and the melting endotherm of the crystalline phase becomes more pronounced. The size of this endotherm increases with time at the expense of the liquid crystal endotherm which we attribute to the liquid crystal being converted into the crystalline solid. The liquid crystal endotherm is absent at crystallization times greater than 45 minutes and the crystal endotherm reaches its maximum size at approximately 80 minutes. The behaviour for crystallization at other temperatures below T_i was found to be similar: at each temperature there was a rapid development of the liquid crystalline phase followed by its slower conversion into the crystalline phase.

Crystallization from the isotropic phase (T_c > 79 °C) was similar to that observed for semicrystalline polymers. The liquid crystal to isotropic endotherm was not present and only the crystal melting endotherms were observed. The size of the melting endotherm increases with t_c, the increase being slower for higher crystallization temperatures.

---

[1] The 80 °C quoted here is about 3-4 °C higher than the 76-77 °C obtained in the course of the other experiments for T_i throughout this work. When this difference was noticed at the time of writing there was no more material available to assess whether this difference is real or due to some systematic error. Regrettable as it is that this uncertainty needs to remain unresolved. The numerical discrepancy is small compared to the large T difference between the two peaks, hence cannot affect their attribution and consequently the argument based on them.

The rate of the overall crystallization, thus assessed through the evolution of the endotherm at T_C both above and below the isotropization temperature is illustrated in Figure 11. Here, for a single parameter representation of the rates, we take the time required to reach a melting endotherm of 10J/g ($logt_{10\ J/g}$ vs. T_C plots). The dashed line represents the boundary between the crystallization from the isotropic and the liquid crystal states. The interesting feature of the overall crystallization behaviour is the change in the crystallization rate immediately above and below T_i. At lower temperatures the material crystallizes rapidly and the rate decreases with increasing T_C as indicated by the slope of the line of 0.132. There is an abrupt change in the slope upon going to temperatures above T_i. Now the material crystallizes more slowly, and the decrease in the crystallization rate is greater with increasing temperature as evident by the much larger slope of 0.536.

The above results show that, although ClBPE-9 can crystallize from either the isotropic melt or the liquid crystalline phase, the intervention of the metastable liquid crystalline phase changes the crystallization behaviour.

For the morphological assessment of the rates we can subdivide the overall crystallization rate into nucleation and growth. Within the isotropic region (region 1) this follows the established pattern in crystallization studies by respectively counting spherulites and measuring their diameter as a function of time. Thanks to seeing visible spherulites even below T_i this procedure can now be extended into the LC region 2, but only so far as spherulite entities remain discernible for measuring the rates of nucleation, and as long as their boundary remains sufficiently distinct to enable measurement of their diameter. As seen from Figs. 8,9 the range of visibility could be substantially extended below T_i by the use of the first order red plate which enabled spherulites to be detected and measured even when without the use of this plate the image of the spherulite merges indistinguishably into the grainy background. Clearly, these measurements could only be pursued down to the low T limit of the region we defined as 2a.

Figure 12 shows the linear growth rates of the crystallites as a function of crystallization temperature, the dashed line again representing T_i. We see that the liquid crystal phase does not dramatically change the linear growth rates. In contrast to the overall rate measured by DSC here the growth rates increase continuously with decreasing temperature in the vicinity of T_i. At approximately 73 °C, the behaviour becomes more complicated as two morphologies are growing simultaneously. The

linear growth rates of both morphologies increase with decreasing T_c but M1 grows faster by a factor of approximately 1.5 compared to the more slower growing entity M2.

The nucleation density per unit time was determined as a function of crystallization temperature. Figure 12 shows a plot of the nucleation density per unit time versus the crystallization temperature, The nucleation densities observed during crystallization from the isotropic state are low and the values range between 0.038 and 0.51 nuclei/mm^{2}hr for crystallizations at 81 and 76 °C respectively. On lowering T_c into the liquid crystal region the nucleation density increases. A decrease of 14 °C from 76 to 62 °C results in nearly a five order increase in the magnitude of the nucleation density. Nevertheless, there is no obvious discontinuity at T_i, an impression confirmed when plotting on a logarithmic scale (including further date points at the high rate end) which gave a perfect straight line (not shown here separately).

The two morphologies observed below 72 °C exhibit dramatically different nucleation densities. The values used in Figure 13 are those of M2, the slower growing morphology. Its nucleation density greatly exceeded that of M1. In a typical sample area of 2 cm^2, the number of M1 crystallites would never exceed 12 compared to the number of the M2 crystallites which would number in the hundreds or thousands. For this reason no meaningful measurement of nucleation rates of M1 was feasible.

The most important point to note is that neither growth (Fig. 12) nor nucleation (Fig. 13) did display any obvious discontinuity when passing through T_i in contrast to the clear discontinuity observed in the calormetrically assessed overall increase of crystallinity.

Optical Observations on Melting Effects

The spherulitic structure in Fig. 6 was seen to melt at around 98 °C on heating as to be expected from crystal entities on the basis of the DSC thermograms. When cooling fast to below 70 °C then the mottled structure appeared as already described. Heating immediately after its emergence this mottled structure disappeared at ~ 76 °C. In contrast, if the sample was cooled rapidly to say 45 °C and held there for times commensurate with crystallisation, as judged by DSC (e.g. appearance of lower exotherm in Fig. 2), then the same mottled structure only cleared at 98 °C. All the above is fully consistent with expectations from our phase assignment, including the metastable T_i transition. Specifically, it distinguishes between crystal morphology formed in region 1 and LC morphology below T_i (region 2) and further, within the

confines of the mottled LC type morphology it discriminates between the true LC structure and the crystalline structure of otherwise identical appearance into which it transforms in the T region 2b. This is as might be expected. More interesting, however, is the behaviour on heating of textures arising in the T region 2a.

In the T region 2a we have three kinds of morphology, the overall grainy texture, the M1 and the M2 spherulites. The heating experiments to be described were to test and compare their thermal stability as seen under the polarizing optical microscope. The series of photographs in fig. 9c to 9e display the melting process of ClBPE-9 crystallized at 72.3 °C, i.e. resorting to the same sample and to the identical field of view as in Figs. 9a and b in the course of heating at 5 °C/min. To recall, Figs. 9a and 9b show the morphology as arising after crystallization for 60 minutes. A single bright M1 entity is apparent within the fine grained matrix and through the use of a full-wave retardation plate several M2 crystal entities can be identified. As already stated, the same M2 entities are hardly discernible when viewed without the full wave plate (Fig. 9a). They remain hidden within this background during the first stages of heating but they become distinct even without the full-wave retardation plate (Fig. 9c) when the temperature 74.5 °C is reached in the course of the heating experiments. The reasons for the visibility of the M2 entities rests in two factors: the decrease in the intensity of the grainy background and the increase of the intensity of the M2 entities where the latter effect is the larger up to a temperature of closely 76 °C. That the above assertion on the changes in brightness is real also in the absolute sense was ascertained by standardising exposure and photographic processing conditions.

Eventually at 76.5 °C the grainy background starts fading away altogether and the crystal entities, both M1 and M2, stand out clearly against a dark background with, particularly M2, greatly enhanced brightness even on an absolute scale. At 77.5 °C the last trace of the grainy background has disappeared (Fig. 9d). At this stage the edges of the M1 morphology appear to be rescinding as apparent by the decrease in size upon going from 74.5 °C to 77.5 °C. The edges of the M1 spherulites have now taken on their jagged appearance. The M1 morphology doesn't melt entirely and its final size remains constant until total melting at higher temperatures. The M2 morphology does not change size but its brightness has increased further. Beyond this stage there is no further change in either M1 or M2 until approximately 94.5 °C. At this point there is a loss in birefringence intensity in both M1 and M2, but the effect is more apparent and unusual in M2. Here the loss of birefringence occurs mainly in the centre until the only remaining birefringence is a bright rim which surrounds the area once occupied by the crystallite (Figure 9e taken at 94.5 °C). At this stage the M1 crystallite still remains

although there is an even loss of birefringence intensity across the crystal entity and a decrease in its size. With further heating to 98 °C both the remnants of the M1 morphology and the M2 rims melt simultaneously.

If the sample is quenched to room temperature from 94.5 °C the liquid crystal background again quickly develops. The M1 crystallites have increased in size and in birefringent intensity. The rim of the M2 crystals is still evident, and the birefringence intensity within the rim is greater than that of the liquid crystal background outside the rim (see Figure 9f).

The sequence of Fig. 9c - 9f will be discussed further below. At this stage we only make the comment that the main features are consistent with the grainy background corresponding to material in the LC state disappearing at T_i while the M1 and M2 entities, corresponding to crystalline material, disappear at T_m where, in addition, more crystalline material arises in the course of heating, particularly within the M2 variety However, the effects in Figs 9c and 9f are altogether novel and lie beyond the scope of a straightforward interpretation.

For completeness we add Fig. 14. This corresponds to a stage in heating equivalent to Fig. 9c but for a sample initially crystallized at 75.3 °C, i.e. again in region 2a but now closer to T_i. Here the M2 entities are apparent even without using a retardation plate, even at room temperature (as in Fig. 7). They become much more pronounced displaying a clear Maltese Cross above T_i thus now appearing more like conventional spherulites, yet still possessing a mottled structure.

Another characteristic of the crystallites formed from the liquid crystal state is the appearance of signs of faceting of the edges. The faceting is most apparent for the M2 morphologies. In Figures 9d and e) the M2 morphologies are roughly faceted into hexagons with the regularity of the edges varying from crystallite to crystallite. The faceting is not as apparent in the M1 morphologies because of the lack of a distinct boundary.

Memory Effect

When investigating the melting behaviour an interesting memory effect was observed. This is associated with the formation of the LC phase arising after melting a previously crystallized sample. Figure 15 is from a sample which had been crystallized at 73 °C and was then heated to 130 °C for several minutes. Upon quickly cooling to below T_i ,

the liquid crystal phase developed but the birefringence intensity was very much reduced within the areas previously occupied by the crystallites. At this stage the material is not crystalline, as evident by the fact that the entire birefringent background disappears at T_i upon heating. In fact, new crystals can grow from the centre of the dark areas. Fig. 15 shows a crystal entity growing from the interior of one of the dark areas. This entity displays a Maltese Cross like a spherulite yet also exhibits the faceting already described. It must be pointed out that this behaviour exists only for samples which had been previously crystallized, **and** has only been kept within the melt region for a limited length of time (few minutes). After a prolonged time, e.g. longer than 4 minutes, the material returns to normal behaviour.

DISCUSSION

General Considerations

The principal objective was to compare crystallization from the nematic LC state (LC $\rightarrow$ C) transition with crystallization from the isotropic state (L $\rightarrow$ C transition). Such a comparison, using the same material, has become possible thanks to the monotropic nature of the system chosen (see Fig. 1a). To recapitulate, here the crystal is the ultimately stable phase from T_m downwards. However, at T_i where $T_i < T_m$, a further phase, here LC, can appear which is metastable in the sense that it is stable w.r. to L but less stable than C. As already stated in the Introduction, this metastable LC phase will appear first in the course of usual cooling, subsequently transforming into the ultimately stable C phase. It is in the nature of monotropicity that on subsequent heating nothing will happen while passing through T_i (hence no re-emergence of LC phase) the system going over directly into the melt (L) at T_m. The DSC traces in Fig. 2 are fully consistent with the above assignment: they display the monotropic behaviour in a clear cut manner providing the actual values for T_m and T_i in the phase diagrams (Fig. 1a and abscissa of Fig. 16). The overall optical observations are in full accord with this assignment and so are the qualitative tests for consistency which could distinguish between the LC, L and LC phases by the higher deformability (fluidity) of the LC phase, thus identifying in its own way the metastable LC regime.

The most conspicuous difference between the L $\rightarrow$ C and the LC $\rightarrow$ C transition is morphological even as assessed on the level of the polarizing optical microscope. Transition L $\rightarrow$ C as conducted in T region 1 (Fig. 6) gives rise to spherulites as familiar in polymer crystallization studies, while transition LC $\rightarrow$ C at sufficient low T,

i.e. in region 2b (Fig. 3), retains the fine grained structure of the initial LC state even if with enhanced birefringence (brightness) as usually experienced with LCP's. However, a highly unusual situation arises within the T range in between regions 1 and 2b which we here term range 2a (for definition of regions see Fig. 1a) where both features, spherulites and fine grains, are seen together: the spherulites are seen to evolve from a fine grained mottle becoming gradually more pronounced and the spherulites correspondingly less distinct on going deeper into the T_i region. (Figs. 7,8,9, and 14).

For an attempt to interpret the novel structure features we need to go back to the metastable LC phase first. As indicated in the Introduction the reason for the LC phase appearing at all is kinetical: for a given supercooling ΔT (as referred to the respective transition temperature T_m and T_i) the LC phase evolves much faster. Or putting it in another way, a much smaller supercooling is required for the LC phase $(\Delta T)_i$ then for the C phase $(\Delta T)_m$ for it to appear on a practicable time scale, the reason why the LC phase appears under normal conditions of cooling.

From the more restricted view of LC studies the above behaviour may not appear surprising since it is general experience that the formation of the LC phase is faster than that of the C phase under most circumstances irrespective of whether monotropic (Fig. 1a) or enantiotropic (Fig. 1b), when compared at identical respective ΔT (which can be close to $\Delta T = O$, in fact the LC phase is normally considered as requiring no supercooling at all). Nevertheless, the situation relating to monotropicity has wider implications. Namely, as already stated in the Introduction, in a situation where the formation of two phases are in competition, it is the one that is metastable which usually "wins". This in the case of a transformation from a disordered liquid to an ordered solid means that it is the state which is intermediate between the liquid and the crystal form of ultimate stability which appears first on a normal cooling experiment (where this intermediate state can be an LC or some other mesophasic state or a less perfect or stable crystal polymorph). As already referred to this general experience is embodied in Ostwalds Rule of Stages which states that a transformation from one ultimately stable state to another proceeds via stages of metastable states in the sequence of increasing stability whenever such metostable states exist.

Although Ostwald originally considered the Stage Rule to be an expression of some intrinsic property of matter any rational justification of the underlying empirical experience on which the Rule has been founded must rely on rate considerations along the lines laid out above (see ref 8). In wider generality, to predict which phase will appear first in noticeable amount we need to compare their evolution as a function of T

(which of course will relate to the respective ΔT -s) i.e. enter rates as a separate co-ordinate into the phase diagram. For a single component system this is easily done in a two dimensional representation. The general base on which to scrutinise Ostwald's Stage Rule and which , also pertinent to our present monotropic LC system, is as in Fig. 16. As seen, the rate for the stable system will start off only very slowly as from $(T_m)_{stable}$ (which is $(T_m)_c$ in our case) while for the metastable phase it rises much faster as from $(T_m)_{meta}$ (which is T_i in our system). This means that the two rates cross at T^+. Fig. 16 thus defines the T regime where the metastable phase is expected to dominate and with it also sets limits to the validity of Oswald's Rule of Stages, namely confining it to below T^+. Above T_m we only have the stable phase and in between, in the range of T_m - T^+ the two phases will compete on more or less equal terms. The relevance of Fig. 16 to our system (and vice-versa) will be immediately obvious). We see that the regions defined by $(T_m)_{stable}$, $(T_m)_{meta}$ and T^+ as in Fig. 16 the correspond to the division into T regions 1) 2a) and 2b) adopted already in this paper[2]. now defined in terms or rates.

To pursue the subject still along the present general lines somewhat further we need to consider that the overall rate (R) of the phase evolution is composed of nucleation and growth where growth itself may be nucleation controlled (secondary nucleation), or at least controlled by an activation barrier, associated with successful attachment probability (α) and inception of new surface (β). Collectively this can be expressed as

$$R \equiv N = \alpha e \frac{-\beta}{T\Delta T} \qquad 1$$

where N stands for nucleation rate (primary or secondary in the above sense, whichever the overall rate determining factor) and α and β contain the parameters relevant for a given system, β also depending on the dimensionality of the nucleation. Where several phase variants are possible as end products e.q. 1 will hold for each with the appropriate values for α and β. A general treatment of the situation for two competing phase variants [8] has shown that the situation such as in Fig. 16 with one cross-over point closely below $(T_m)_{meta}$ will arise when the conditions

---

[2] The above procedure of taking $(T_m)_{meta}$ and T^+ as the explicit boundaries between the T regions as defined by rates is adopted for ease of presentation so as to have some identifiable fixed points. In reality region 2a) will start somewhere below $(T_m)_{meta}$ because the rate at $(T_m)_{meta}$ itself is still zero, and region 2b will start somewhat below T^+ where the rate for the metastable phase becomes much faster.

$$\alpha_{meta} \geq \alpha_{stable} \quad \text{a)}$$

and (2)

$$\beta_{meta} \leq \beta_{stable} \quad \text{b)}$$

are simultaneously fulfilled. It could then be shown by separate argumentation[8] that conditions 2a and b are indeed the most plausible ones for the situation under consideration.[3] In summary at this stage: metostable phases are, as a rule, the first to appear in the course of the usual phase transformation in accordance with Ostwald's Rule of Stages, nevertheless this is only one, even if the most feasible one, out of several other possibilities which could arise from rate considerations based on Eq. 1. Even in the usually occurring case where eq.2 applies, the prominence of metastable phases (hence validity of Ostwald's Stage Rule) has an upper T limit as defined by (or related to) the cross-over in rates as depicted by Fig. 15. We maintain that the observations on the presently used monotropic LCP system reported in this paper are interpretable in terms of the general considerations just outlined, or conversely, they provide an illustration to the reality of the most frequently occurring situation such as represented by Fig. 16.

Specific Interpretation

For the monotropic (ClPBE-9 polymer the rate curves in Figs. 11,12,13 fall into the pattern of the curve marked "stable" in Fig. 16. We do not have the rate curves corresponding to the one marked "meta" in ClPBE-9 because here the rates were too fast to measure with our techniques by which, for all intents and purposes, LC formation appeared instantaneous as soon as a critical T was reached on cooling (clearly equal or close to $(T_m)_{meta} \equiv T_i$.) Nevertheless, even by a priori considerations the L $\rightarrow$ LC transformation cannot be infinitely fast and thus must occur over a finite time span at the appropriate temperature. Concrete evidence for this is provided by Fig. 5a. Here there is a pronounced downward shift of the L $\rightarrow$ LC exotherm along the T axis with increasing cooling rate, about 7 °C when going from 5 °C/min to 40 °C/min. As the peak corresponds to the steepest slope in a curve depicting degree of phase transformation v. time, hence approximately to the half time of the phase

---

[3] Under conditions other than specified by eq.2 the following situations can arise: for $\alpha_{meta} \leq \alpha_{stable}$ and $\beta_{meta} \leq \beta_{stable}$ two cross - over po int s; for $\alpha_{meta} \geq \alpha_{stable}$ and $\beta_{meta} \leq \beta_{stable}$ single cross-over point but very far below $(T_m)_{meta}$; for $\alpha_{meta} \leq \alpha_{stable}$ and $\beta_{meta} \geq \beta_{stable}$ no cross-over points. While all these cases are possible analytically they are less reasonable or outright unreasonable physically and, except for one possible instance of a double cross-over [9], are not observed experimentally.

transformation, the above peak shift with cooling rate demonstrates in the first place, that the rate of LC formation is finite, and further, that in the present case it should have half times ranging from a few seconds to about 1 minute in the temperature interval in question. Hence, equipped with suitably sensitive detector rates of LC formation should be measurable. At this point all we can say is that qualitatively rate relations such as in Fig. 16 must apply, i.e. the equivalents of the "stable" and "meta" curves must cross with the "meta" transformation rate, while fast, being finite.

Fig. 11 reveals a discontinuity in overall rate at T_i (77 °C) in a sense that crystallization speeds up at the temperature where LC also forms by all the evidence listed. This is readily interpretable by the expectation that at T_i most of the material undergoes L $\rightarrow$ LC transformation first with an LC $\rightarrow$ C transformation to follow where the latter is faster than the direct L $\rightarrow$ C transformation; in other words that crystallization is faster from the nematic than from the isotropic state.

A similar effect, even in a more pronounced form, again as assessed by DSC, has also been observed independently in a different work [10], with which one of us has had association, from which we shall briefly quote here. In that work by Pardey et al. the materials were a series of monotropic polyimides were the positions of T_i w.r. to T_m (and chiefly T_g) varied systematically according to chemical composition (length of spacer segments). On the whole, the T_i values were much further below T_m than in the present polyether, in fact at T-s which are below the maximum in the crystallization rate (R) v. T curves, i.e. where R is falling with decreasing T (in other words T_i is approaching T_g). Here this drop in R with decreasing T is in fact reversed on reaching T_i (as approached from above) leading to an actual pronounced rise in R with falling T passing through a second maximum before becoming zero at T_g. One of such R v. T curves is reproduced in Fig. 17. Clearly Figs. 11 and 17 are complementary providing examples for acceleration of crystallization at T_i (and below), in the first case at the T_m side in the second at the T_g side of the respective R v. T curves.

However, a discontinuity such as in Fig. 10 is not discernible in the rate v . temperature curves as assessed visually under the optical microscope, neither in the growth (Fig. 12) nor in the nucleation (Fig. 13) process which by this technique could be identified and followed separately. (There is no corresponding information available in the case of the polyimides from which Fig. 17 was taken). To account for this difference the following interpretation suggests itself. The DSC technique records all the transformations that are taking place, i.e. L $\rightarrow$ C plus LC $\rightarrow$ C, which shows the discontinuity in rates as anticipated. In contrast, the optical image reflects the

characteristics of the familiar crystallization from the isotropic state (namely spherulite formation). If we therefore assume that the optical image records L → C transformation even below T_i then, qualitatively at least, all the main observations fall into place. Above T_i, i.e. in range 1, the situation is clear: all the phase transformation is of the L → C kind in any case. Beneath T_i the above attribution implied that we still have some untransformed isotropic material, and it is the crystallization of this material that we are recording.

All the above is fully consistent with the foregoings, namely that we have two processes L → LC and L → C which are competing in range 2a in accordance with Fig. 16. Accordingly, the L → LC process should give rise to the grainy texture and the L → C one to the spherulite. The further we go downward in T the stronger will be the dominance of the L → LC over the L → C process; hence the consequent graininess of the spherulites until the spherulites become indiscernible, and we enter the T region which we have been denoting as 2b (see Figs. 1a and 3). Here, the direct crystallization, namely the L → C process should become negligible and crystallinity will be attainable only through the LC → C process; i.e. through transformation within the LC domains leaving the grainy texture, as seen on the level of the light microscope, unaltered. The latter process, namely LC → C transformation within the LC grains, is expected to take place already in region 2a where it should be partly subsequent to and partly simultaneous with the direct L → C process which gives rise to the spherulites. In addition to providing consistency with the main visual observations the above picture would also tie in with the differences in rate behaviour as assessed by DSC and POL microscopy. Namely POL microscopy would only register the rate of the L → C transformation which is not expected to show any disconuity at T_i while the DSC the combined process of L → C plus LC → L with the anticipated acceleration of the overall rate due to the latter.

While the above scheme would account for the overall features linking the combined consideration of phase diagram and kinetics (as in Fig. 16) with the microscopic morphology it has further implications raising some conceptual issues and also some unanswered problems to which we shall now turn.

The first implication is that the L → C process starts from widely separated nuclei and spreads outwards creating long range order of circular symmetry within thin film samples despite the facts that, by the above picture, LC grains are arising in its way. Alternatively, the LC grains may already be present throughout but not yet comprising all untransformed isotropic material. In either way the situation arises that the

spherulite has liquid crystal content, and in the second alternative, in addition, that the liquid crystal itself has an isotropic, hence amorphous content. Further, as a combination of the two, a spherulite may have both liquid crystal and isotropic contents. The latter would be in addition to the conventional "amorphous content" as constituting the crystallinity deficiency of a traditional semi crystalline polymer. The new conceptional possibility thus arising would be the "liquid crystal content" of a crystalline polymer (thus a C:LC ratio) and the amorphous content of a liquid crystal (thus on LC:L ratio). In the first instance such a situation should mainly be envisaged as a transient state where all liquid crystal would eventually become true crystal, and similarly, all isotropic liquid associated with LC domains become liquid crystal which in turn would then become crystal thereafter turning the whole system into a conventional semi crystalline polymer with its appropriate amorphous content.

On further thought, within such a multi level structure and phase hierarchy, one may envisage an extension of the conventional picture of amorphous material being trapped between crystals giving rise to the familiar limited crystallinity, hence amorphous - crystalline ratio even beyond the final stage of crystallization. Thus, one may envisage the possibility of a trapped LC content within the final crystal aggregates, and even trapped L content within the final LC texture component thus arisen imparting a widened meaning to the conventionally understood concept of "degree of crystallinity", or to the here suggested "degree of liquid crystallinity", also allowing for a combination of the two. It is to be strongly emphasized that all the above refers to departures from equilibrium (including metastable "equilibrium") situations where the system is prevented from attaining its minimum free energy, be it on absolute or (for metastable phases) "local" minimum, through steric hindrances, entanglements etc. and is not related to order deficiencies characteristic of an equilibrium state (such as e.g. expressed by a T dependant order parameter in LC systems).

The morphological effects observed on heating reinforce some of the above arguments but also create new issues. The most salient effect is that the field between the spherulites darkens and the grainy structure there disappears close to T_i as seen between crossed polaroids. (Figs. 9c, d). This means that the underlying material there is still in the LC and not yet in the C state. This immediately raises the question of the origin of the acceleration of the overall crystallization rate of T_i indicated by Fig. 11 (and Fig. 17 in a different work). Namely, even if in the T range 2a the L $\rightarrow$ LC and the L $\rightarrow$ C rates are broadly comparable (as envisaged throughout range 2a) the evolution of the crystal is expected to accelerate once in the LC state. There is however, no sign of this by the microscopic observations, at least for the interspherulitic grainy background.

This at the T_c of the initial isothermal crystallizaiton experiment stays in the LC state, at least on the time scale in question, while the spherulites, in their appropriate mottled form, are seen to grow at a rate appropriate to the particular T_c (Fig. 12).

However, in contrast to the grains of the interspherulitic material, the spherulites themselves, hence also the grains contained by them, become noticeably brighter on subsequent heating. (Fig. 9c). This must mean that their birefringe, hence their state of order increases on heating even at the temperature (T_i) where the grains outside the spherulites melt (Fig. 9d). If all grains have LC structure initially then this must mean that grains within the spherulites are crystalline, certainly at the stage of their final melting at T_m. They may have crystallized from the LC state on heating or may already have become crystalline while still at the intended T_c in the initial isothermal crystallization experiment. It is this latter case (LC $\rightarrow$ C transformation still while at T_c and perfectioning on heating) which we prefer as it allows for the most comprehensive interpretation of our experiments. First, because a primary phase transformation, such as L $\rightarrow$ C or LC $\rightarrow$ C, is not expected to become faster on raising the temperature; the increase in birefringence on heating therefore indicates a secondary, i.e. annealing process, facilitated by the increase in mobility at the higher temperature, consistent with the grainy structure having become crystalline before heating. This of course implies an initial state of lower "degree of crystallinity" so as to allow for the perfecting of order on subsequent heating indicated by the increase in birefringence.

The above interpretation has the added attraction that it would allow for the acceleration of total crystallization following LC formation, missed in the preceding paragraph dealing with the interspherulitic material. The additional fact that now emerges is that such an effect would only apply to those LC domains which are located within the spherulites, but not to those outside. This situation would restore our original suggestion on the distinction between the rate curves of Fig. 11 and Figs. 12,13 with the added qualification that not all LC domains are equally effective in promoting subsequent crystallization: those within a spherulite circumference should be more effective than those lying outside. The above explanation implies that some pre-existing crystallinity is needed for creating an enhanced LC $\rightarrow$ C transformation rate. As in a monotropic system $T_i \leq T_m$ it follows that a certain amount of crystal will always be possible when cooling to below T_i, hence the precondition for the rate enhancement of the overall crystallization actually observed (Fig. 11 and even more conspicuously in Fig. 17) would be present.

Some further, apparently puzzling effects may also follow (or can be accommodated) by the above scheme. Such is the bright rim left in the M2 spherulites close to melting (Fig. 9e). According to the foregoings we should have two kinds of crystal: i) those formed from the L state d[illegible]v and ii) those arising from the LC state (aided by some of the type i) already p[illegible]as inferred above). In our present case much of the spherulite interior would be constituted of type ii) which in their perfectioned form melt at a slightly lower T than the rim. As the rim only appears above T_i it seems reasonable to assume that it has formed (or has been reinforced) by crystallisation from the L state, itself arisen on heating above T_i where we do know that L $\rightarrow$ C transformation, slow as it is, still occurs at a finite rate.

There are still some further puzzling observations the explanation of which seems to be beyond our present scope of comprehension. Such is, in the first place, the duality of spherulite type, in region 2a, specifically the existence of the M1 type, much rarer but growing faster.[4] Similarly unaccountable at [illegible]are the persistent memory effects due to the more common M2 spherulites, as [illegible]y Fig. 15. Clearly, where an M2 spherulite has been once the subsequent phase behaviour can be basically affected: not only the crystallization behaviour but also the L $\rightarrow$ LC transformation product unless this memory is wiped out by going to sufficiently high m[illegible] temperatures. Not only is the origin of these effects (M1 spherulites and the memory effects) unknown at present but we are lacking even the understanding of what the relevant structure features are, even in purely descriptive terms.

Finally a comment on the occasionally yet, where appropriate, unmistakably observable faceting of the spherulitic entities (both M1 and M2), particularly when the grainy background has melted away (Figs. 9d.e). Besides placing this on record, we remark on their resemblance to the so called "hedrites" [12]. Such objects, all products of growth in the form of thin film or on surfaces, bear clear relation to flat on views of single crystals suggesting that they may have arisen from such, as lying flat on a substrate and bushing out into spherulite-like aggregates subsequently.

---

[4] While it does not help understanding it could be useful for the future to mention that this situation seems to have a counterpart in nylons, observed in the 1960's and revived currently [11] in the form of minority entities which in the nylon case have been termed "aggregates". These have striking visual resemblance to the present M1 spherulites with similarly faster growth rates. Incidentally recent observations on nylons also suggest monotropic LC type behaviour near the melting region.

Concluding Remarks

To end with it needs remarking that all the above was dealing only with macroscopic heat (DSC calorimetry) and large scale structure effects on the level of the optical microscope. We regard the present microscopic and associated large scale structure mapping as prerequisites for further enquiries into the nature of the electron microscopic fine structure and ultimately into the underlying molecular processes involved in the crystallization of LCP systems. Before embarking on the much more selective and labour consuming direct attack on the fine scale structure and molecular issues, undoubtedly more central for ultimate understanding, clearly we need to know where we stand on the broader canvas, to which the present enquiry has been directed, first. And, as will have become apparent, even on the latter plane there are basic questions which still need to be answered.

References

1. N.J. Alderman and M.R. Mackley, *Faraday Disc. Chem. Soc.* **79** 149 (1985).
2. A.H. Windle, C. Viney, R. Golombok, A.M. Donald and G.R. Mitchell, *Faraday Disc. Chem. Soc.* **79**, 55 (1985).
3. J.L. Feijoo, G. Ungar, A.J. Owen, A. Keller and V. Percec *Mol. Cryst. Liq. Cryst.* **155**, 487 (1988).
4. E.L. Thomas and B.A. Wood, *Faraday Disc. Chem. Soc.* **79**, 229 (1985).
5. S.D. Hudson, E.L. Thomas and R.W. Lenz, *Mol. Cryst. Liq. Cryst.* **79**, 229 (1985).
6. S.L. Kent, D. Lin, D. Dean, J. Liu, F. Rybnikar and P.H. Geil in "Crystallization of Polymers" Ed. M. Dosière, NATO ASI Series, υ. 405, p. 177 (1993), Kluwer Academic Publishers, Dordrecht, Boston, London.
7. W. Ostwald, *Z. Physik, Chem.* **22,** 286 (1987).
8. A. Keller, M. Hikosaka, S. Rastogi, A. Toda, P.J. Barham and G. Goldbeck-Wood, *J. Materials Sci.* **29**, 2579 (1994).
9. J. Varga, Poster A2, EPS conference on "Transitions in oligomer and polymer systems" Ulm, 1993.
10. R. Pardey, S.S. Wu, J. Cheng, F.W. Harris, S.Z. Cheng and A. Keller, *Macromolecules*, in press.
11. C. Ramesh, A. Keller and S.J.E.A. Eltink, *Polymer*, in press.
12. P.H. Geil, Polymer Single Crystals, Interscience Publ. (New York, London, Sydney), 1963.

Figure Captions

Fig. 1 "Phase diagram" of one component LCP systems. a) Monotropic system with numbers for T_m and T_i as pertinent for the present ClBPE-9 compound. b) Enantiotropic system, unspecified.

Fig. 2 DSC thermogram of compound ClBPE-9 recorded on cooling (dashed) and subsequent heating (full line) at rates of 10 °C/min.

Fig. 3 Fine grain liquid crystal texture of ClBPE-9 formed in the range of 77 °C - 73 °C during cooling. Polarizing optical micrograph 300X.

Fig. 4 X-ray diffraction pattern of a sample of ClBPE-9 after cooling from the melt to room temperature.

Fig. 5 a) DSC traces of ClBPE-9 recorded on cooling from the isotropic melt with rates indicated.
b) DSC traces of same samples as in Fig. 5a recorded on subsequent heating at 10 °C/min. The preceding cooling rates are as indicated.

Fig. 6 Spherulitic morphology of ClBPE-9 as developed from the isotropic state at 80 °C. Polarizing optical micrograph 400X.

Fig. 7 Spherulites (M2 type) with grainy substructure and in a grainy background formed at 74 °C after 60 minutes. Polarizing optical micrograph 300X.

Fig. 8 Spherulites (M2 type) showing a grainy structure grown at 73 °C for 75 minutes. Polarizing optical micrograph 440X.
a) as seen between crossed polaroids, displaying no Maltese cross effect.
b) same area as a) with addition of a full wave retardation plate displaying discernible quadrants which correspond to addition and subtraction of retardation, seen as blue (here darker) and orange (here lighter) in original colour.

Fig. 9 ClBPE-9 crystallized at 72.3 °C for 60 minutes displaying both M1 and M2 spherulites. Polarizing optical micrograph 300X.

a) Between crossed polaroids revealing a distinct M1 spherulite (large circular entity on the right) within an otherwise uniformly mottled background.

b) Same area as a) with the addition of a first order retardation plate. Here distinct quadrants become discernible corresponding to addition (blue, here dark) and substraction (orange, here light) of retardation. These quadrants allow the identification of M2 spherulites (2 are arrowed) which otherwise would remain undetected.

c) Same area as in a) after heating to 74.5 °C when M2 spherulites become visible also without retardation plate as in this photograph.

d) Same area as in a) after further heating to 77.5 °C when the grainy background disappears.

e) Same area as in a) after further heating to 94.5 °C when only a rim of spherulite, M2 remain.

f) Same area as in e) after quenching from 94.5 °C to room temperature.

Fig. 10 DSC heating traces of ClBPE-9 recorded after holding sample at 72.7 °C, where both liquid crystal formation and crystallization can occur, for the times indicated.

Fig. 11 The logarithm of the time to reach a crystal melting endotherm of 10J/g for ClBPE-9 crystallized at various temperatures. The dashed line represents division between crystallization from the isotropic state (high temperatures) and liquid crystal state (low temperatures).

Fig. 12 The linear growth rates of ClBPE-9 crystal entities as a function of crystallization temperature. The dashed line has the same meaning as in Figure 11.

Fig. 13 Nucleation rate of ClBPE-9 as a function of crystallization temperature. The dashed line has the same meaning as in Figure 11.

Fig. 14 Spherulites (type M2) grown at 75.3 °C (i.e. close to but below T_i). It was heated to 83 °C to remove the grainy background arising at the crystallization temperature and then quenched to room temperature. Polarizing optical micrograph, 400X.

Fig. 15 An example of "memory" effect in ClBPE-9. The sample had been crystallized at 73 °C, then heated to 130 °C and held there for 2 minutes and then cooled rapidly to 70 °C. Polarizing optical micrograph, 600X.

Fig. 16 Illustration of competition between a stable and a metastable phase. Schematic plot of rates of phase evolution (R) as a function of temperature in a situation where the respective rates cross-over, applying, amongst other, to monotropic LCP-s. The T regions denoted as 1, 2 with subdivision 2a and 2b are meant to correspond to those in Fig. 1a) (see also Ref. 8).

Fig. 17 Rates of crystallization in a segmented polyimid displaying monotropic LCP behaviour (see text and ref. 10; $t_p \equiv$ time of peak position in heat development in isothermal DSC traces). Reproduced from ref. 10 to provide an example where the temperature coefficient of the rate of crystallization actually changes sign at the onset of liquid crystallization leading to a second maximum in the rate $v.T_c$ curves.

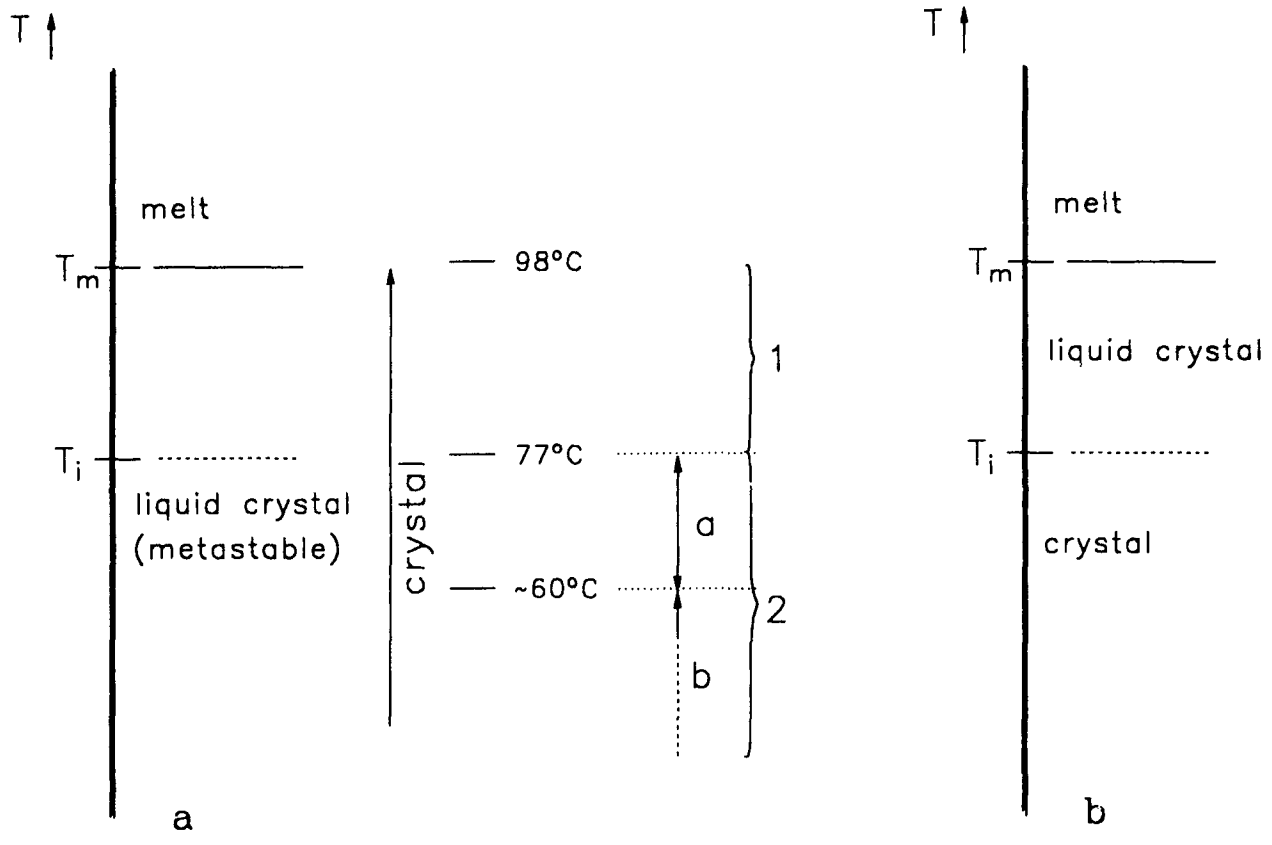
T
melt
T_m
T_i
liquid crystal
(metastable)
crystal
98°C
77°C
~60°C
1
2
a
b
a
T
melt
T_m
liquid crystal
T_i
crystal
b

Figure 1

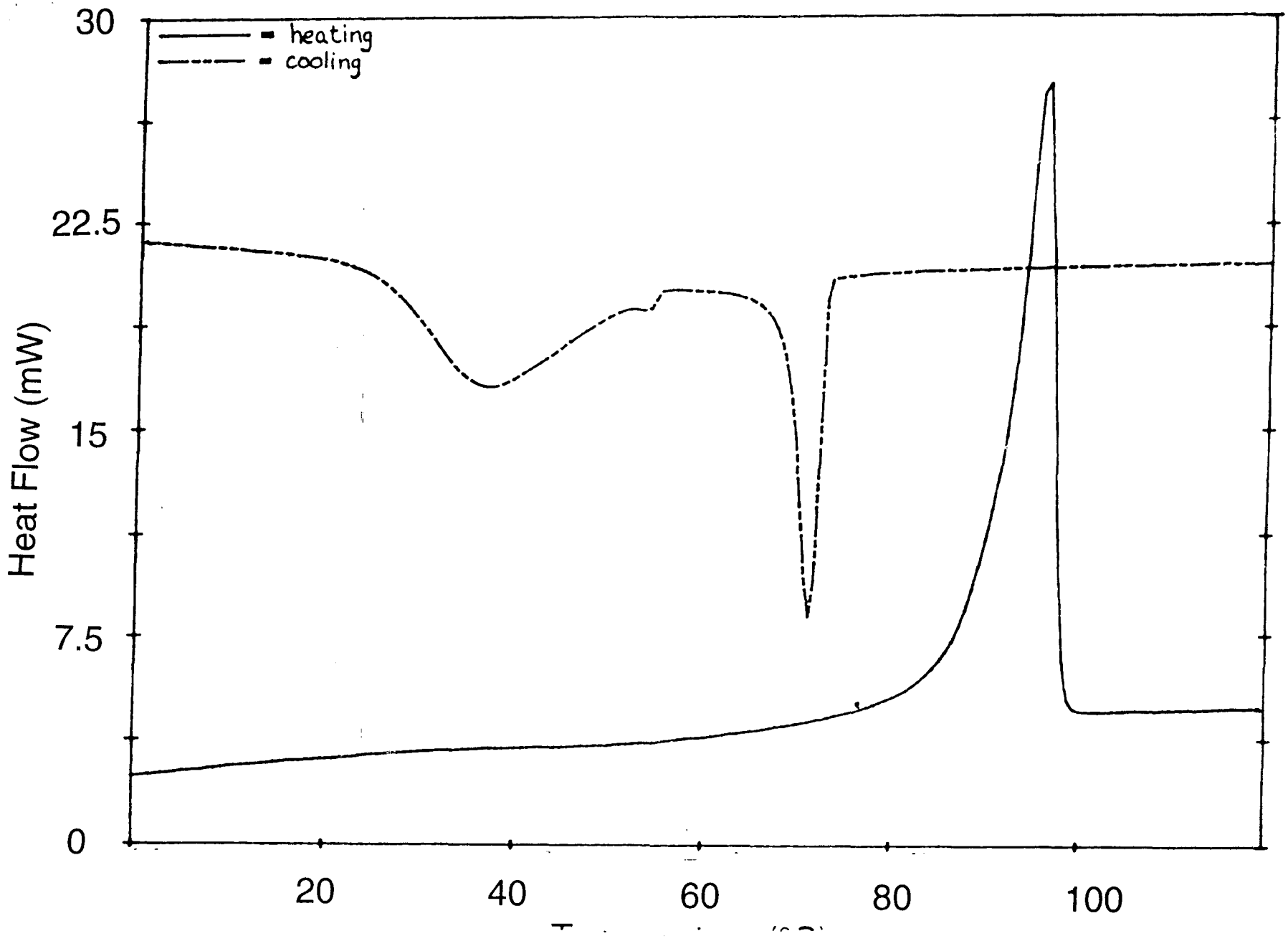
30
22.5
15
7.5
0
Heat Flow (mW)
heating
cooling
20
40
60
80
100

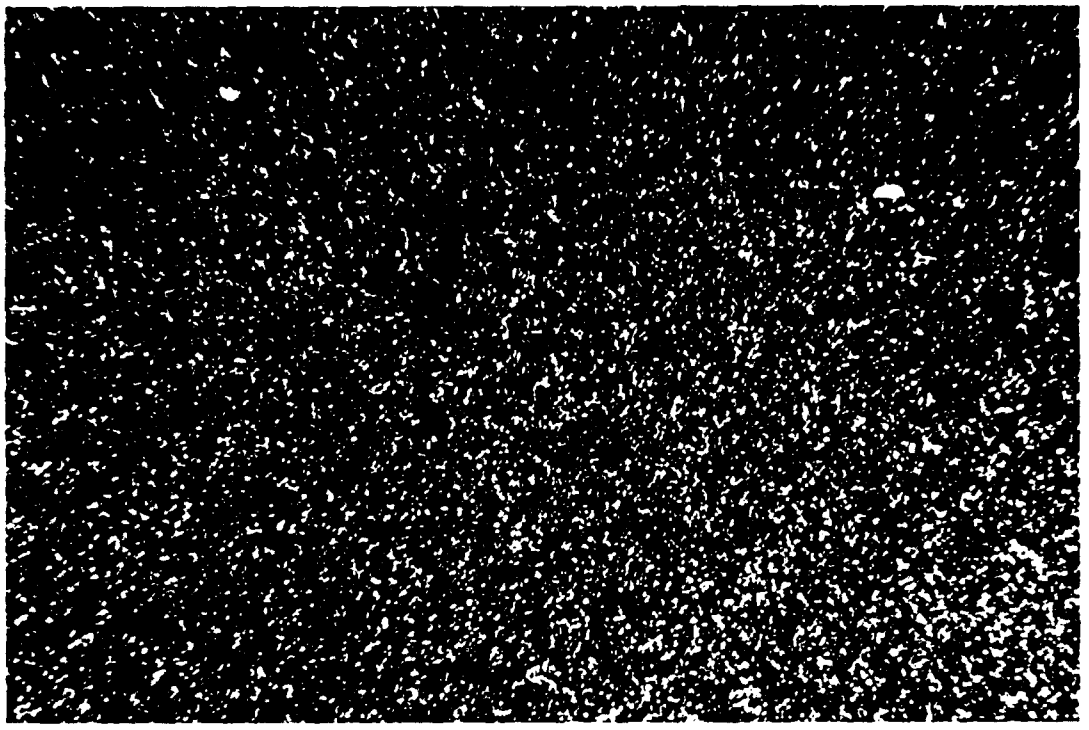

Figure 3

Figure 4

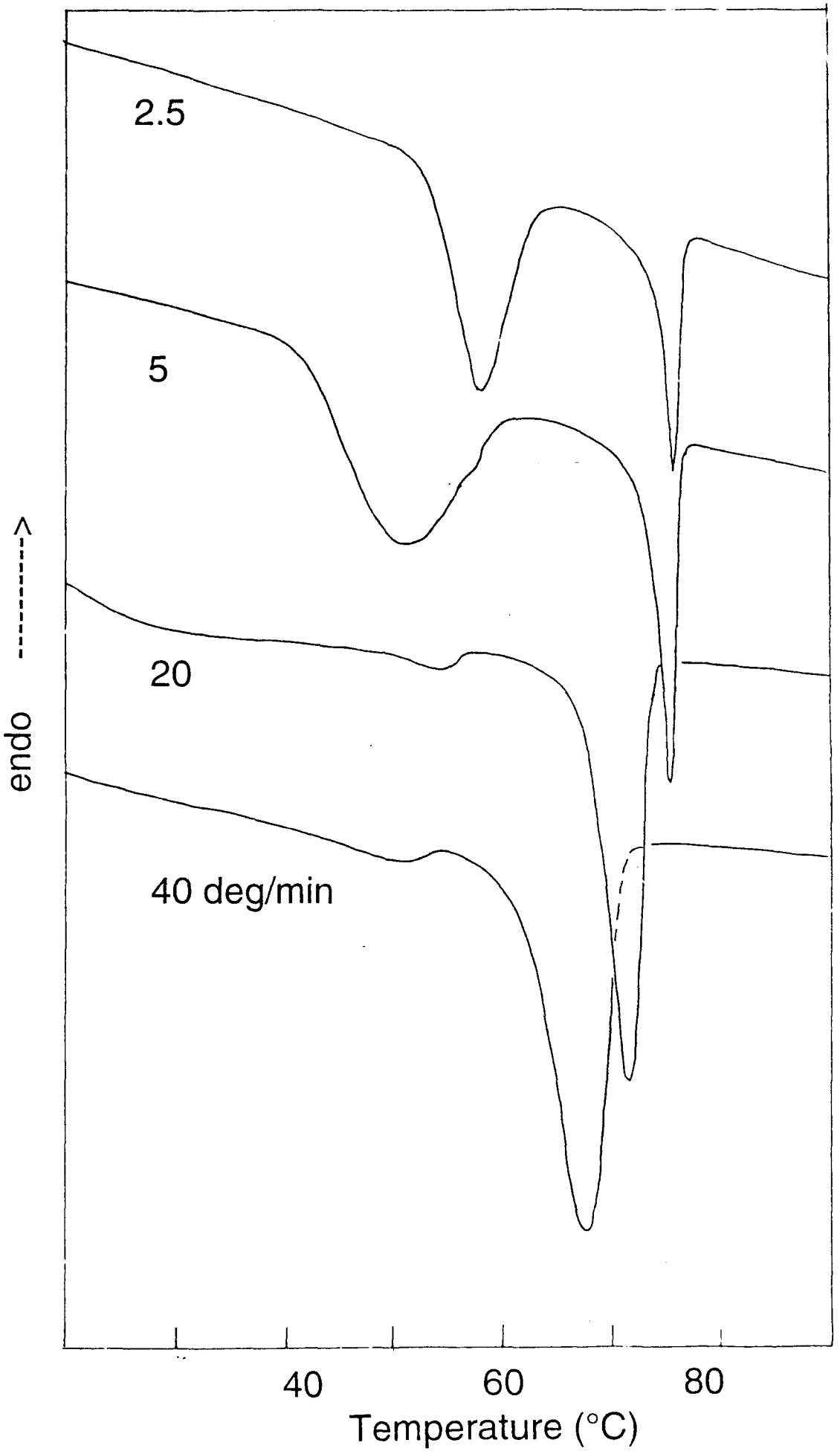

Figure 5a

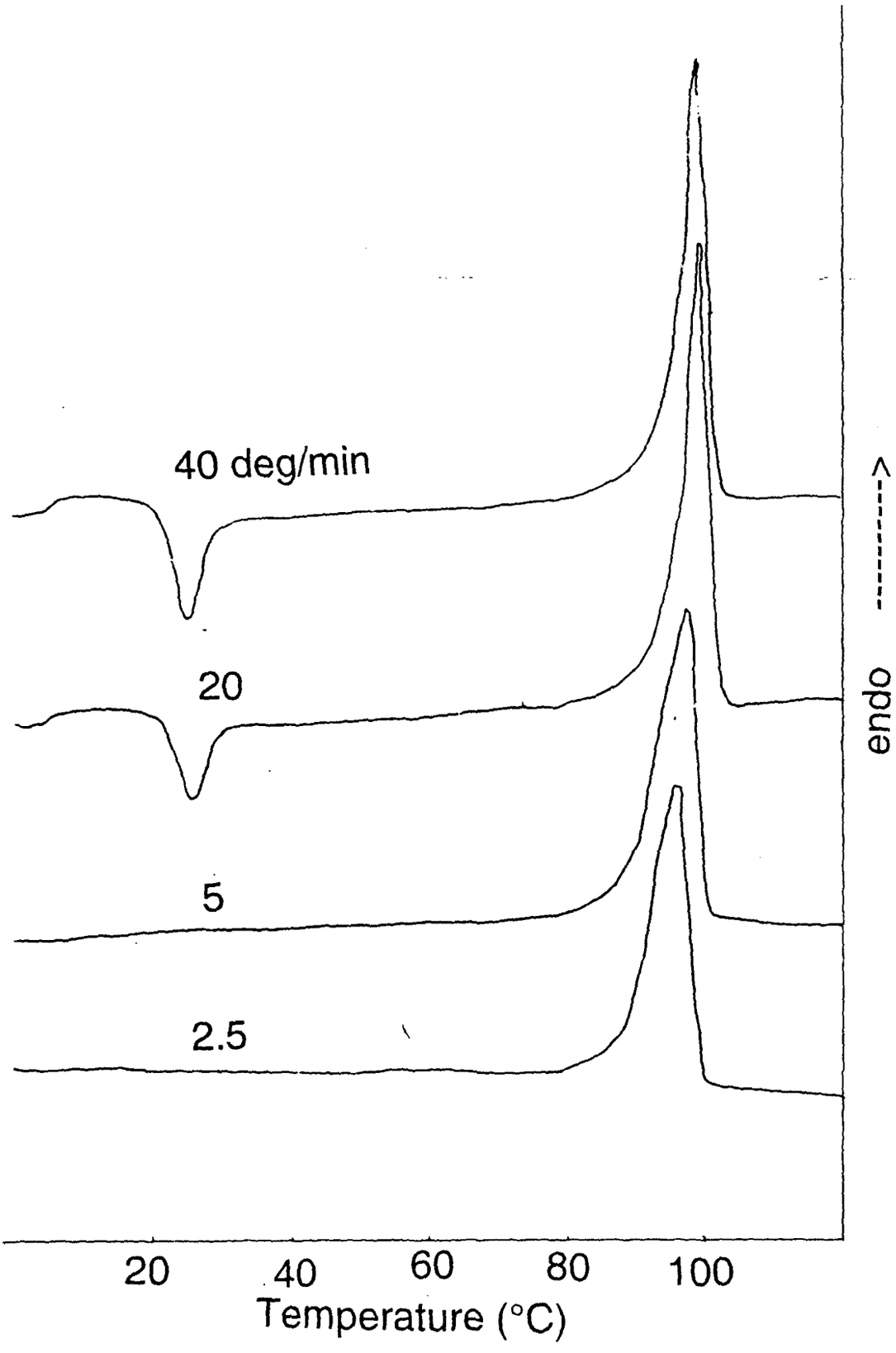

Figure 5b

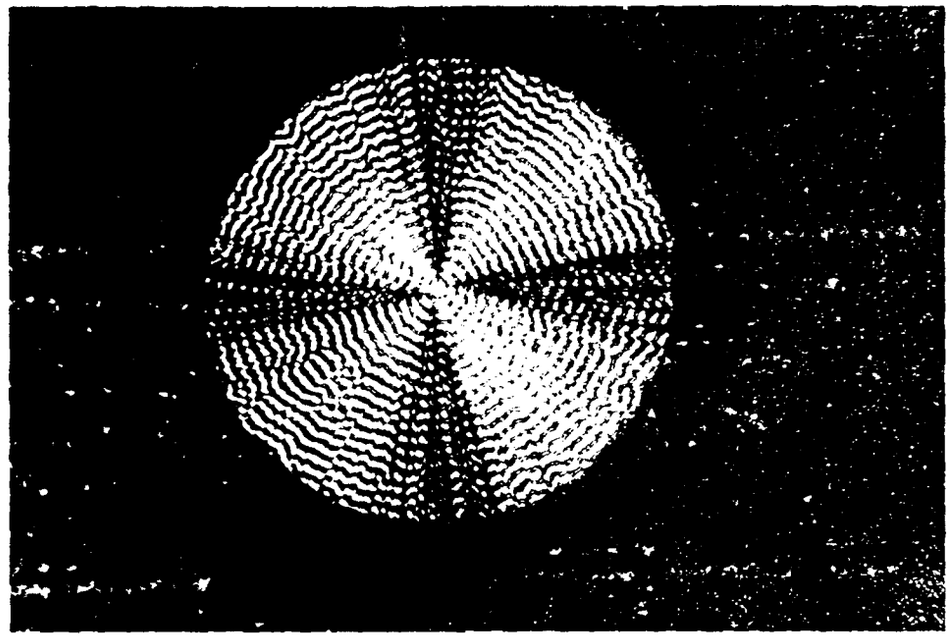

Figure 6

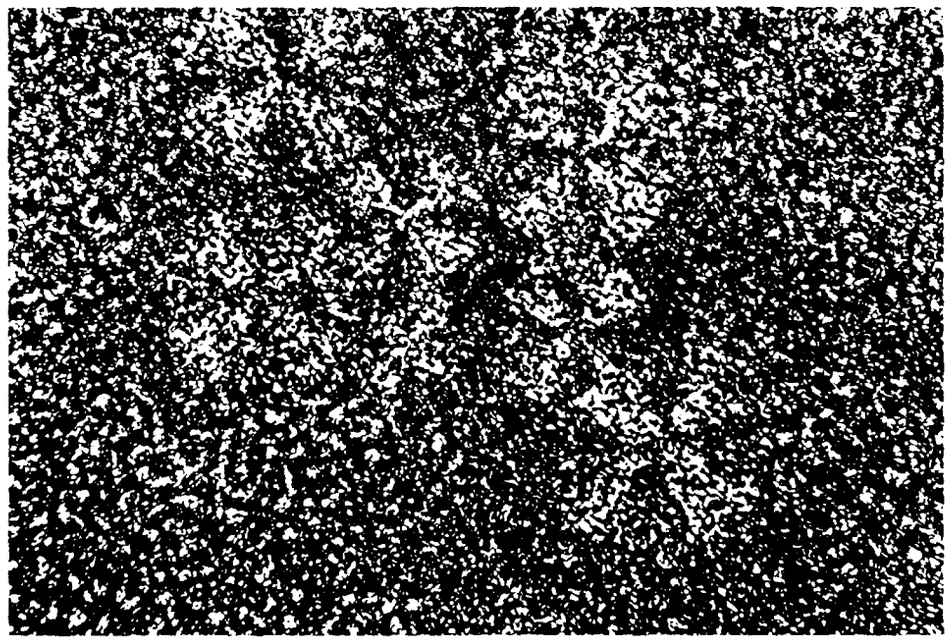

Figure 7

Figure 8a

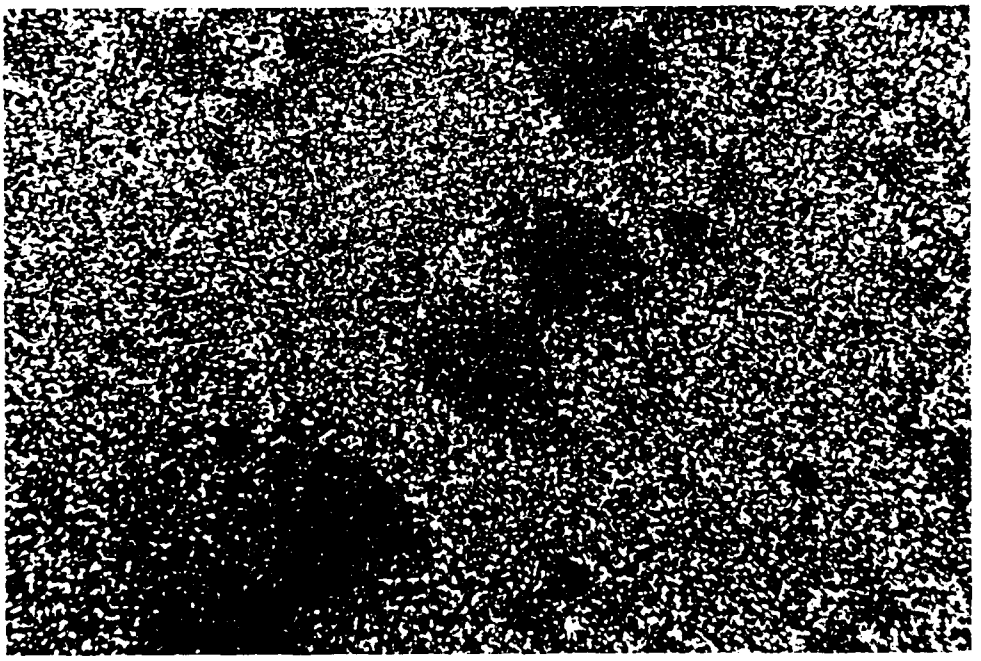

Figure 8b

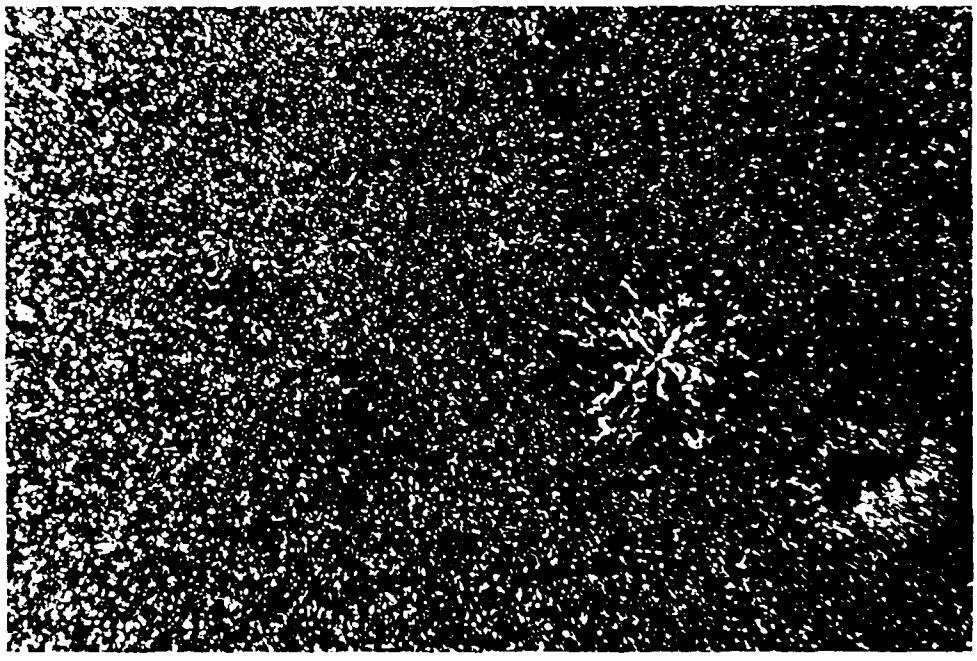

Figure 9a

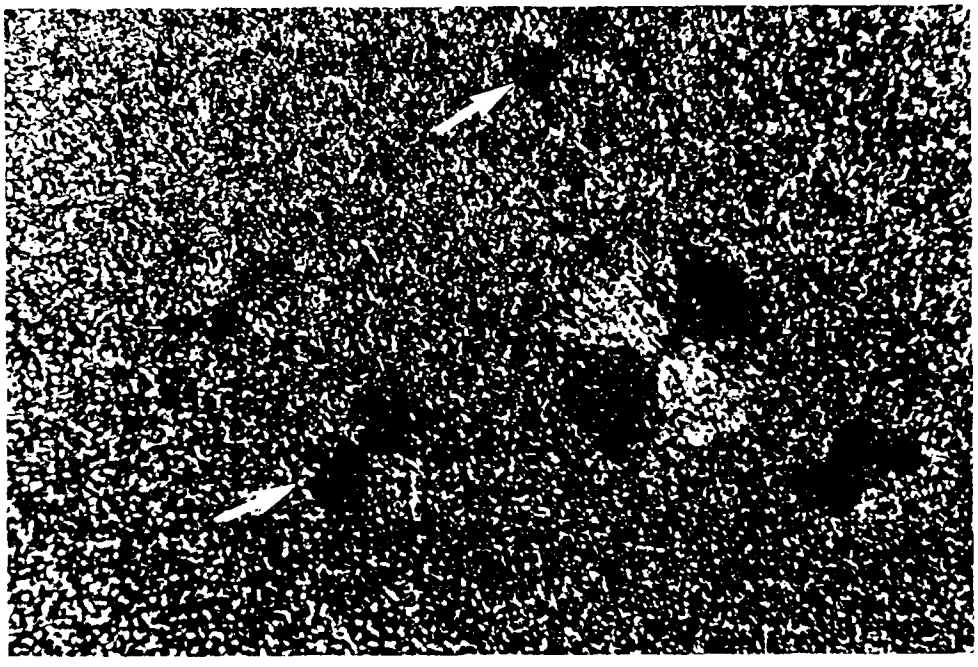

Figure 9b

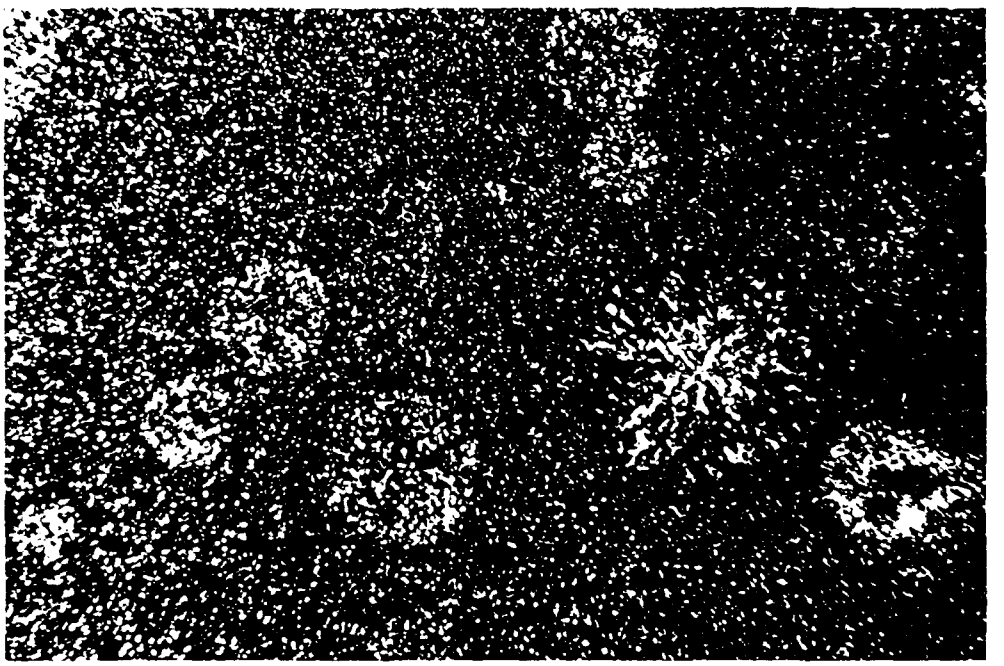

Figure 9c

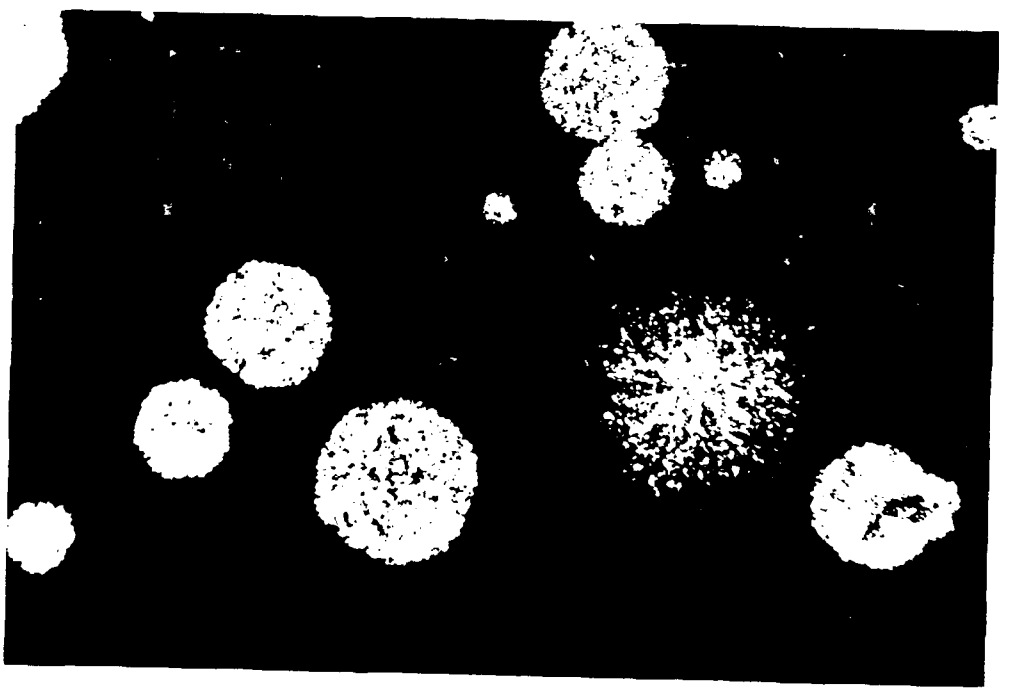

Figure 9d

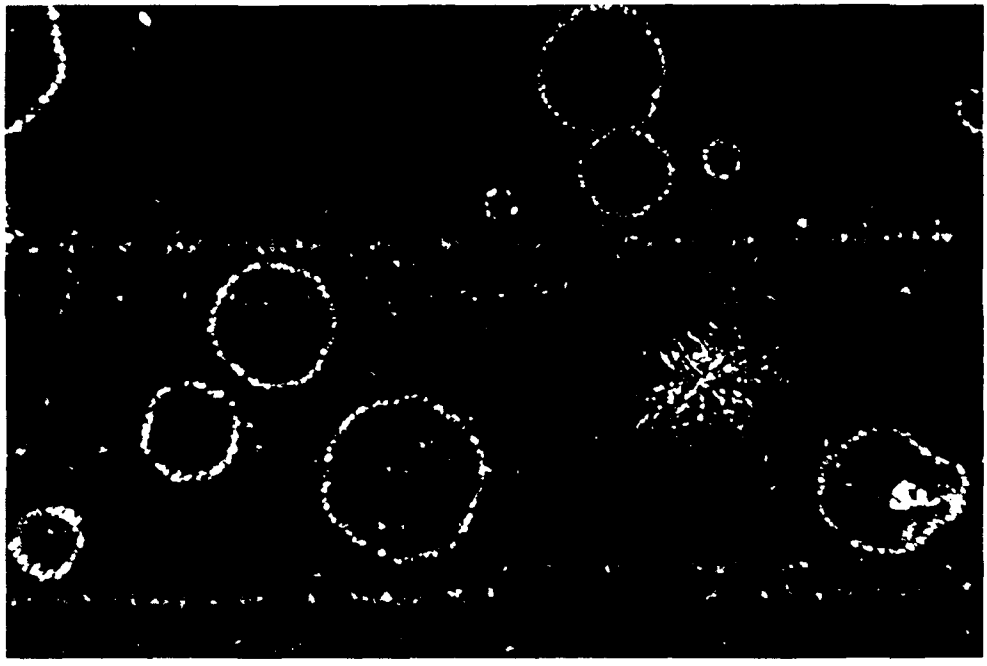

Figure 9e

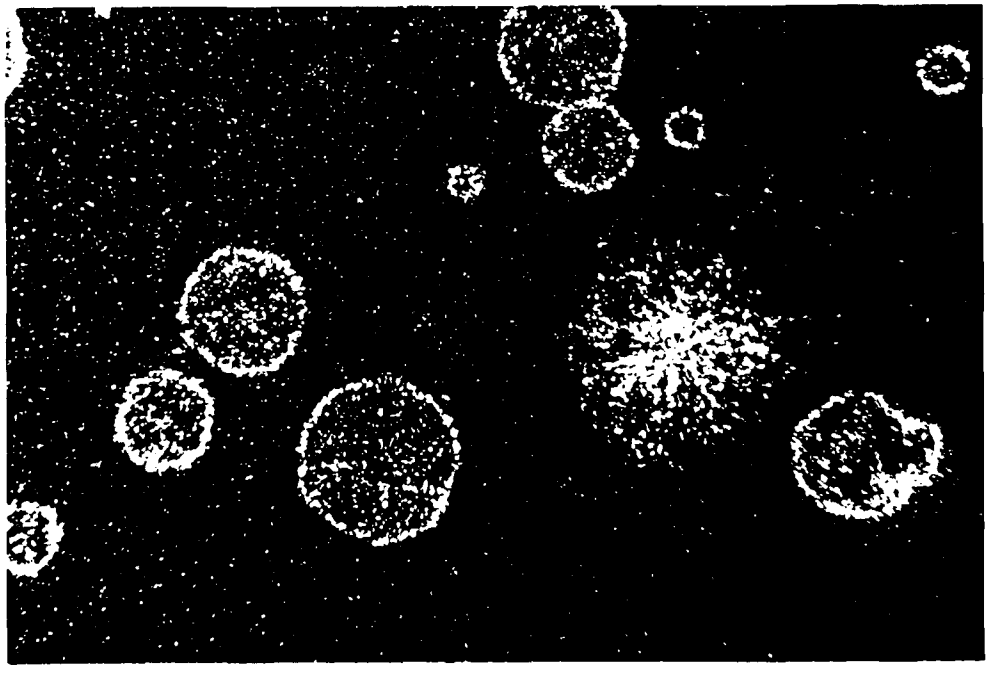

Figure 9f

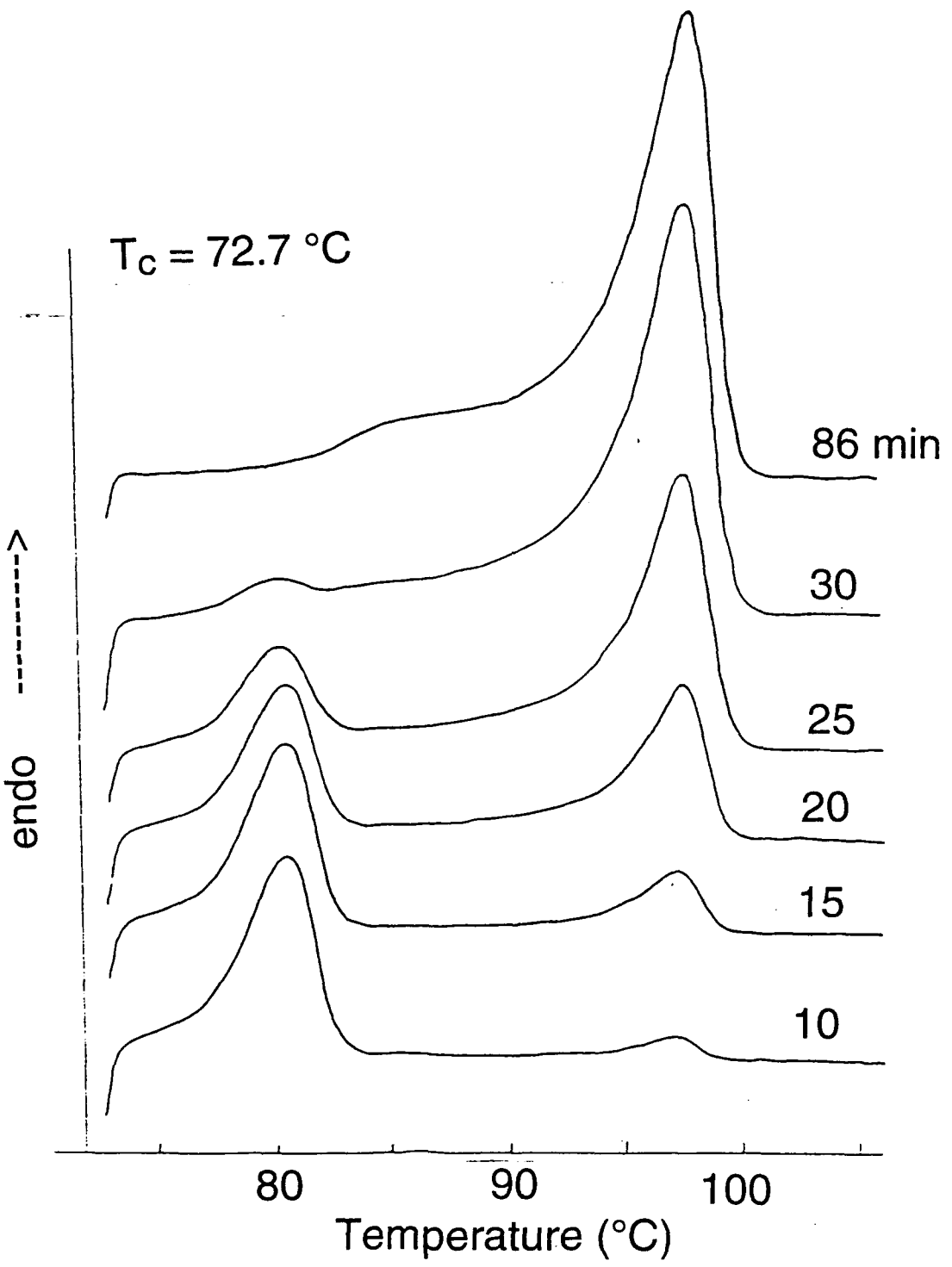

Figure 10

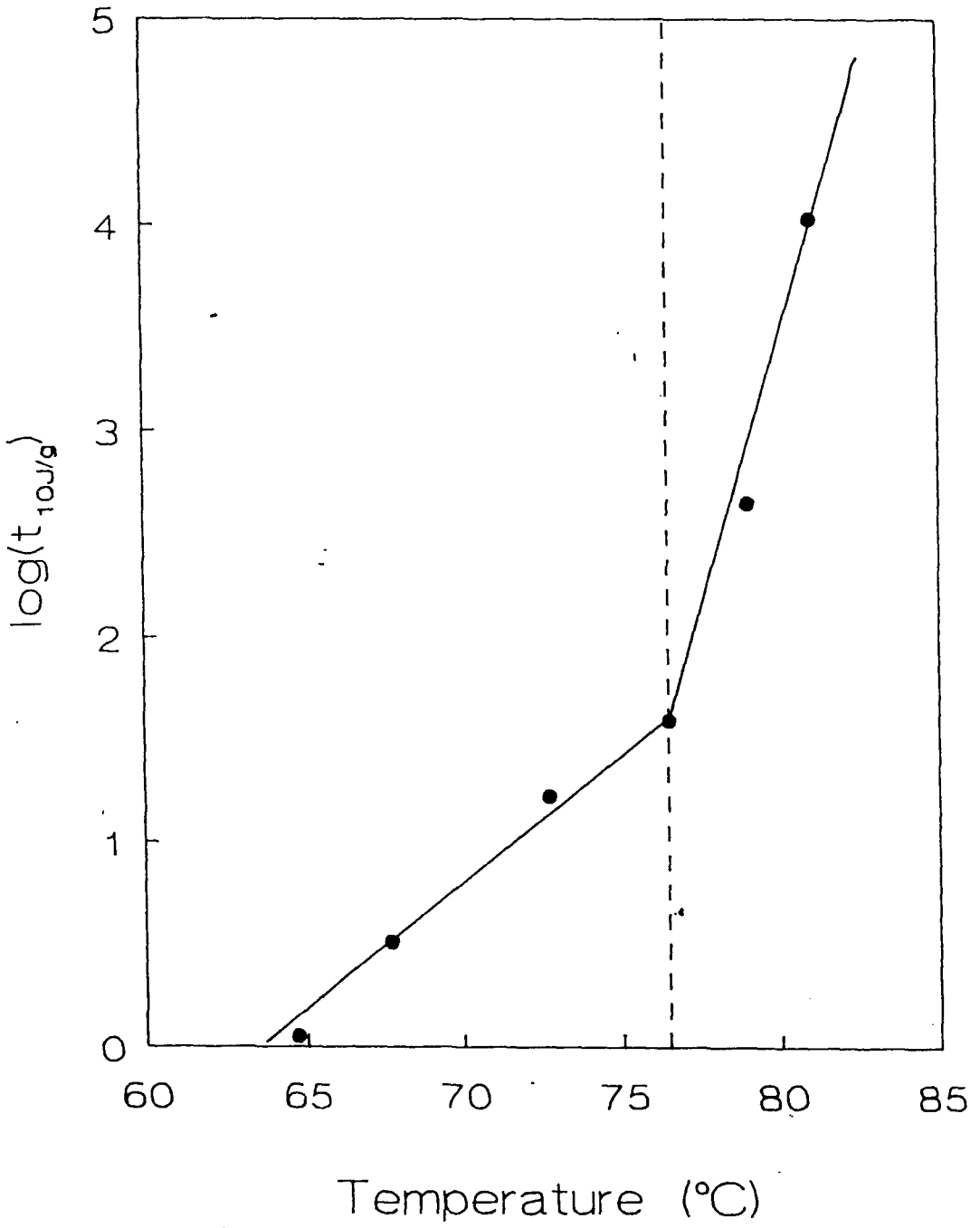

Figure 11

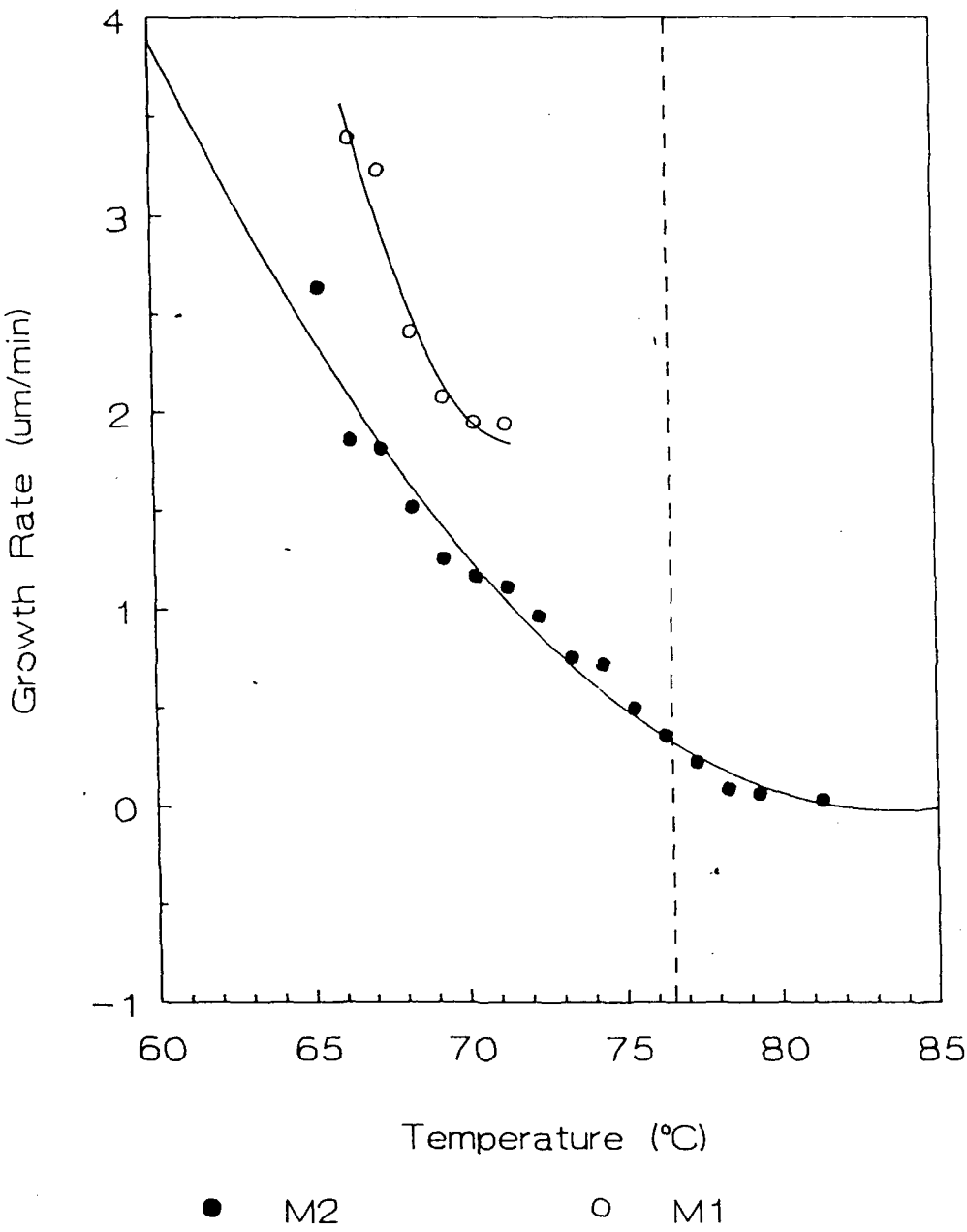

Figure 12

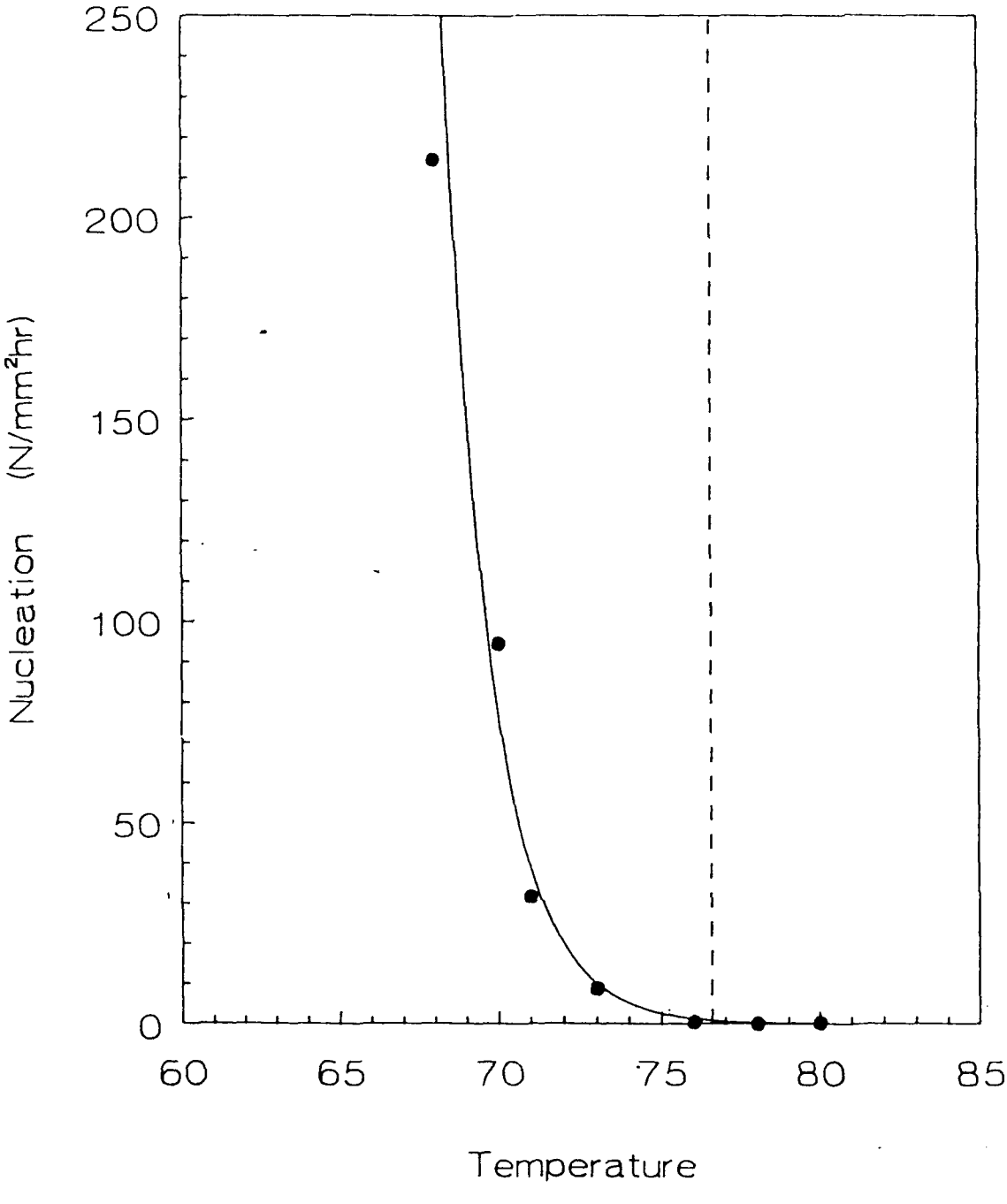
250
200
150
100
50
0
Nucleation (N/mm²hr)
60
65
70
75
80
85
Temperature

Figure 13

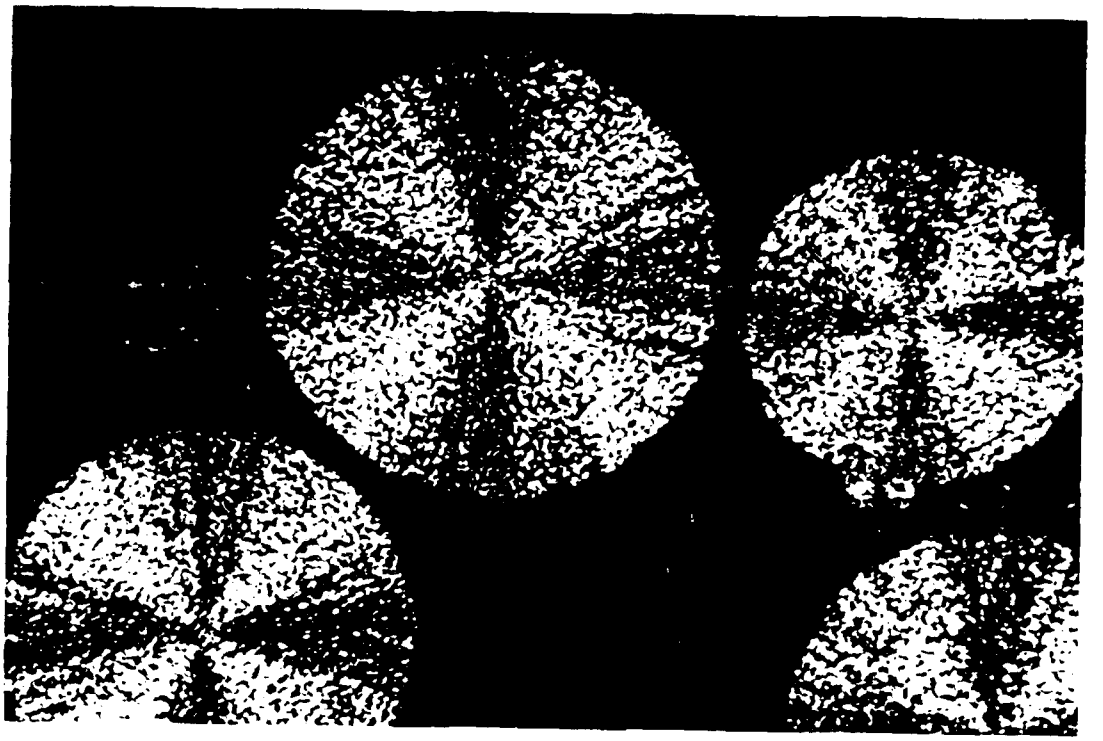

Figure 14

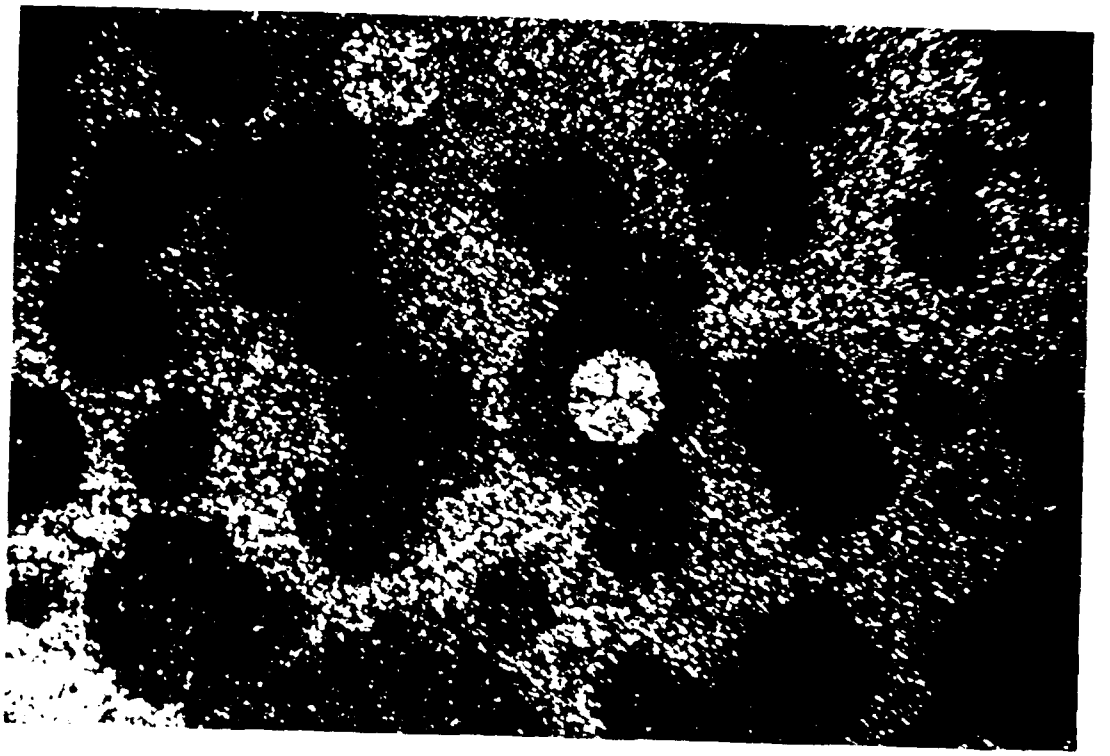

Figure 15

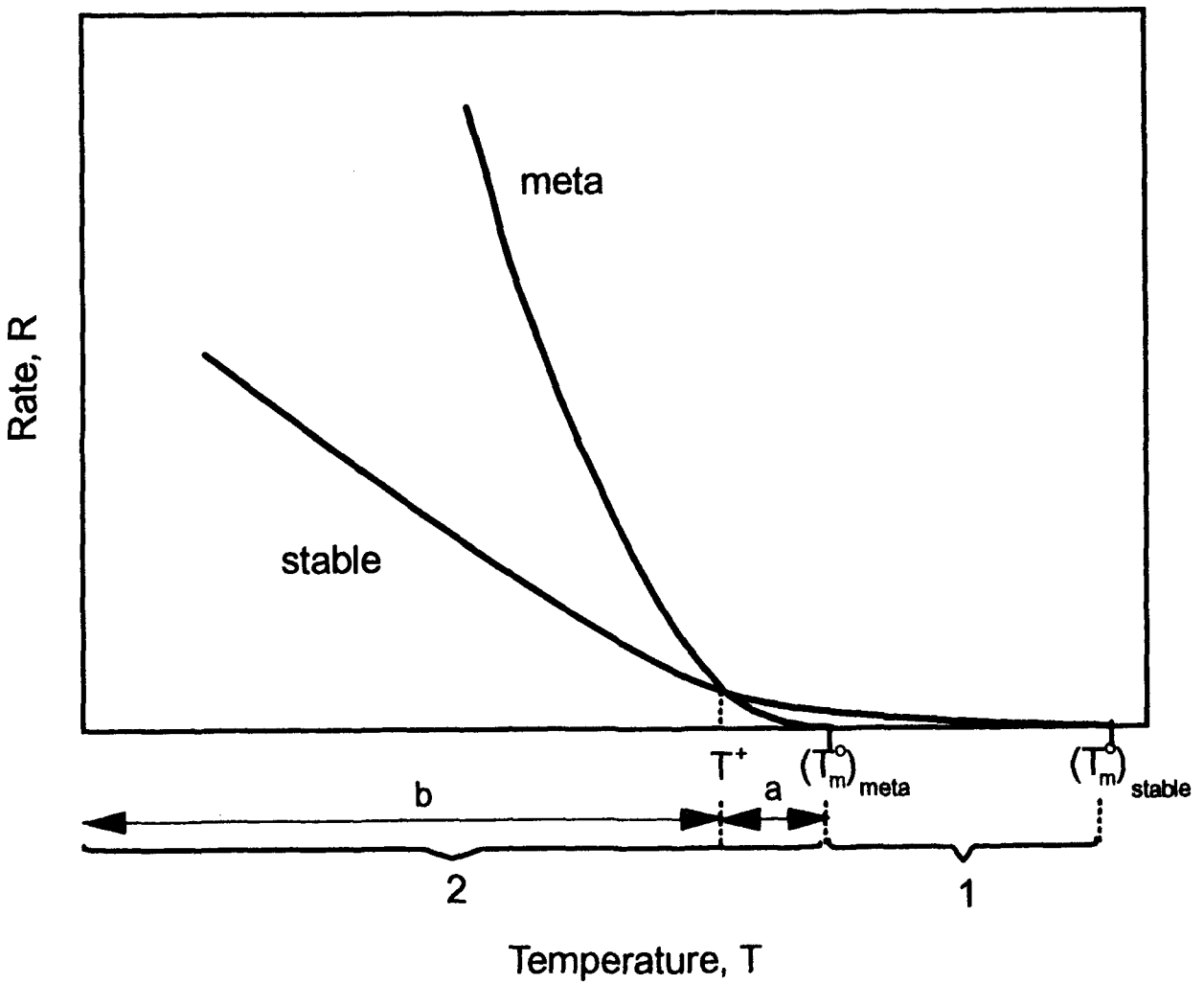

Figure 16

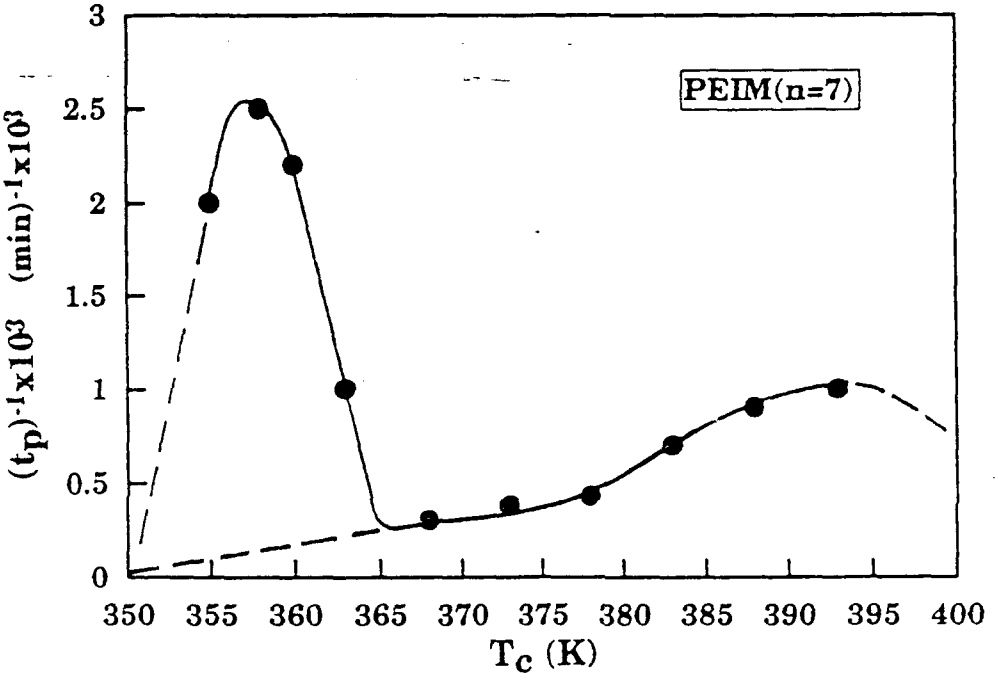
PEIM(n=7)
$(t_p)^{-1}x10^3$ $(min)^{-1}x10^3$
3
2.5
2
1.5
1
0.5
0
350 355 360 365 370 375 380 385 390 395 400
T_c (K)

Figure 17

SECTION 4: PHASE BEHAVIOUR - CRYSTAL SOLVATES AND SOLVENT STRUCTURE

A better understanding of equilibrium phases and their structures and of the possible transitions between them should permit better control of processing of stiff chain polymers in solution, the process of crystal formation and the final resulting fibre structure. The results presented here focus on the interest on the understanding the phase behaviour of liquid crystalline solutions of PBZT and PBO in PPA. Previous investigations have shown that solutions show a more or less complex behaviour including the formation of different kinds of crystal solvates depending upon water content and temperature. There are some hints that there are two different kinds of solvent molecules present in the solution, molecules that are somehow adsorbed or bonded to the dissolved macromolecules and free solvent molecules in between them. This has been underlined mainly by the **investigation of the phase diagram PBZT/PPA/water**, a system of major commercial interest. Therefore the work has been focused on this system (report 5 and 8).

The system Hydroxypropylcellulose (HPC) / water provides an easy to handle model system for stiff chain polymers in solution. It was one of the first systems where liquid crystallinity in solutions of polymers has been recognised. This system is also known to exhibit a complex phase behaviour including the formation of an isotropic and a mesomorphic phase but also a reversible phase transition upon heating. However, the nature of the phases at equilibrium at high temperatures and even the structures of the homogenous phases at lower temperatures are still not known. Some authors understand the anisotropic phase as solution consisting of discrete clusters of HPC chains the majority is convinced, that structuring of water through H-bonds plays an important role in the structure of the different phases. The investigations described here have been carried out to understand the nature of the solid phase at high temperatures and to understand principle features of phase diagrams of lyotropic polymeric systems.

On The Phase Diagram of the System PBZT/Polyphosphoric Acid/Water*

H. Fischer, M. Murray*, J. A. Odell and A. Keller

H. H. Wills Physics Laboratory, University of Bristol, Tyndall Avenue, Royal Fort, Bristol, BS 8 - 1 TL

* School of Chemistry, University of Bristol, Cantrocks Close, Bristol BS 8 - 1 TS

ABSTRACT:

The phase diagram of the System PBZT/Polyphosphoric Acid/Water has been investigated using DSC, optical microscopy and ^{31}P NMR-spectroscopy. A peritectic line at higher temperatures and an eutectic line at lower temperatures have been found independent from the polycondensation degree of the polyphosphoric acid (PPA). The phase transitions between the different regions in the phase diagram are strongly dependent on the condensation degree of the solvent. All phase transitions are completely reversible. The formation of crystal solvate phases is connected with the water content of the system and therefore with polycondensation reaction of the PPA. The solvent molecules are strongly associated with the macromolecules. The nematic phase is formed by interaction of 6 solvent molecules per monomeric unit of the polymer and proton transfer from the solvent towards the polymer in the nematic phase.

INTRODUCTION

In the past interest in high performance material has been focussed on an improvement of mechanical properties, especially compressional strength. The transition from the dissolved state to the solid state is therefore of major interest in order to understand the final mechanical properties of the material obtained. During coagulation a transition from a liquid to a solid phase occurs either by diffusion of a nonsolvent or by decrease of temperature. The structure initially formed by this coagulation process is therefore the basis for the final fibre structure. A better understanding of equilibrium phases and their structures and of the possible transitions between them should permit better control of the final resulting fibre structure. The results presented here focus on the interest on the understanding the phase behaviour of liquid crystalline solutions of PBZT and PBO in PPA.

* *J. Mater. Sci.*, **29**, 1025 (1994)

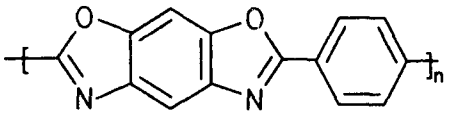

PBO

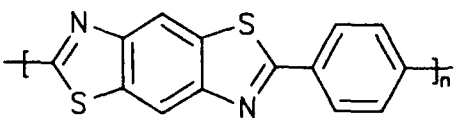

PBZT

Previous investigations have shown that solutions show a more or less complex behaviour including the formation of different kinds of crystal solvates depending upon water content and temperature [1-6]. Orientation and relaxation of the dissolved macromolecules and the solvent molecules have been observed during shear experiments. There are some hints that there are two different kinds of solvent molecules present in the solution, molecules which are somehow adsorbed or bonded to the dissolved macromolecules and free solvent molecules in between them [7].

EXPERIMENTAL

The different mixtures investigated were prepared by dilution of a mother solution of 9 % PBZT in Orthophosphoric acid (OPA) by deuterated Polyphosphoric acid (PPA) with a composition of 82 % P_2O_5 in the system P_2O_5/D_2O. The deuterated PPA was obtained by dissolving anhydrous P_2O_5 in a solution of 85 % D_3PO_4 in D_2O under dry conditions with stirring. Liquid crystalline behaviour was determined visually using a Linkam THM 600 hot stage mounted on a Zeiss Ultraphot optical microscope. A Sony videorecorder was used to record crystal solvate formation and phase transitions from the nematic to the isotropic phase or to the mixed phase. Thermal analysis was carried out using a Perkin Elmer DSC 7 with heating and cooling rates of 20K/min to a temperature limit of 200 °C. Samples were prepared in stainless steel high pressure pans from Perkin Elmer. The ^{31}P NMR-spectra were obtained using a JEOL Alpha 500 or a JEOL FX 90 Q.

RESULTS AND DISCUSSION

Optical microscopical studies with polarized light were used to examine the phase diagram of the System PBZT/PPA/H_2O. At room temperature between crossed polarisers a 9 % solution show a fine grainy texture which is more or less unspecific with respect to a typical texture known for types of mesophases. By heating up to 100 °C and annealing

at this temperature for 48 hr. the development of a large scale ***threaded*** texture could be observed (see Figure 2). This is the texture typical of for nematic liquid crystals and is comparable with textures displayed by low molecular weight compounds [8].

With further heating the formation of crystal solvates could be observed starting at 133 °C in solutions in OPA and at 270 °C in solutions in PPA. The formation of the crystal solvates is associated with a change in colour of the solution from dark green to bright green and further to orange and dark red, also crystallisation of a different structure could be detected under the polarizing microscope. The Figures 3a and 3b show the development of a crystal solvate out of a large scale texture nematic solution at 140 °C. Finally an orange to dark red crystal solvate is formed, which exhibits much smaller crystal sizes and which irreversibly disturbs the large scale monodomain structure at 150 - 180 °C (see Figure 4). Those crystal solvates no longer show the properties of a solution, no flow under shear conditions can be observed. The crystal solvate behaves like a network of macroscopic crystals. Together with the crystal solvate the presence of some isotropic liquid is observable.

With a change in temperature, there is a change in the degree of polymerization with splitting off of water into the gas phase. Water is acting in the polymer solution as a nonsolvent. At elevated temperatures above 100 °C the amount of water which is split off could be large enough to attract the nematic solution and therefore to force the formation of crystal solvates or a precipitation of the polymer.

The formation of the crystal solvates is reversible. By cooling to 25 °C for solutions in OPA and to 60 °C for solutions in PPA a biphasic solution of crystals (bright green) and the nematic solution is present. The crystals melt again in the 9 % solution at approximately 60 °C. The texture exhibits again very small monodomains and is grainy. The reformation of the nematic phase is associated with a change in colour back to dark green.

For the more diluted solutions (3-5 %) phase transitions in the heating mode from a homogeneous nematic into a biphasic nematic/isotropic and finally into a homogeneous isotropic solution have been detected (see Figure 5). Cooling to - 30 °C forces the rapid formation of crystals (see Fig. 6a). Additionally an increase of birefringence of the isotropic parts of the biphasic region of the 4.62 % solution with the growing of the crystals could be observed. The crystals are well defined and more similar to crystals of a low molecular weight compound, than to the crystals of a polymer. Those crystals are again stable upon subsequent heating up to a temperature of app. 30 °C, beyond which they melt into the nematic solution (see Figure 6b). We assume that the crystals are formed by crystallization of OPA, which has a reported melting point of 42.3 °C, but in a

mixture with other polyphosphoric acids a melting point of 34.6 °C. A similar behaviour is observed for solutions in PPA. Here the formation of crystals starts at 60 °C. The phase transition is reversible and we believe is due to the formation of DPA crystals, which melt at 61 °C, (64 °C for deuterated DPA).

Similar behaviour could be observed by DSC (see Figure 7). The graph obtained from the PBZT solution shows two phase transitions and a recrystallisation at the heating curve. The first phase transition at 31 °C would correspond to a melting temperature of the crystals as observed optically into a nematic solution, the second phase transition to the formation of the crystal solvate at high temperatures. A recrystallisation of the crystal solvate takes place afterwards. On cooling, the transition from the red crystal solvate to the nematic solution is supercoolable by 45 K. Similar results have been obtained by COHEN et.al. [6].

The DSC traces of the pure solvent, polyphosphoric acid has shown a broad endothermic peak at 250 °C which is obviously due to structural and chemical changes of the solvent. This was sufficient reason to look closer at the nature of the solvent. In the literature of the nematic solutions of rigid rod polymers polyphosphoric acid (PPA) is only described as a mixture of P_2O_5 and H_2O with a content of P_2O_5 of about 82 - 84 %. A characterization with respect to the molecular weight or polymerization degree and the molecular weight distribution of the phosphoric acids is only described in general terms in GMELIN Volume Phosphorus [11, 13]. This is possible by chromatography, by IR spectroscopy or by ^{31}P-NMR spectroscopy of aqueous solutions of the neutral salts of the polyphosphoric acid. Difficulties arise due to the fact that, on neutralisation of the free acids the degree of condensation degree can change. The concentration of 84 % would correspond to a polymerization degree of 4 (tetraphosphoric acid). In the present method of synthesis a formation of cyclic polyphosphoric acids (metaphosphoric acids) can be excluded. However, the PPA is not one single compound but rather a mixture of polyphosphoric acids with polymerization degrees ranging from 1 to more than 9 (see Figure 8). "Free" water, connected with orthophosphoric acid is also present. The composition of the crystal solvate (orange to dark red phase) could be calculated by separation of the isotropic liquid phase from the solid crystal solvate and comparing the weight of the dry crystal solvate thus obtained with the calculated amount of PBZT in the solution used. The crystal solvate was found to consist of approximately 4 phosphoric acid units per monomeric unit of PBZT and hence will be described as crystal solvate 4 (CS 4).

One of the best methods for the investigation of the structure of the different liquid and solid phases in the system PBZT /PPA/ H_2O should be ^{31}P-NMR

spectroscopy, where the investigation should be possible in solution without changing the character or the chemical structure and the condensation degree of the solvent. Surprisingly sharp lines have been obtained from pure isotropic and nematic solutions, even from solutions with a comparatively high viscosity (see Fig. 9). All spectra show, beside the line at app. 0 ppm (OPA), one line at app. -14 ppm (DPA, end groups of PPA). In no spectra wwere lines at 29 ppm (middle groups of PPA) or at 44 ppm (crosslinked PO_4-groups) observed [13]. This means that the solvent is only a mixture with a rather high content of OPA and a low content of DPA; polymeric phosphoric acid and crosslinked phosphoric acid are not present. Unfortunately most of the spectra show no significant splitting of the lines due to different degrees of protonation of the different phosphorous nuclei. Only one sample, a solution with a concentration of 6.4 % and a condensation degree of the polyphosphoric acid of about 2 did show a splitting of the OPA line due to different species of the acid present in the solution Figure 9b). Therefore we believe that the interacting molecules are mostly OPA molecules, and from the shift towards lower field, it is quite clear that the interaction, at least in the nematic solution, involves a proton transfer from the OPA to the polymer. The number of OPA molecules which are involved in the formation of the nematic phase could be estimated from the NMR spectra and is about 6. An investigation of the differences between the interaction of the solvent with the polymer in the nematic solution and the two crystal solvate phases was not possible.

Spectra at room temperature from solutions with higher concentrations of PBZT (9 %) show a line broadening effect and a solid state like spectrum of the DPA part. This is due to the solidification process during the formation of the crystalline DPA. It is clear that at concentrations > 8 % at temperatures in the range from 25 °C to 30 °C there are solid particles present in the solutions, even when there is no visible sign of them, because they are too small (see Fig. 10a and b).

After application of vacuum to the different solutions at 150 °C, a significant increase of the condensation degree of the polyphosphoric acid could be detected.

^{31}P NMR-spectra were also recorded at high temperatures. Fig. 11 shows the spectra of an 8 % solution of PBZT in OPA at 40 °C in the nematic phase and a spectra of the same sample at 200 °C in the mixed phase crystal solvate 4 / isotropic solution. The spectrum at the higher temperature shows not only broader lines than the spectrum of the nematic solution, but also the intensities of the lines have changed. The calculated content of diphosphoric acid has increased from 5 % in the nematic solution to 9.6 % in the mixed phase. This increase is due to the condensation of the OPA at elevated temperature. Diphosphoric acid forms, water splits off at the condensation temperature

which induces the formation of the mixed phase and the precipitation of the crystal solvate 4. These results are contrary to the assumptions by COHEN et.al. [2]; it is quite clear that at elevated temperatures there is no indication for a hydrolysis of PPA.

Finally, it is possible to construct phase diagrams for different condensation degrees of the polyphosphoric acid (see Figure 12, 13). The different regions are marked in the phase diagrams. This type of phase diagram is well known for systems of stiff polymers in solution and has been theoretically predicted by FLORY [15].

A quite general change was detected by changing the polycondensation degree of the PPA from OPA with app. 5 % DPA to a PPA with a condensation degree of 2. At first a large shift of the phase transition line [nematic] - biphasic region [isotropic / crystal solvate 4] towards higher temperatures (270 °C) takes place. This is in good agreement with the results obtained for PPA (83 % P_2O_5 in the system P_2O_5/H_2O) [6]. The temperature shift is basically due to the higher condensation degree of the PPA, and therefore due to higher temperatures required to split off of a sufficient amount of water for the formation of the crystal solvate 4. This is in agreement with the results obtained by thermal condensation of OPA [9, 10, 12]. Secondly the width of the chimney became much broader than in the system PBZT - OPA. This is visible by a shift of the transition line between the biphasic region [nematic] / [isotropic] towards the homogeneous nematic region. Also a significant shift of the eutectic line /formation of crystalline phases at lower temperatures took place. This is basically due to the change in the composition of the PPA and the resulting amounts of the different species of polyphosphoric acids and changing their melting temperatures. The melting temperature of DPA is 61 °C whereas the melting temperature of OPA in a mixture of different species of PPA is only 34.6 °C. These melting temperatures of the major components have a strong influence on the solidification temperature of the crystalline phase at lower temperatures as is usual in eutectic systems.

CONCLUSIONS

The System PBZT/PPA/H_2O show a quite complex phase behaviour. The phase transitions between the different regions in the phase diagram are strongly dependent on the condensation degree of the solvent. At high temperatures a precipitation of a crystal solvate phase is forced due to an increase in the condensation degree of the solvent and the elimination of water as a nonsolvent. The nematic phase is formed by interaction of 6 solvent molecules per monomeric unit of the polymer and proton transfer from the solvent towards the polymer.

REFERENCES

[1] Cohen, Y. and Thomas, E. L., *Polymer Eng. Sci.*, **25** (1985) 1093

[2] Cohen, Y. and Thomas, E. L., *Mol.Cryst.Liqu.Cryst.*, **153** (1987) 375

[3] Cohen, Y., *MRS Symposium Proceedings*, **134** (1989) 195

[4] Cohen, Y. and Thomas, E. L., *Macromolecules*, **23** (1990) 4419

[5] Cohen, Y., Saruyama, Y. and Thomas, E. L., *Macromolecules*, **24** (1991) 1161

[6] Cohen, Y., Buchner, S., Zachmann, H. G. and Davidov, D., *Polymer*, **33** (1992) 3811

[7] Feijo, L. J., Odell, J. A. and Keller, A., *Polymer Commun.* **31** (1990) 42

[8] Demus, D. and Richter, L. in "Textures of Liquid Crystals" (Verlag Chemie Weinheim, N. Y. 1978)

[9] Wee, E. L. and Miller, W. G., *J.Phys.Chem.*, **75** (1971) 1446

[10] Bassett, H., *J.chem.Soc.*, **55** (1958) 2949

[11] GMELINS HANDBUCH DER ANORGANISCHEN CHEMIE, Volume Phosphoros, Part C, 8th Edition (Verlag Chemie Weinheim) p. 157, 166, 218-221

[12] Balarew, D., *Z.anorg.Chem.*, **67**, 243 (1910)

[13] Huhti, A.-L. and Gartaganis, P. A., *Canad.J.Chem.*, **34** (1956) 785

[14] Mark, V.,Dungau, C.,Crutchfield, M. and van Wazer, J., in "Topics in Phosphorus Chemistry", Vol. 5, "Compilation of ^{31}P-NMR data", Intersiecnce (N.Y., London, Sydney, 1967) 319

[15] Flory, P. J. *Proc. R. Soc. London, Ser. A*, **234** (1956) 73

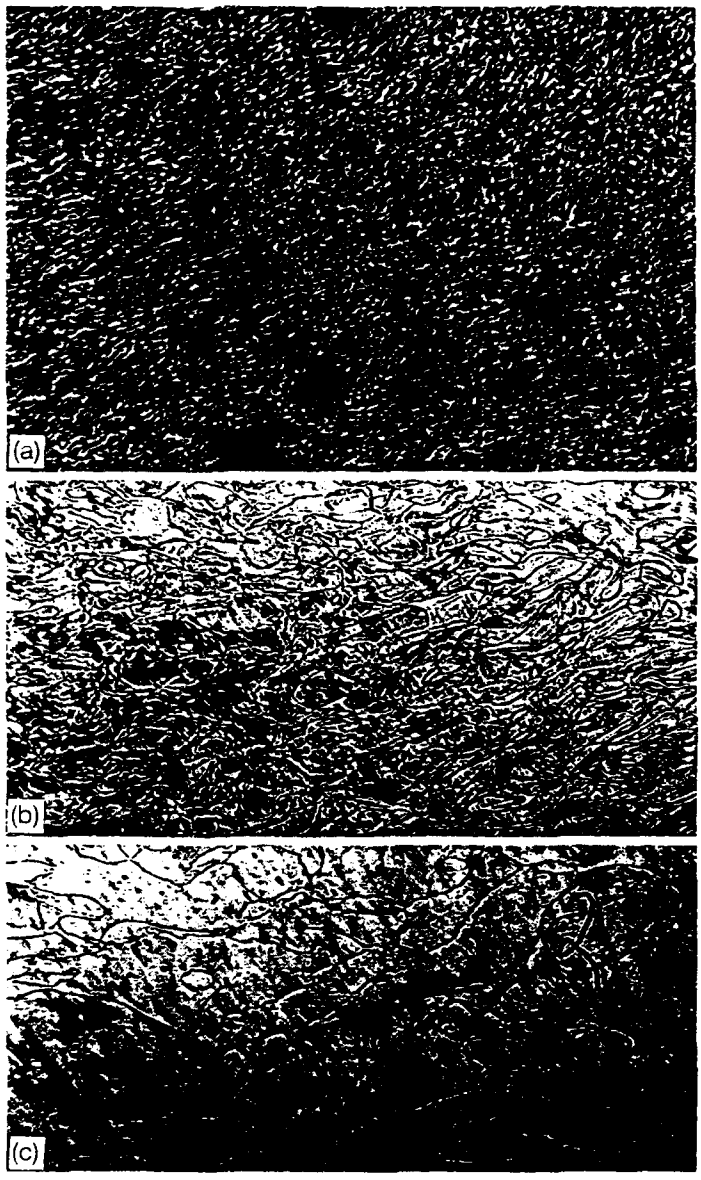

Figure 2 Development of a large-scale threaded texture out of (a) a grainy texture of a solution of PBZT (8%) in PPA after annealing at 100 °C for (b) 24 h and (c) 48 h, × 160

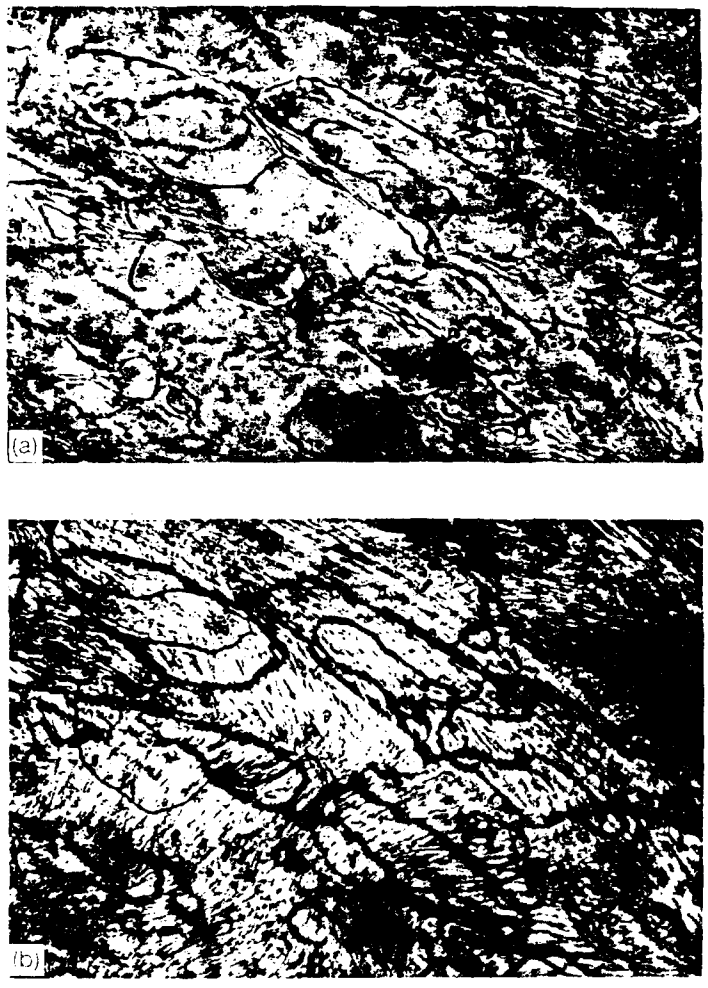

Figure 3 Development of a crystal solvate (b) out of a large-scale threaded texture (a) at 140° C. × 320.

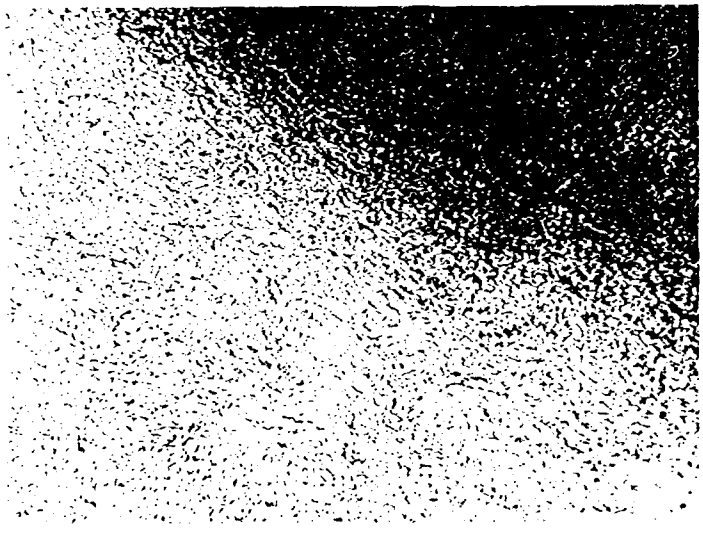

Figure 4 Growth of the red crystal solvate out of a nematic homogeneous solution of PBZT (8%) in PPA at 160° C. × 320.

Figure 5 Transition of the nematic to the isotropic phase (biphasic region) of a 3.8% solution of PBZT in OPA at 74.2 °C.

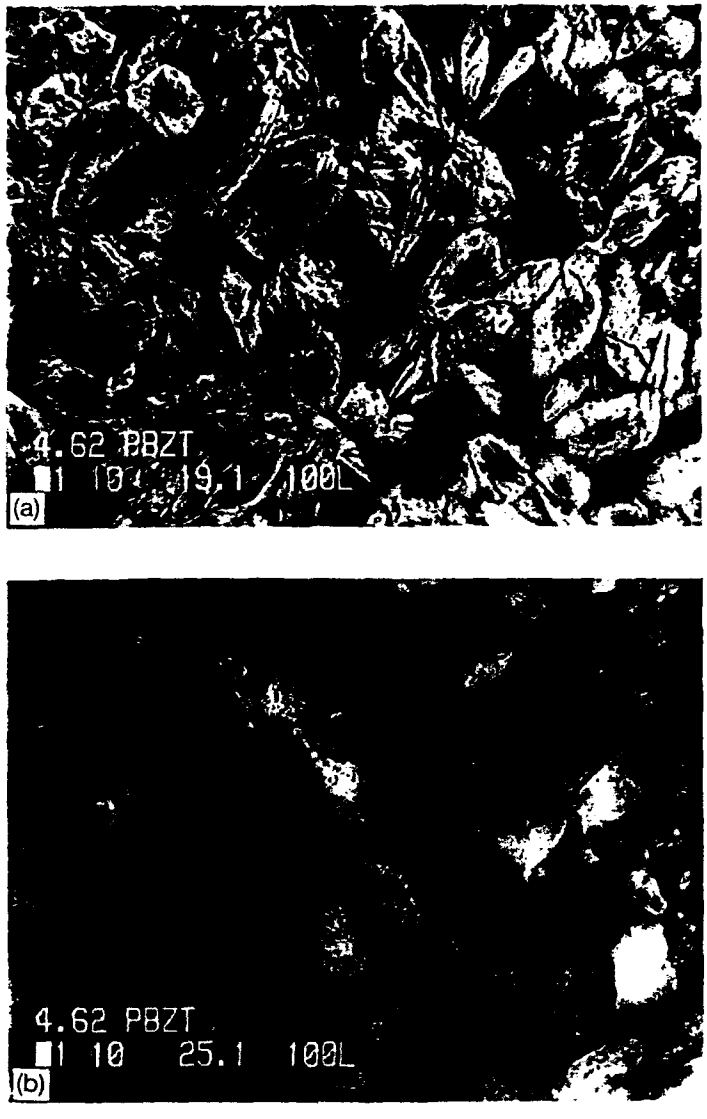

Figure 6 (a) Formation (19.1 °C) and (b) melting (25.1 °C) of the crystalline phase at low temperatures in a 4.62% solution of PBZT in OPA.

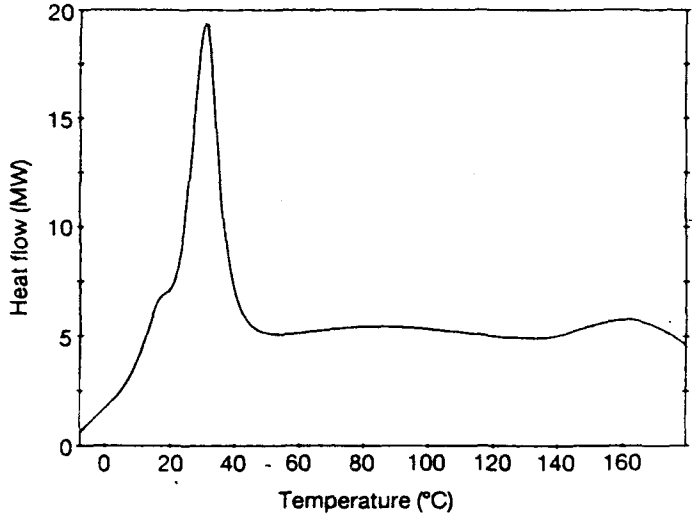

Figure 7 DSC heating trace of an 8.5% solution of PBZT in OPA.

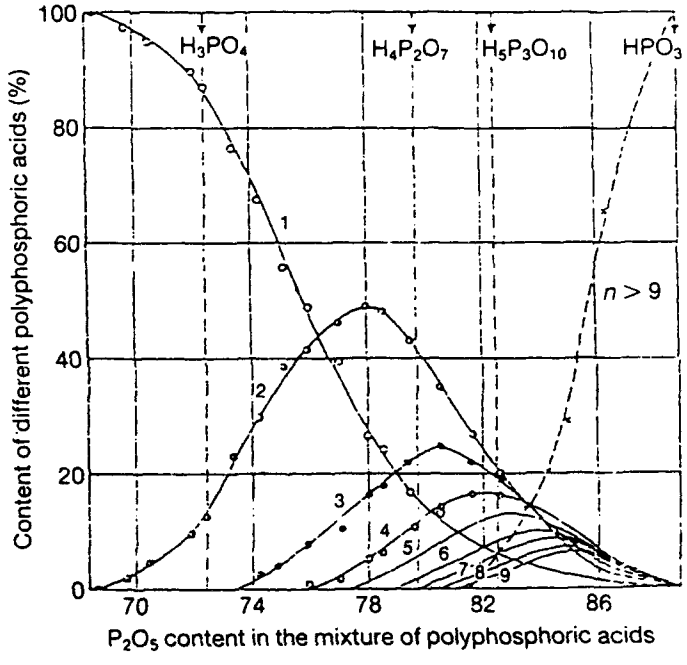

Figure 8 Distribution of the molecular weight of polyphosphoric acids in the system P_2O_5/H_2O in a concentration range between 68% and 89% P_2O_5.

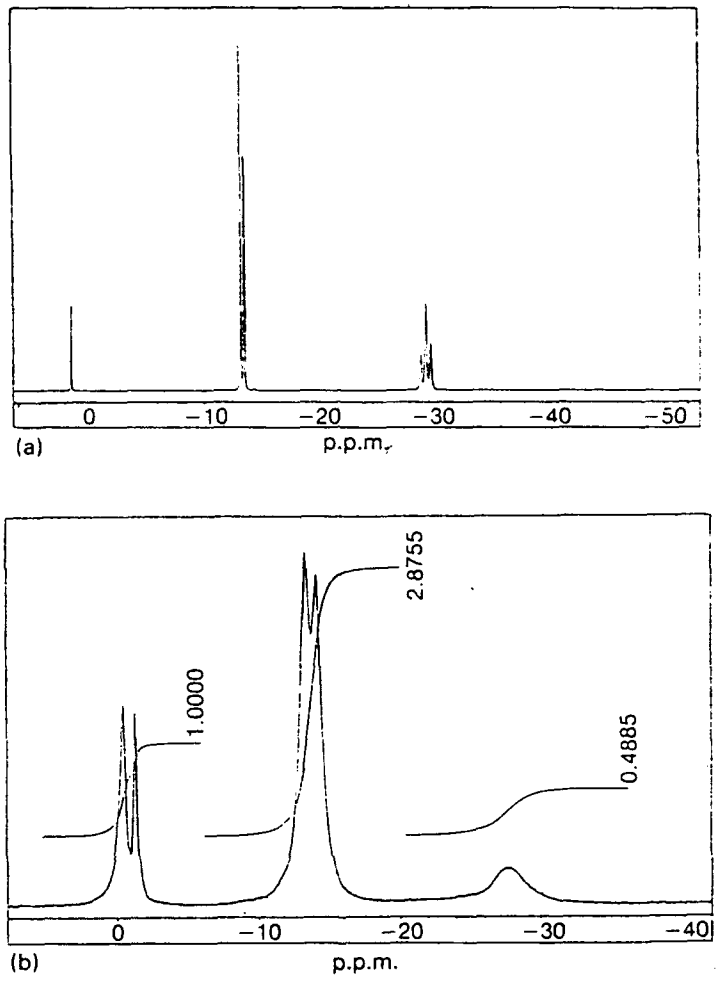

Figure 9 ^{31}P NMR spectra of (a) deuterated PPA, 500 MHz; and (b) 6.4% solution of PBZT in deuterated DPA, 500 MHz.

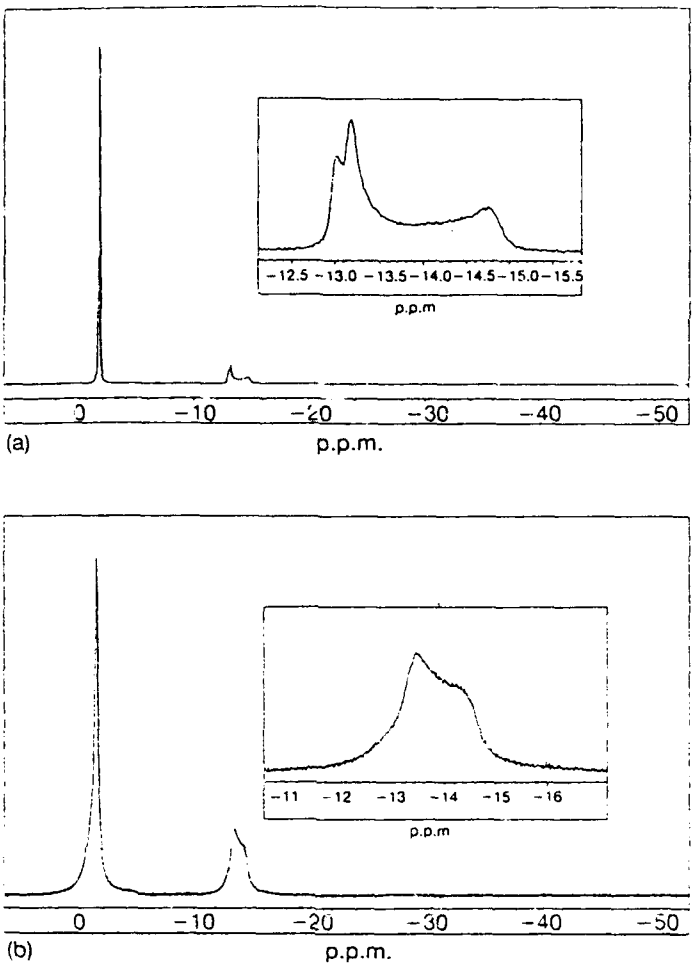

Figure 10 ^{31}P NMR spectra of (a) 8.5% and (b) 9% solutions of PBZT in deuterated OPA, 500 MHz.

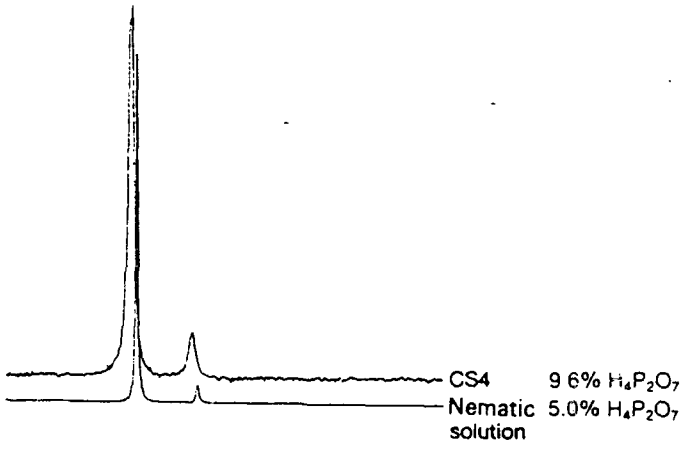

Figure 11 ^{31}P NMR spectra of 8% PBZT in deuterated OPA; spectra obtained from the nematic solution at 40° C, and from the crystal solvate 4 at 200 °C, 90 MHz.

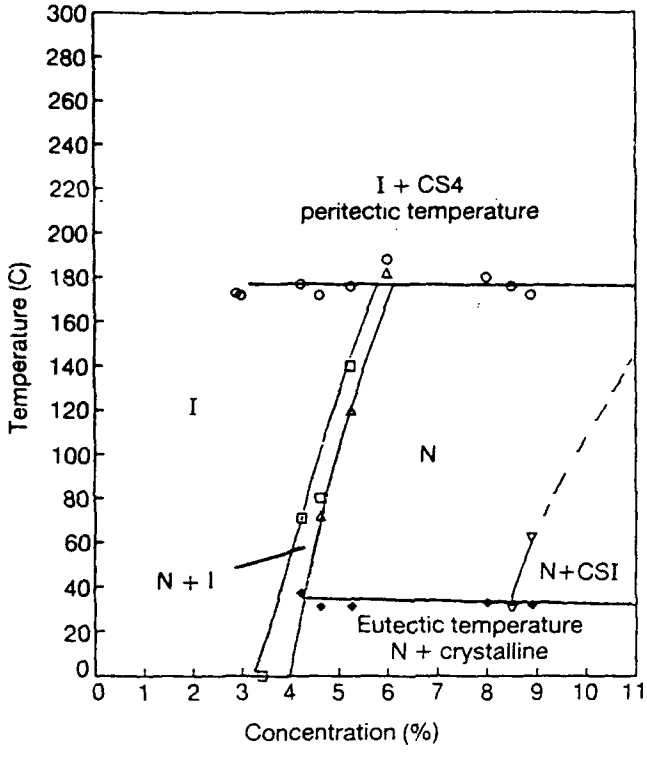

Figure 12 Phase diagram of the system PBZT/OPA.

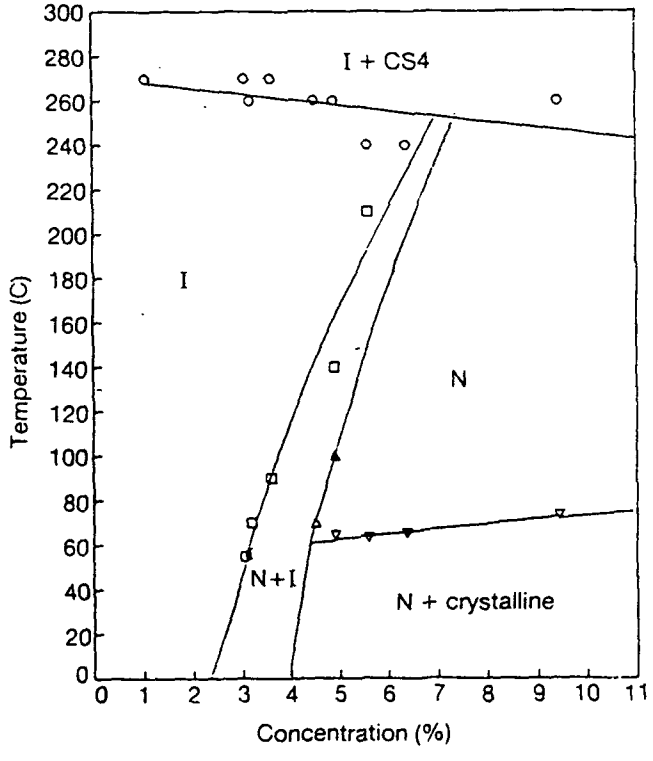

Figure 13 Phase diagram of the system PBZT/DPA.

On The Phase Diagram of the System Hydroxypropylcellulose/Water*

H. Fischer, M. Murray*, A. Keller and J. A. Odell

H. H. Wills Physics Laboratory, University of Bristol, Tyndall Avenue,
Royal Fort, Bristol, BS 8 - 1 TL
* School of Chemistry, University of Bristol, Cantocks Close,
Bristol BS 8 - 1 TS

ABSTRACT: The phase diagram of the System Hydroxypropylcellulose/Water has been investigated using DSC, X-ray diffraction, optical microscopy and ^{1}H NMR-spectroscopy. A peritectic line at higher temperatures has been found similar to the lytropic systems described before. This phase transition from a solution consisting of solvate aggregates and free solvent into a crystal solvate/isotropic phase system is completely reversible. The formation of crystal solvate phases is independent of the water content of the system until the system transforms into a thermotropic system. The solvent molecules are strongly associated with the macromolecules.

INTRODUCTION

The system Hydroxypropylcellulose (HPC) / water is one of the first systems where liquid crystallinity in solutions of polymers has been recognised [1]. An idealised structure of HPC is shown in Figure 1. This system is known to exhibit a complex phase behaviour including the formation of an isotropic and a mesomorphic phase, but also a reversible phase transition upon heating [1-5]. However, the nature of the phases at equilibrium at high temperatures is still not known. The occurrence of a "white gel" is often mentioned, and the phase behaviour is described as a LCST behaviour [1,2]. Other authors describe this phase as a mesophase with cholesteric order [4]. The other phase present at high temperatures is described as infinitely diluted solution [2,4]. However, not even the structures of the homogenous phases at lower temperatures are clear. Some authors understand the anisotropic phase as a solution consisting of discrete clusters of HPC chains [6] most are convinced that structuring of water through H-bonds plays an important role in the structure of the different phases [1,2,4,5,7]. There are some

* submitted to *J.Mater.Sci.*

investigations by means of light scattering [1] and X-ray diffraction [7] which suggest a strong aggregation of water molecules with each HPC chain.

Previous investigations on the system Poly-*p*-phenylene-benzbisthiazol (PBZT)/Polyphosphoric acid (PPA)/H_2O which is similar to system HPC/water have shown that solutions exhibit a more or less complex behaviour including the formation of different kinds of crystal solvates depending upon solvent content and temperature [8]. Orientation and relaxation of the dissolved macromolecules and the solvent molecules in this system have been observed during shear experiments [9]. There are some hints that there are two different kinds of solvent molecules present in the solution, molecules which are somehow adsorbed or bonded to the dissolved macromolecules and free solvent molecules in between them.

The investigations described in this paper have been carried out in order to understand the nature of the solid phase at high temperatures and to understand the principal features of phase diagrams of lyotropic polymeric systems.

EXPERIMENTAL

The different mixtures investigated were prepared by the following procedure. Air dry HPC was mixed with the calculated amount of distilled water in a teflon sealed sample vial. The vial was heated to about 70 °C until a white precipitate was formed. After cooling to 25 °C, the solution became transparent. Using several cycles the solution homogenised and was ready for the investigations. A GPC with two aquagel Polymer Laboratories (OH60 and OH 40) was used to check the molecular weight distribution before and after the dissolving process. Liquid crystalline behaviour was determined visually with a Linkam THM 600 hot stage mounted on a Zeiss Ultraphot optical microscope. A Sony video recorder was used to record crystal solvate formation and phase transitions from the nematic or the isotropic phase to the mixed phase. Thermal analysis was carried out using a Perkin Elmer DSC 7 with heating and cooling rates of 10 K/min to a temperature limit of 200 °C. Samples were prepared in stainless steel high pressure pans from Perkin Elmer. The 1H NMR-spectra were obtained using a JEOL Alpha 500. X-ray experiments were done on a GX 21 rotating anode with copper target, equipped with a graphite crystal monochromator and a 2-D GADDS detector X-1000 from Siemens. The usual time for collection of data for one frame was 180 seconds.

RESULTS AND DISCUSSION

The thermal behaviour of the system HPC/water was studied by DSC using a sample with an isotropic phase (35 % HPC) and a sample with a mesophase (65 % HPC). The traces obtained from both solutions show a phase transition in the heating and cooling mode (see Figure 2). This phase transition at 46 °C/ 61 °C corresponds to the formation of the "white gel" as reported by several authors before [1-5]. On cooling, the transition from the white gel / isotropic phase to the anisotropic or to the isotropic solution is supercoolable by 15 K. Similar results have been obtained in the system PBZT/PPA/H_2O [8]. There the phase transition was attributed to a formation of a mixed phase crystal solvate /solvent out of a homogeneous phase. Therefore we believe the behaviour in HPC/water is essentially similar.

Optical microscopy studies with polarised light were used to examine the isotropic and the anisotropic phase, and especially the formation of the "white gel" at higher temperatures. A 65 % solution shows an anisotropic texture at room temperature between crossed polarisers which is a typical texture known for nematic/cholesteric mesophases. By heating up to 65 °C a phase separation connected with the formation of a crystal solvate and a very low viscosity isotropic phase could be observed. The formation of the crystal solvates is associated with a change in transparency; also crystallisation of a different structure could be detected under the polarizing microscope. The Figures 3a and 3b show the development of a crystal solvate out of an anisotropic (a) and of an isotropic (b) solution. The crystal solvate exhibits very small crystal sizes. It no longer shows, the properties of a solution: no flow under shear conditions can be observed. The crystal solvate behaves like a network of macroscopic crystals. Together with the crystal solvate the presence of some isotropic liquid is observable. The formation of the crystal solvates is reversible. By cooling to 25 °C a single phase solution is present again.

The composition of the crystal solvate could be calculated by separation of the isotropic liquid phase from the solid crystal solvate at 70 °C and subtracting the weight of the isotropic phase (water) from the original amount of water in the solution used. The crystal solvate was found to consist of approximately 6 water molecules per monomeric unit of HPC and hence will be described as crystal solvate 6 (CS 6). This value corresponds to an association of approximately two water molecules per functional group (OH-group). Again a similar result has been found in the system PBZT/PPA/H_2O [8], where a crystal solvate consisting of 4 phosphoric acid groups per monomeric unit was estimated. Hence the maximum concentration of HPC in the system HPC/water is approximately 76 % before the lyotropic system becomes a thermotropic system. A

similar value has been reported by Fortin and Charlet [4]. They observed no discontinuity in the reflection wavelength for solutions with a weight fraction above 75 % HPC with increasing temperature. Also only a small amount of separated isotropic phase and only a minor change in turbidity has been reported by these authors [4] for solutions around 80 % during heating.

Interestingly enough, it was estimated by Fortin and Charlet that the concentration where the pure anisotropic phase is stable (50 - 55 %) corresponds to about 18 molecules of water per monomer or six molecules of water per hydroxyl group.

The isotropic phase was described by Fortin and Charlet [4] as an infinitely diluted solution. This has now been proved by ^{1}H-NMR spectroscopy. The NMR spectra did show a very small concentration of monomeric and oligomeric HPC. The existence of monomers in the isotropic solution could be concluded from the appearance of a signal corresponding to aldehyde groups which can only be explained by the existence of the ring opened monomer of HPC. With a change in temperature there is a change in the degree of associated water per monomeric unit, which includes either the formation of crystal solvates or a precipitation of the polymer. Therefore the isotropic phase is formed by the split off water, which is not associated with the crystal solvate.

X-ray diffraction patterns were taken from the isotropic phase and the anisotropic phase at room temperature and at 65 °C (see Figure 4). The diffractograms and the pattern show a clear difference between the isotropic and the anisotropic phase; the low angle reflection of the anisotropic phase is much more resolved and clear [7]. However, the patterns at 65 °C are very similar for both samples. Both display a very sharp small angle reflection and a more or less sharp wide angle reflection indicating the existence of some crystallinity. The small angle reflection is slightly shifted to larger angles compared with the pattern obtained from the anisotropic solution. This indicates closer packing of the chains in the crystal solvate phase due to the split off water molecules and the formation of the coexisting isotropic solution at higher temperatures.

X-ray diffraction patterns were also recorded while shearing the anisotropic solution (Figure 5). There is clear evidence that not only the main chains are oriented due to the shear (reflection 1), but also some orientation of the wide angle reflection associated with the water could be recorded (reflection 2). This observation is very similar to that reported by Feijo et al. [9] for sheared PBZT/PPA/H_2O samples. An association of water molecules with the main chain in the system HPC/H_2O is very likely and has been found before from Keates et al. [7] by means of X-ray diffraction and by Werbowij and Gray by light scatting methods [1]. Time resolved X-ray studies show a quick decay in the Hermans orientation parameter of the reflection 1 and 2 after cessation of shear (Figure

6). This decay is very similar and suggests also a strong association of water with the HPC.

One of the most informative methods for the investigation of the structure of the different liquid and solid phases in the system HPC/H_2O should be ^{1}H-NMR spectroscopy. The isotropic sample, a solution with a concentration of 35 % HPC did not show a clear splitting of the H_2O line at 4.75 ppm at room temperature (Figure 7a). Spectra at room temperature from solutions with higher concentrations of HPC (65 %) show a line broadening effect and a solid state like spectrum of the HPC part. ^{1}H NMR-spectra were also recorded at higher temperatures. Figure 7b shows a spectrum of the 35 % solution at 65 °C in the mixed phase crystal solvate / isotropic solution. There are two different lines observable at the range of the water resonance. It is assumed that there is free water present (small line at 4.4 ppm) as well as aggregated water on HPC chains (broader line shifted to higher field). An investigation of the differences between the interaction of the solvent with the polymer in the cholesteric solution and the crystal solvate phase was not possible. The spectrum shows broader lines than the spectrum at room temperature and is now comparable with the spectrum discussed by Werbowyj and Gray [1]. They also noticed the splitting of the water signal into two lines, a line with small line width associated with the free water in the solvent and a broad line corresponding to the HPC associated protons. There are two different lines observable in the region of the water resonance.

CONCLUSIONS

It is possible to modify the existing phase diagram (see Figure 8) [1, 3, 4]. The different regions are marked in the phase diagrams. The similarity of the phase diagrams of different systems of stiff main chain polymers in solution is obvious [8,10]. All show the main features of the theoretically described phase diagram of stiff rods in solution [11]. Moreover, all systems display a peritectic line connected with the formation of a crystal solvate at high temperatures. These crystal solvate phases have very similar constitutions, specifically the systems PBZT/PPA/H_2O [8] and HPC/H_2O forming a crystal solvate where **two** solvent molecules are aggregated to one H-bond active site (NH-group and OH group). The association of solvent molecules is also present in all systems in the homogeneous phases, in the isotropic phase, and in the anisotropic phase [8].

The question now arises, what is the nature of the homogeneous phases? We think that there is no clear distinction between the so called lyotropic liquid crystalline polymers formed from "solutions" of stiff main chain polymers and thermotropic polymers. The association of solvent molecules is very strong in the case of the lyotropic polymers and very little solvent is left. So the main action of the solvent is the lowering of the melting temperature of the stiff chain polymers by formation of a "new" substance, the solvate aggregate. This is clearly the case for the HPC/water system where the pure, single phase anisotropic area starts at a concentration, which corresponds to about 18 molecules of water per monomeric unit . A monomeric unit contains nine oxygen atoms, so that almost all the water could be well fixed to the whole monomeric unit with little or no "free" water left.

The knowledge of the phase diagram and the composition of the phases has led to a novel technique for preparation of highly concentrated solutions by an easy and quick way. As described in the experimental part, the solutions were prepared by heating a mixture of water and dry HPC until the crystal solvate was formed. This happened in a short time due to the high vapour pressure of water at high temperatures and the shortening of the swelling time of HPC. Once the crystal solvate is formed, one can prepare any concentration by simple "dilution" of the crystal solvate with the amount of water required and cooling down to the homogeneous region. No change in the molecular weight distribution has been recorded (Figure 9). This procedure is only applicable up to a final concentration of about 76 % HPC (composition of the crystal solvate). Mixtures with higher concentration can be achieved by application of a controlled vacuum to the crystal solvate. The technique of solution preparation may have general applicability to lyotropic systems.

SUMMARY

At high temperatures a precipitation of a crystal solvate phase of HPC is forced due to an increase in the condensation degree of the solvent and the elimination of water as a non solvent. Optics, X-ray shear experiments and NMR experiments point to the existence of closely associated water with approximately two water molecules per functional group (OH) of HPC. A novel preparation technique has been introduced which enables a quick and easy preparation of highly concentrated solutions of stiff chain polymers.

REFERENCES

[1] Werbowyj, R. S. and Gray, D. G., *Macromolecules*, **13**, 69, (1980)

[2] Aspler, S. A., and Gray, D. G., *Macromolecules*, **14**, 1546, (1981)

[3] Conio, G., Bianchi, E., Ciferri, A., Tealdi A. and Aden, M. A., *Macromolecules*, **16**, 1264, (1983)

[4] Fortin, S. and Charlet, G., *Macromolecules*, **22**, 2286, (1989)

[5] Winnik, F. M., *Macromolecules*, **20**, 2745, (1987)

[6] Wignall, G. D., Annis, B. K. and Triolo, R. *J.Polym.Sci.Polym.Phys.Ed.*, **29**, 349 (1991)

[7] Keates, P, Mitchell, G. R. and Peuvrel, E., *Polymer*, **33**, 3298 (1992)

[8] Fischer, H. Odell, J. A., Keller, A and Murray, M., *J. Mater. Sci.*, **29**, 1025 (1994)

[9] Feijo, L. J., Odell, J. A. and Keller, A., *Polymer Commun.*, **31** (1990) 42

[10] Förster, G., Reussner, J., Jankowski, A., Kuschel, F. and Wagner R., *Cryst. Res. Techn.*, **24**, 11 (1989)

[10] Flory, P. J. *Proc. R. Soc. London, Ser. A*, **234**, 73 (1956)

FIGURE CAPTIONS

Figure 1: idealised structure of HPC

Figure 2: DSC heating and cooling trace of an
a. 35 % isotropic solution of HPC in water (solid line)
b. 65 % anisotropic solution of HPC in water (dashed line)

Figure 3: microscopically picture of the formation of the white crystal solvate out of an a. 35 % isotropic solution of HPC in water at 65 °C
b. 65 % anisotropic solution of HPC in water at 65 °C

Figure 4: X-ray diffraction patterns and diffractograms from the
a: isotropic phase at room temperature, b: at room temperature
c: isotropic phase at 65 °C, d: anisotropic phase at 65 °C

Figure 5: a: X-ray diffraction pattern recorded while shearing the anisotropic solution, b: plot of the azimuthal intensity of the reflections 1 and 2.

Figure 6: Hermans orientation parameter of the reflection 1 and 2 after cessation of shear, determined by X-ray diffraction

Figure 7: H-NMR spectra of a 35 % solution of HPC in D_2O, 500 MHz
a. 25 °C, b. 65 °C

Figure 8: modified phase diagram of the system HPC/water

Figure 9: GPC traces of the HPC, solid line: as supplied, dashed line: after the dissolving process

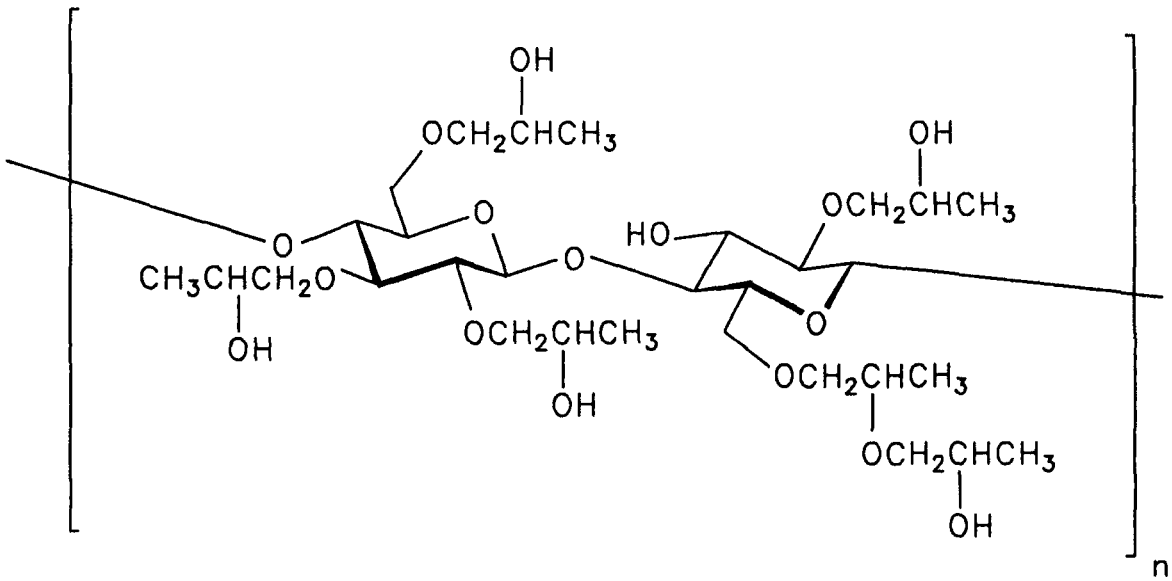
OH
OCH2CHCH3
O
O
CH3CHCH2O
OH
O
OCH2CHCH3
OH
HO
OH
OCH2CHCH3
O
OCH2CHCH3
OCH2CHCH3
OH
n

Figure 1

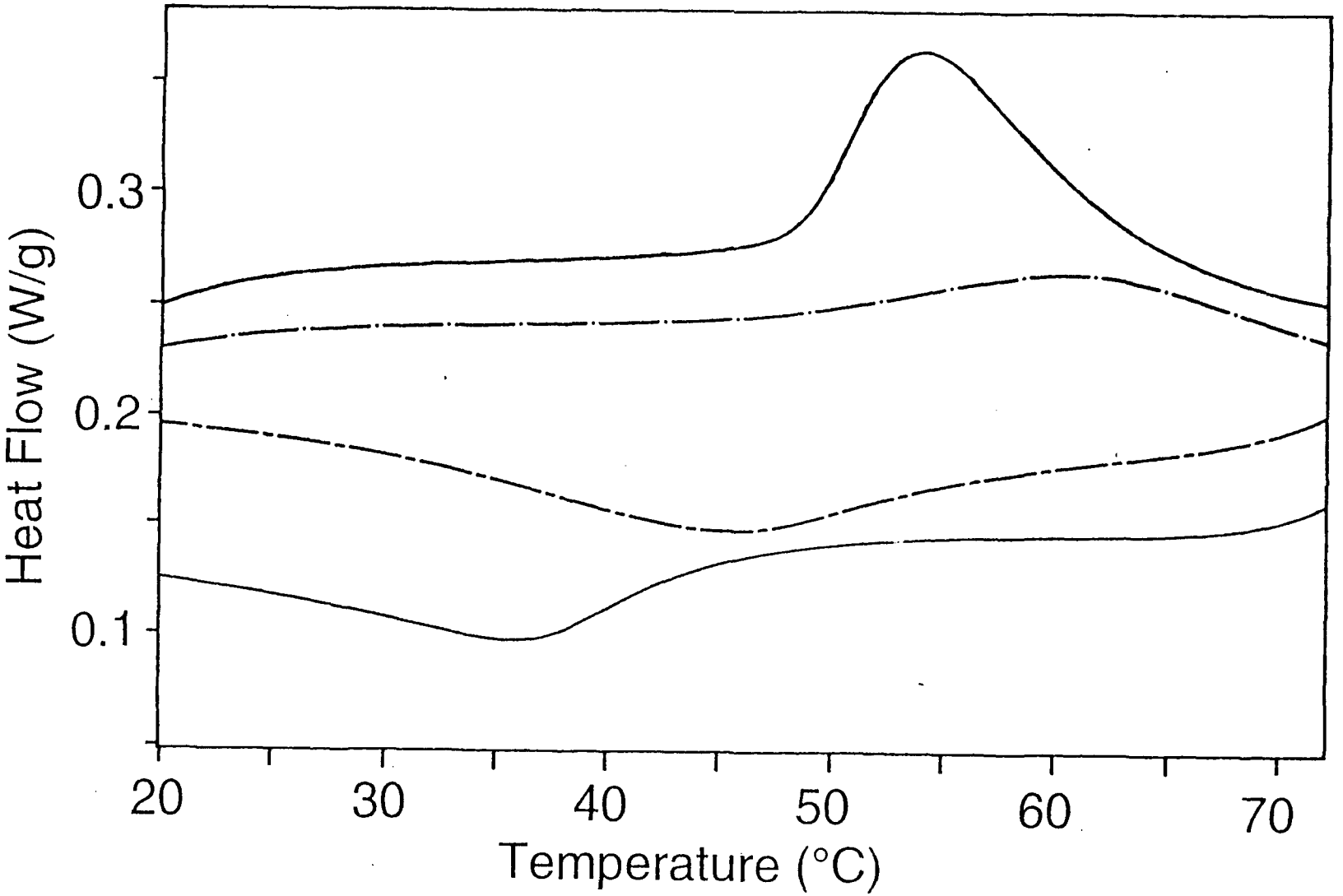

Figure 2

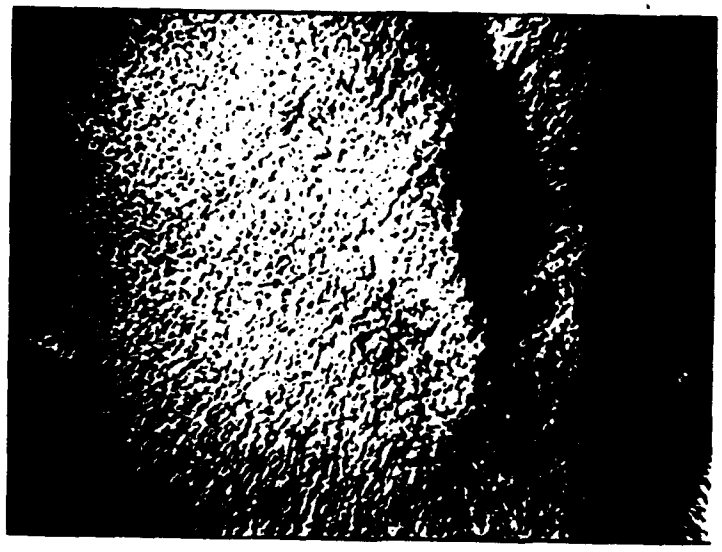

Figure 3a

Figure 3b

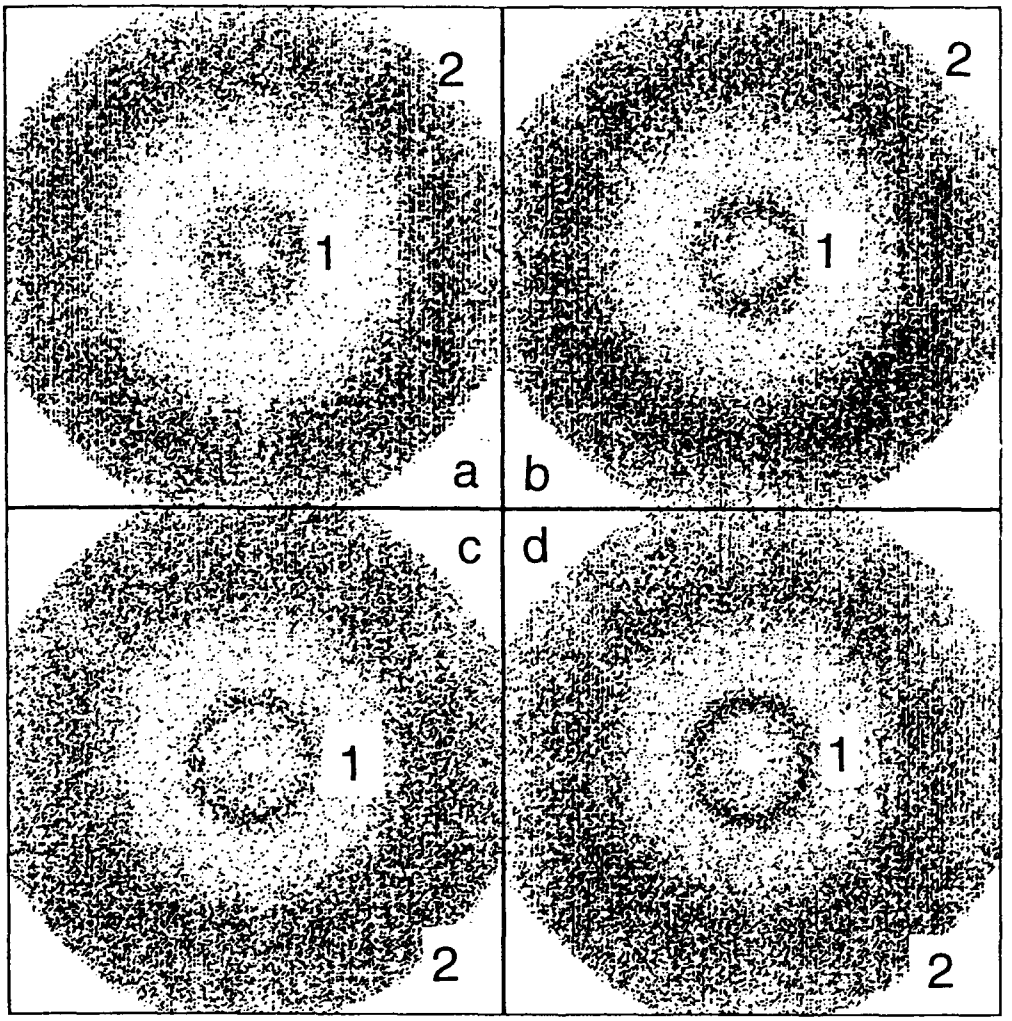

Figure 4

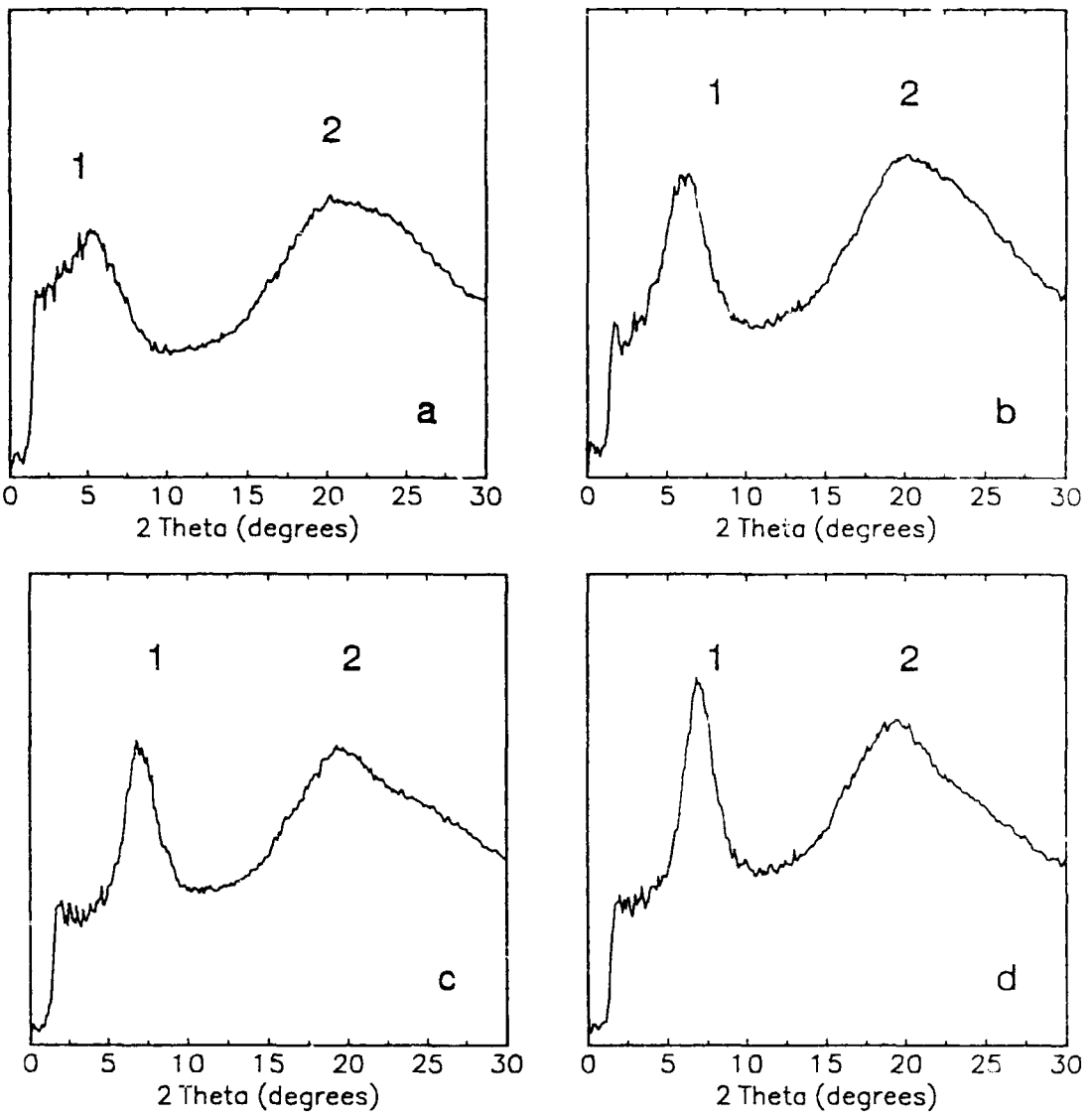
1
2
a
0 5 10 15 20 25 30
2 Theta (degrees)
1
2
b
0 5 10 15 20 25 30
2 Theta (degrees)
1
2
c
0 5 10 15 20 25 30
2 Theta (degrees)
1
2
d
0 5 10 15 20 25 30
2 Theta (degrees)

Figure 4

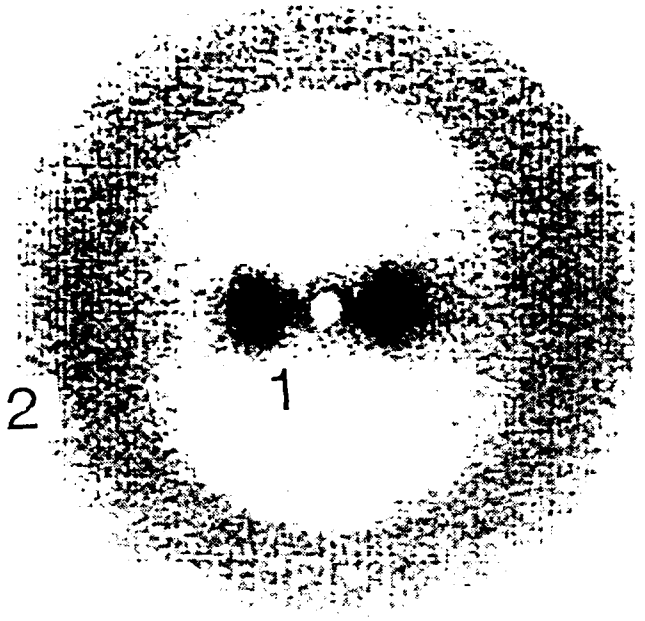

Figure 5a

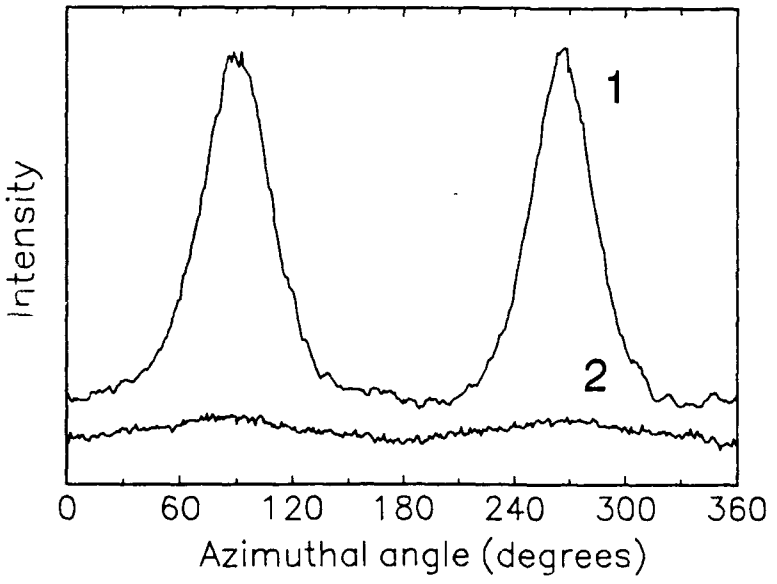

Figure 5b

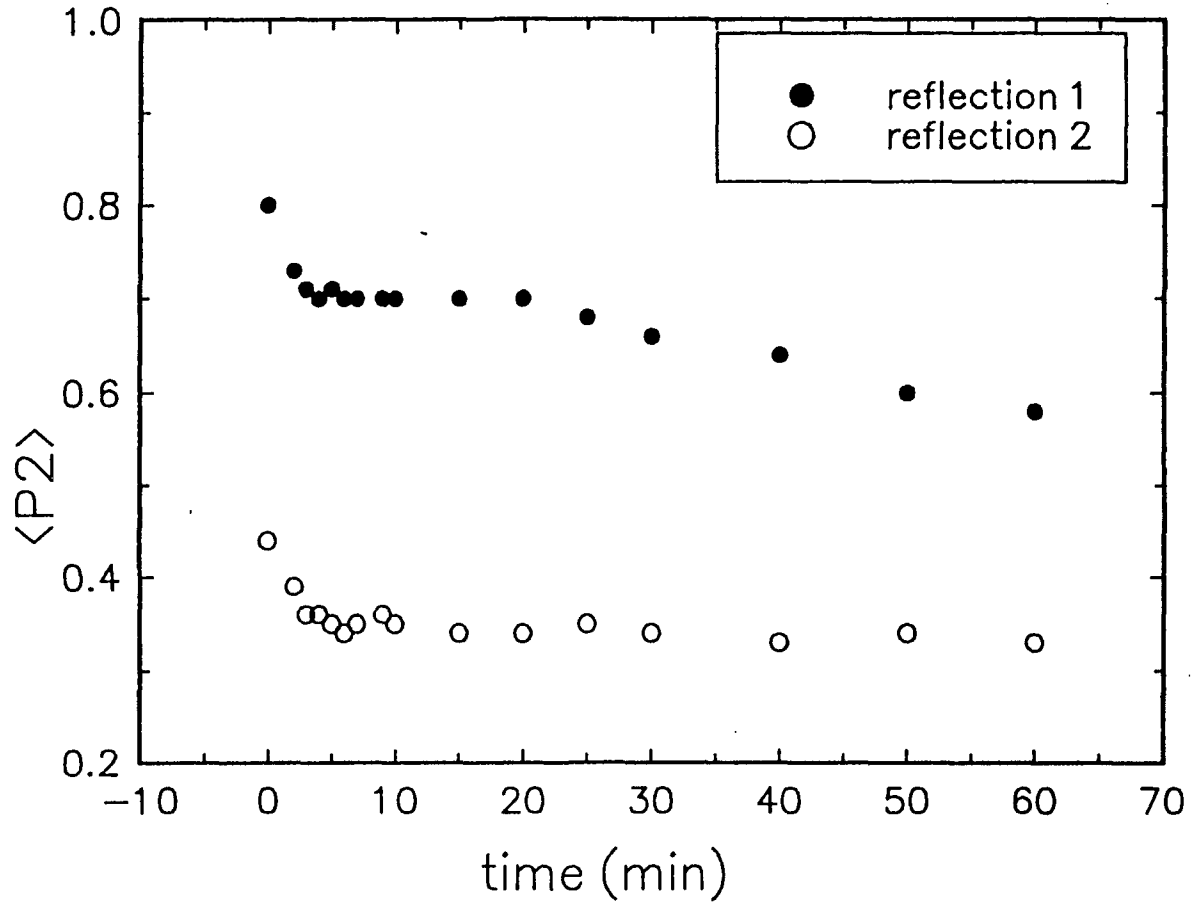
1.0
0.8
0.6
0.4
0.2
<P2>
−10
0
10
20
30
40
50
60
70
time (min)
reflection 1
reflection 2

Figure 6

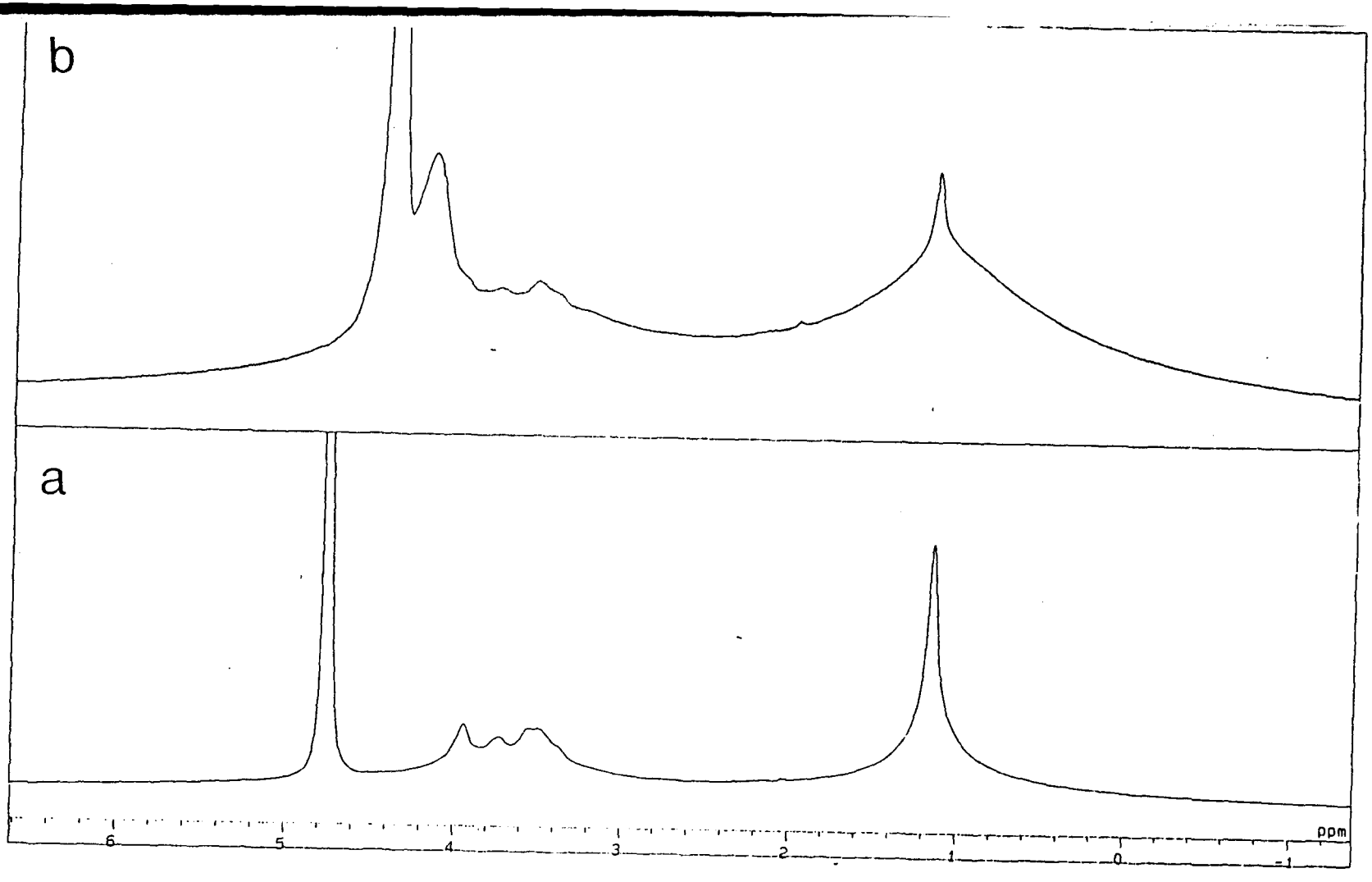

Figure 7

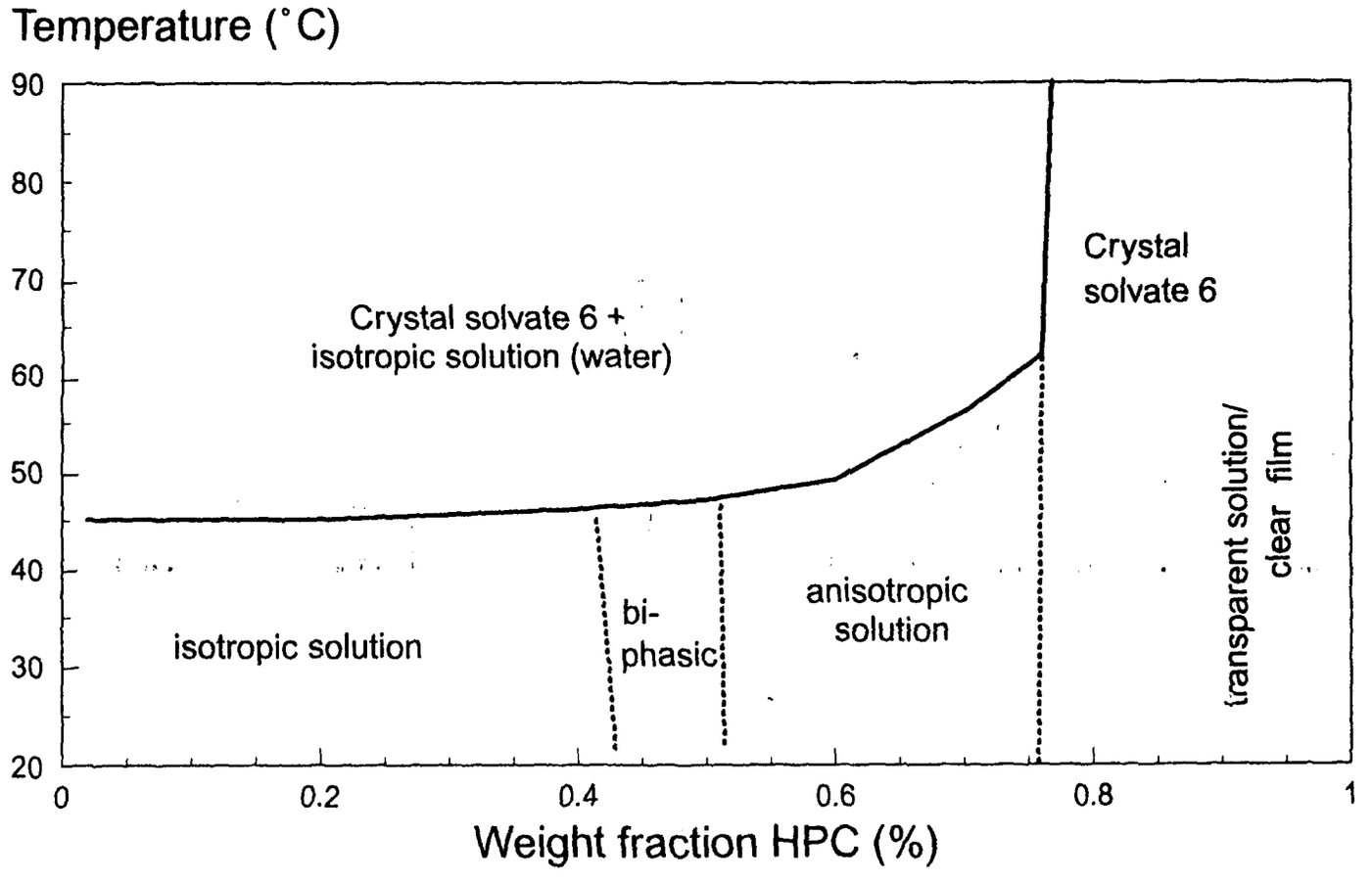
Temperature (˚C)
90
80
70
60
50
40
30
20
0
0.2
0.4
0.6
0.8
1
Weight fraction HPC (%)
Crystal solvate 6 + isotropic solution (water)
Crystal solvate 6
isotropic solution
bi-phasic
anisotropic solution
transparent solution/ clear film

Figure 8

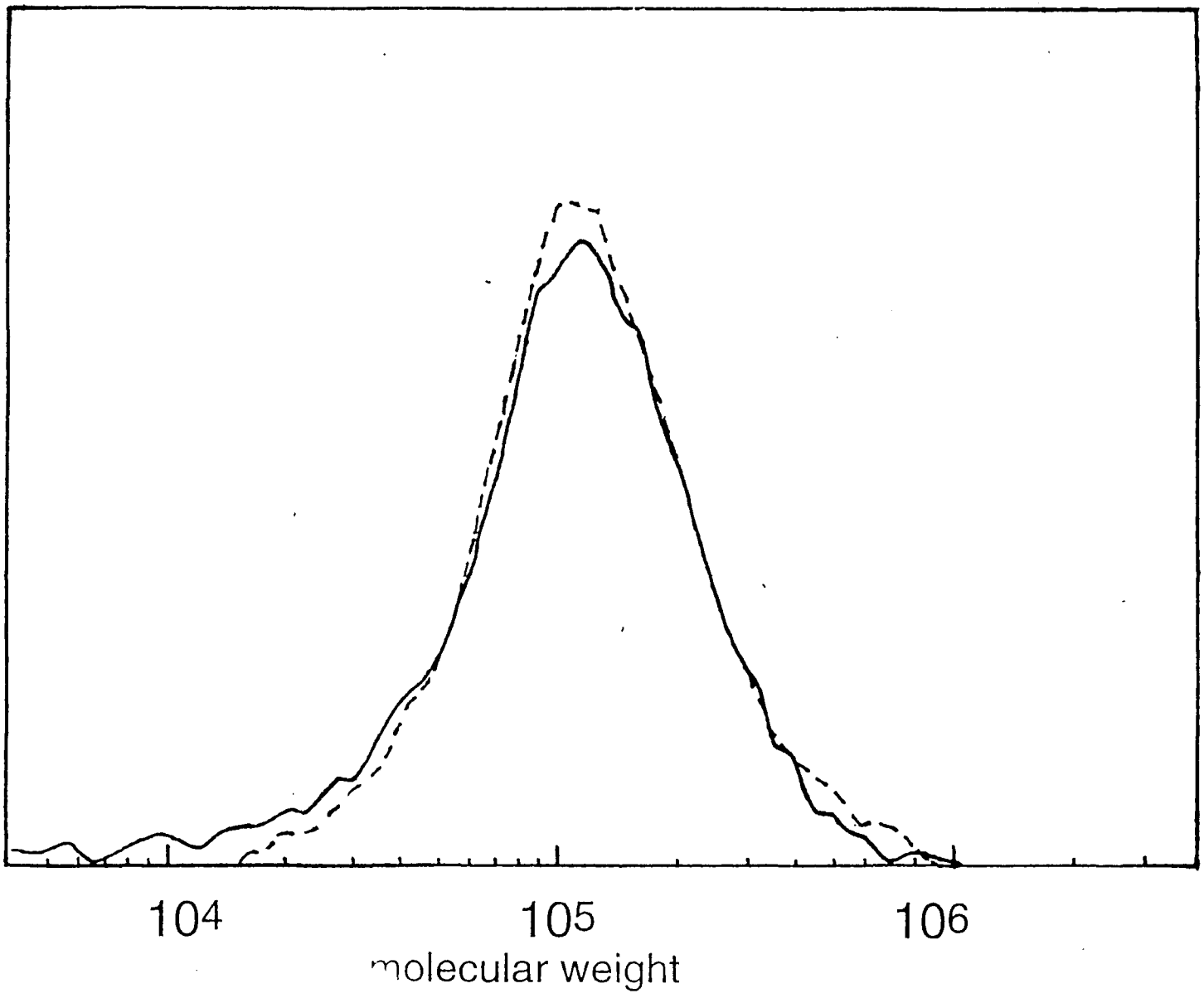

Figure 9

SECTION 5: STRUCTURE FORMATION IN BLOCK COPOLYMERS WITH ONE LIQUID CRYSTALLINE BLOCK

Additional work has been done on AB and BAB block copolymers, consisting of an amorphous A-block (for example styrene, butadiene) and one or two liquid crystalline B-blocks. Block copolymers composed of incompatible block segments form in general a micro domain morphology in the solid state. In this class of polymers it is possible to combine the properties of two completely different polymers with no macroscopic phase separation occurring. Owing to the chemical link between the non compatible polymers, the phase separation is limited to a microscopic scale, and is dependent on the thermodynamic interaction parameter χ, on the temperature, on the molecular weights of the constituent block chains and on the volume fraction of the different blocks. .Several different morphologies have been predicted and observed. These morphologies are spheres in a cubic lattice, rods in a hexagonal lattice embedded in the matrix of the other component of the block copolymers or lamellae of both. Recently, ordered bicontinuous morphologies were also found. These double-diamond structures, space group P_n3m, (OBDD) were found for volume fractions inbetween the lamellar and the rodlike hexagonal phase. If one of the blocks is a liquid crystalline side group polymer (LC), two different scales of phase separation might be obtained. It is now the aim to study the influence of the morphology of the block copolymer on the phase structure of the LC-block. Questions of interest are also:

- Is there any difference in the structure of the LC phase at the surface or in bulk?
- Is there a dependency of the equilibrium phase of the LC part (substructure) on the dimensions of the morphological structure?

Initial investigations on the AB type cpolymers Poly-styren-*b*-2-(3-cholsteryl-oxycarbonyloxy)-ethylmethacrylates (PS-PChEMA) and Poly-butadien-*b*-2-(3-cholsteryl-oxycarbonyloxy)-ethylmethacrylates (PB-PChEMA) suggested an influence of the amorphous block on the phase structure of the LC-block for a lamellar structure. Now we are interested in varying the block length ratios for the A-B block copolymers to obtain different volume ratios of the two parts. The phase separation of the block copolymer should lead to different morphologies in these block copolymers. Di- (AB) and triblock-copolymers (BAB) of Poly-styren-*b*-2-(3-cholsteryl-oxycarbonyloxy)-ethylmethacrylates (PS-PChEMA and PChEMA-PS-PChEMA) have been studied to determine the influence of the different block lengths and thus the change in the morphology, on the phase behaviour of the LC phase (see abstracts of papers 1 and 2). A change in morphology was

observed with respect to the morphology consisting of PS-rods embedded in a PChEMA-matrix. Here a tetragonal arrangement of the rods has been found instead of the hexagonal structure known from the system PS-*b*-PB (see attached paper and abstract 3). This structural change may also be produced due the interaction between morphological structure and phase behaviour of a LC side chain block copolymer. Other work has been performed to investigated the structure of the interface between the blocks and the interaction between morphology and LC phase behaviour (see attached abstracts of papers 4 and 5).

(1) Arnold, M, Poser, S.; Fischer, H.; Frank, W.; and Utschick, H., "LC side group block copolymers -synthesis, morphology and phase behaviour", *Macromol.Rapid Commun.*, **1994**, *15*, 487

ABSTRACT: LC side chain block copolymer have been synthesised using living anionic polymerisation and a polymeranlogous reaction. All samples of Poly-styren-*block*-2-(3-cholsteryl-oxycarbonyloxy)-ethylmethacrylate (PS-*b*-PChEMA) show a phase separation between the two blocks as investigated by SAXS, DSC, TEM and low angle electron diffraction.. The phase structure of the liquid crystalline sub-phase is dependent on the morphological structure.

(2) Fischer, H., Poser, S., Frank, W. and Arnold, M., "On the influence of the morphology on the LC behaviour of LC side chain block copolymers ", *Macromoleclues*, submitted for publication

ABSTRACT: The influence of the morphology on the phase behaviour of a LC side chain block copolymer has been investigated using SAXS, DSC, TEM and low angle electron diffraction. All samples of Poly-styren-*block*-2-(3-cholsteryl-oxycarbonyloxy)-ethylmethacrylate (PS-PChEMA) show a phase separation between the two blocks. An influence on the phase structure of the liquid crystalline sub-phase, exerted by the morphological structure was observed. It was found that in the case of those samples, where the liquid crystalline sub-phase is not continuous (spheres), only a nematic phase is seen, whereas in all samples in which there is a continuous liquid crystalline sub-phase, the smectic A phase of the homopolymer is formed.

(3) Fischer, H., "The Existence of a tetragonal structure in block Copolymers", *Polymer Commun.*, in press

ABSTRACT: The morphology of AB and BAB block copolymers consisting of one amorphous block (A) and liquid crystalline blocks (B) has been investigated using TEM, low angle electron diffraction and small angle x-ray diffraction. All samples of Poly-styren-*block*-2-(3-cholsteryl-oxycarbonyloxy)-ethylmethacrylate (PS-PChEMA) with a volume fraction ΦPS between 0.3 and 0.4 show a morphology consisting of polystyrene rods in a PChEMA matrix. The rods are organised in a tetragonal lattice rather than the expected hexagonal structure.

(4) Fischer, H., *Polymer Commun.*, "Selective staining of the interfacial region in block copolymers ", submitted for publication

ABSTRACT: The morphology of AB block copolymers consisting of one amorphous block (A) and one liquid crystalline blocks (B) has been investigated using TEM. A selective staining of the interfacial region has been observed if the staining agent (RuO_4) was applied for only a short time. The interface was observed to be about 2.5 ± 1 nm thick, the thickness is independent from the molecular weight of the block copolymers.

(5) Fischer, H., Poser, S. and Arnold, M., " On the interaction of the morphological structure and the LC behaviour of LC side chain block copolymers", submitted to *Liq.Cryst.*

ABSTRACT: The interaction between morphological structure and phase behaviour of a LC side chain block copolymer has been investigated using DSC, TEM and small angle X-ray diffraction. All samples of Poly-styren-*block*-2-(3-cholsteryl-oxycarbonyloxy)-ethylmethacrylate (PS-PChEMA) show a phase separation between the two blocks. It was found that in the case of those samples, where the liquid crystalline sub-phase is not continuous (spheres), only a nematic phase is seen, whereas in all samples in which there is a continuous liquid crystalline sub-phase, the smectic A phase of the homopolymer is formed. On the other hand, the block copolymer seems to stabilize the LC-phase, no dependency of the clearing temperatures from the molecular weight of the LC blocks has been observed.

The Existence of a tetragonal structure in block copolymers*

INTRODUCTION

Block copolymers are an interesting and already well studied variation of polymers. In this class of polymers it is possible to combine the properties of two completely different polymers without macroscopic phase separation occurring. Due to the chemical link between the non-compatible polymers, the phase separation is limited to a microscopic scale, and is dependent on the volume fraction of the different blocks. Several different morphologies have been predicted and observed. These morphologies are dependent from the volume fraction of one block: spheres in a cubic lattice, rods in a hexagonal lattice in each case embedded in the matrix of the other component of the block copolymers or lamellae of both (1). Recently, ordered bicontinuous morphologies were also found (2-4). These double-diamond structures, space group P_{n3m}, (OBDD) were observed for volume fractions in-between the lamellar and the rodlike hexagonal phase. So the scheme for the morphologies of the block copolymers is as described by Bates and Fredericson (1), a sequence of spherical, rodlike hexagonal, double diamond and lamellar phases.

If one of the blocks is a liquid crystalline side group polymer, two different scales of phase separation might be obtained. It is possible to study the influence of the morphology of the block copolymer on the phase structure of the LC-block (5,6). Initial investigations on the AB type cpolymers Poly-styren-*block*-2-(3-cholsteryl-oxycarbonyloxy)-ethylmethacrylates (PS-PChEMA) and Poly-butadien-*block*-2-(3-cholsteryl-oxycarbonyloxy)-ethylmethacrylates (PB-PChEMA) suggested an influence of the amorphous block on the phase structure of the LC-block which was dependent on the type of monomer in the A-block for a lamellar structure (7). More systematic investigations are reported here. Di- (AB) and triblock-copolymers (BAB) of Poly-styren-*block*-2-(3-cholsteryl-oxycarbonyloxy)-ethylmethacrylates (PS-PChEMA and PChEMA-PS-PChEMA) (see Figure 1) have been studied to determine the influence of the different block lengths and thus the change in the morphology, on the phase behaviour of the LC phase (5).

---

* *Polymer Communications*, accepted for publication

EXPERIMENTAL

The block copolymers were synthesised as described previously (6,7) and kindly supplied by S. Poser, Martin-Luther-University Halle-Wittenberg. Samples of the polymers were prepared by casting approximately 1 mm thick films from dilute solutions of the polymers in Toluene, over a period of about 10 days at 25 °C and annealing them afterwards at 130 °C for 24 hrs. under vacuum. The samples were cut using a diamond knife at room temperature and the thin sections (appr. 10 nm thick) were transferred onto Copper grids. In order to get sufficient contrast for transmission electron microscopy (TEM) and low angle electron diffraction studies (8-10), the styrene parts of the samples were stained with RuO_4 vapour at 25 °C for about 30 minutes (11). For the TEM studies and the low angle electron diffraction experiments a Phillips EM 301 was used. The diffraction experiments were performed as described elsewhere (9, 10). X-ray studies were carried out using an Eliott GX 21 with copper target combined with a Rigaku Denki small angle film camera.

RESULTS AND DISCUSSION

The investigated block copolymers were characterised as described in ref. 5 and 6 using GPC, DSC and POM. All the samples reported here show two glass transition temperatures (see Table 1), indicating that phase separation occurred. The phase separation of the two blocks could be confirmed by small angle X-ray diffraction studies (5). Also all samples show the appearance of a smectic A phase in the WAXD pattern. The phase transition temperatures, phase structures and expected morphologies are listed in Table 1 (5). A direct investigation of the morphology of the phase separated block copolymers was possible by TEM using sections of the block copolymers. Figure 2 shows representative pictures of the observed morphology. As expected, PS-rods are formed, embedded in a matrix of the LC-block. It was not possible to obtain completely uniform areas of orientation, but this was an advantage since views in the rod direction as well as perpendicular to the rods could be recorded simultaneously. Top views of the rods are clearly visible. There is a hexagonal arrangement of the rods only in small areas, possibly because of deformation during the cutting process. Larger areas show also a tetragonal arrangement of the rods. This is observed for both, the diblock-copolymer and the triblock-copolymers.

The tetragonal structure is quite new and unexpected, therefore low angle electron diffraction studies have been carried out according to the procedure described by Mahl et

al. (8), Bassett and Keller (9) and Kämpf et al. (10). Compared with X-ray diffraction techniques, the advantages of their method are, firstly, the resolution limit is very much smaller (app. 4000 Å) for low angle electron diffraction (14). Secondly, the exposure time is smaller than in the case of X-ray diffraction. Also, due to the point focus of the electron beam two dimensional resolution is immediately obtained without slit de-smearing approximation procedures etc. Finally the area with a uniform orientation needed for a diffraction experiment can be much smaller (25 μm^2) compared to that required for small angle X-ray diffraction (~ 1 mm^2). Therefore it was possible to select areas with a uniform orientation in the transmission mode prior to switching to the diffraction mode. A disadvantage of low angle electron diffraction is the difficulty in finding a suitable calibration standard. In this case no suitable standard was available so that the diffraction patterns obtained have only qualitative meaning. Figure 3 shows the low angle electron diffraction pattern obtained from the sample DB 7. This was the only sample where larger areas of an uniform orientation of the rods were found. The diffraction pattern can be indexed as that of a tetragonal lattice looking at the [001] plane as shown in the schematic diagram (see Figure 4). The diameter of the dots in Figure 4 is proportional to the expected intensity of the diffraction pattern. Due to the uniformity of the area chosen, it was possible to obtain not only the 100 and 110 reflection, in Figure 3 but also very weak 200 reflections visible. There was now the possibility that a present hexagonal lattice got deformed due to the sectioning process to a tetragonal lattice or a hexagonal lattice was seen under a certain angle and appeared to be tetragonal. Since the low angle electron diffraction represents the Fourier Transform of the observed image, small angle x-ray diffraction studies were carried out on bulk samples to confirm the existence of the tetragonal morphology. Figure 5 shows the small angle x-ray diffraction pattern of sample DB 7. The reflection are not extremely sharp and strong because the phase boundaries are owing to the interfacial region are not very well defined,. However, reflections are observed with a d-spacing of 212 Å, 152 Å and 106 Å, these can be indexed as the 100, 110 and 200 reflections of a tetragonal lattice (see Figure 5b) .

CONCLUSIONS

TEM imaging and low angle electron diffraction reveals a tetragonal arrangement of PS-rods in the block copolymers investigated in this study rather than the expected hexagonal. The tetragonal structure is consistent with small angle x-ray diffraction studies. There is only a small energy difference in-between the hexagonal and the tetragonal lattice, so that it could be well possible, that the system described here prefers the tetragonal lattice to the hexagonal lattice. And in that case, once the tetragonal morphological structure is formed, annealing experiments in order to drive the system towards equilibrium will not change the lattice type towards the hexagonal lattice.

ACKNOWLEDGEMENT:

The supply of the copolymer samples by S. Poser, Martin-Luther-University Halle-Wittenberg is gratefully acknowledged. HF would like to thank M. J. Hill for the help and support during the electron microscopically studies.

REFERENCES

(1) Bates, F. S. and Frederickson, G. H., *Annu.Rev..Phys.Chem.*, **41**, 525 (1991)
(2) Alward, D. B., Kinning, D. J., Thomas, E. L. and Fetters, L. J., *Macromolecules*, **19**, 215, 1288, 2197 (1986)
(3) H. Hasegawa, H. Tanaka, K. Yamasaki and T. Hashimoto, *Macromolecules*, **20**, 1651 (1987)
(4) Spontak, R. J., Smith S. D. and Ashraf, A., *Macromolecules*, **26**, 956 (1993)
(5) Fischer, H., Poser, S., Arnold, M. and Frank, W., *Macromolecules* submitted for publication
(6) Poser, S., Fischer, H., Frank, W., Arnold, M., *Macromol.Chem.,Rapid Commun.*, in press
(7) Zaschke, B., Frank, W., Fischer, H., Arnold, M., *Polymer Bull.*, **27**, 1 (1991)
(8) Mahl, H. von and Weitsch, W., *Z. Naturf.*, **A15**, 1051 (1960)
(9) Basset, G. A. and Keller, A., *Phil. Mag.*, **9**, 817 (1964)
(10) Kämpf, G., Krömer, H. and Hoffmann, M., *J.Macoromol.Sci.Phys.*, **B6**, 167 (1972)
(11) Pan, T., Huang, K., Balasz, A. C., Kunz, M. S., Mayes, A. M. and Russel T. P., *Macromolecules*, **26**, 2860 (1993)

FIGURE CAPTIONS:

Figure 1: Structure of the block copolymers

Figure 2: TEM picture of a rodlike morphology of
a: sample 59, b: sample DB 4 c: sample DB 7

Figure 3: Low angle electron diffraction pattern of sample DB 7,
tetragonal morphology

Figure 4: Schematical diffraction diagram of a tetragonal lattice, [001] plane

Figure 5: Small angle x-ray diffraction pattern of sample DB 7,
a: photographic picture, b: schematic picture

Table 1

sample	Φ_{PS}	phase behaviour (°C)	expected morphology
PS	1.00	g 102 i	
diblock copolymer		PS-PChEMA	
59	0.37	g 103 g 126 S_A 202 i	PS-rods
triblock copolymers		PChEMA-PS-PChEMA	
DB 4	0.29	g 101 g 117 S_A 188 i	PS-rods
DB 7	0.33	g 102 g 118 S_A 193 i	PS-rods
DB 5	0.35	g 98 g 118 S_A 180 i	PS-rods
PChEMA	0.00	g 126 S_A 213 i	

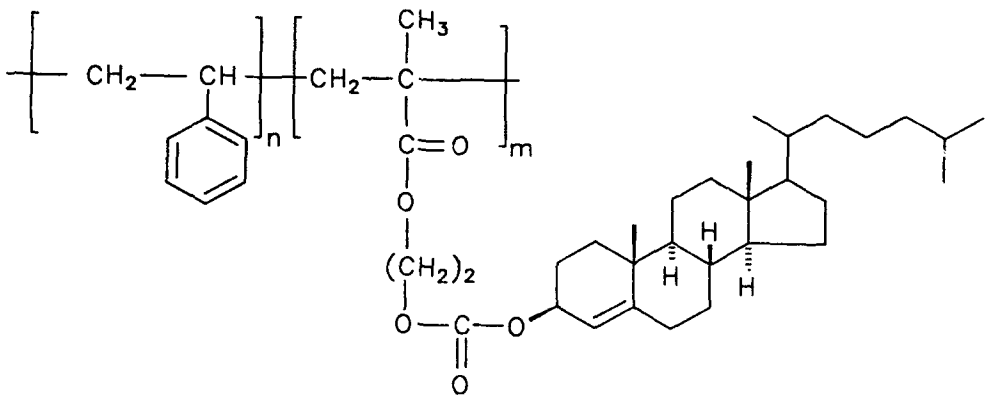

PS-block PChEMA-block

Figure 1

Figure 2a

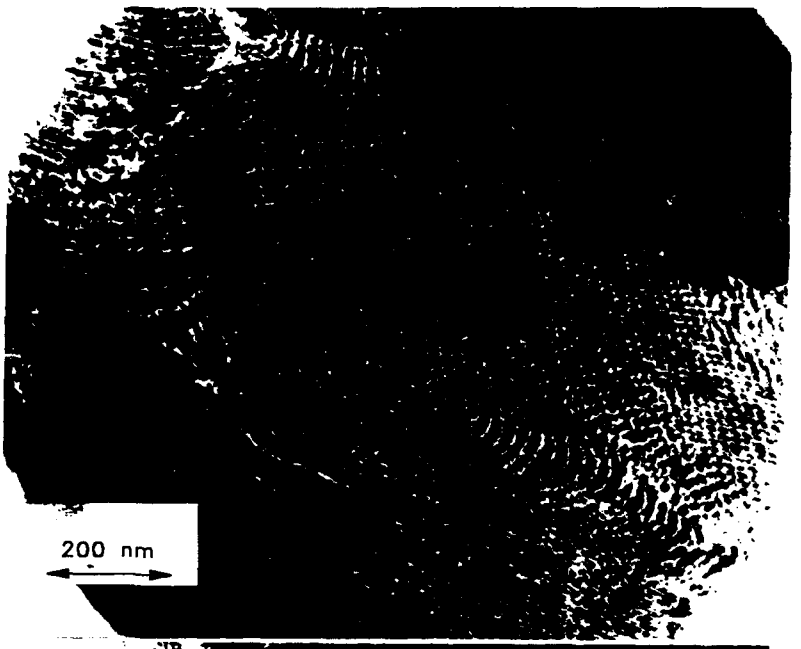

Figure 2b

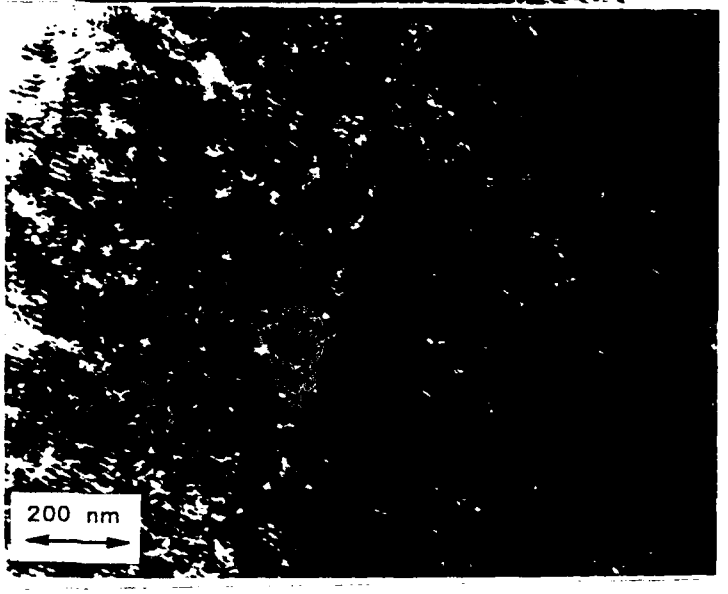

Figure 2c

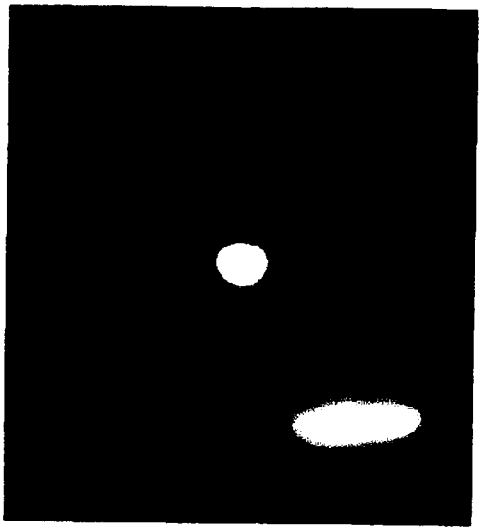

Figure 5a

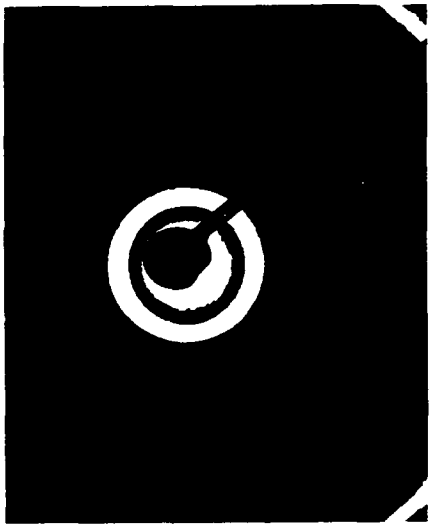

Figure 3

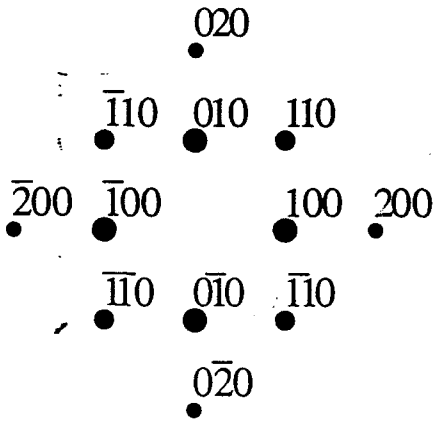

Figure 5b

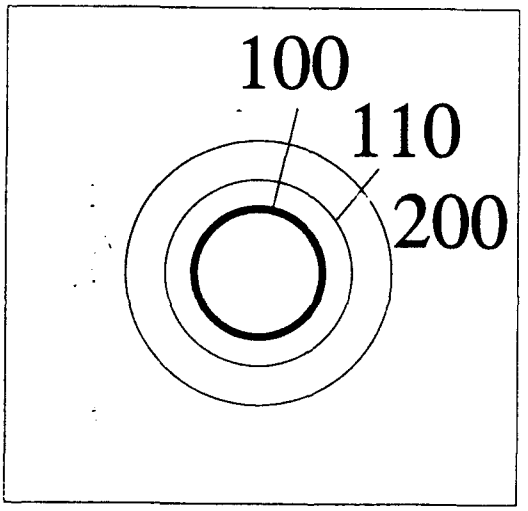

Figure 4